Dissertation

submitted to the

Combined Faculty of Natural Sciences and Mathematics

of the Ruperto Carola University Heidelberg, Germany

for the degree of

Doctor of Natural Sciences

Presented by

M. Sc. Alexa Natalia Lauer

born in Bad Soden am Taunus, Germany

Oral examination:

26.06.2019

A comparative transcriptome analysis of human and porcine choroid plexus cells in response to *Streptococcus suis* Serotype 2 infection

Referees: Prof. Dr. Michael Lanzer

Prof. Dr. Horst Schroten

For my parents

Eidesstattliche Versicherung gemäß § 8 der Promotionsordnung für die Naturwissenschaftlich-Mathematische Gesamtfakultät der Universität Heidelberg

Sworn Affidavit according to § 8 of the doctoral degree regulations of the Combined Faculty of Natural Sciences and Mathematics

1. Bei der eingereichten Dissertation zu dem Thema / The thesis I have submitted entitled

"A comparative transcriptome analysis of human and porcine choroid plexus cells in response to *Streptococcus suis* Serotype 2 infection"

handelt es sich um meine eigenständig erbrachte Leistung / is my own work.

2. Ich habe nur die angegebenen Quellen und Hilfsmittel benutzt und mich keiner unzulässigen Hilfe Dritter bedient. Insbesondere habe ich wörtlich oder sinngemäß aus anderen Werken übernommene Inhalte als solche kenntlich gemacht. / I have only used the sources indicated and have not made unauthorised use of services of a third party. Where the work of others has been quoted or reproduced, the source is always given.

3. Die Arbeit oder Teile davon habe ich ~~wie folgt~~/bislang nicht[1)] an einer Hochschule des In- oder Auslands als Bestandteil einer Prüfungs- oder Qualifikationsleistung vorgelegt. / I have not yet~~/have already~~[1)] presented this thesis or parts thereof to a university as part of an examination or degree.

4. Die Richtigkeit der vorstehenden Erklärungen bestätige ich. / I confirm that the declarations made above are correct.

5. Die Bedeutung der eidesstattlichen Versicherung und die strafrechtlichen Folgen einer unrichtigen oder unvollständigen eidesstattlichen Versicherung sind mir bekannt. / I am aware of the importance of a sworn affidavit and the criminal prosecution in case of a false or incomplete affidavit

Ich versichere an Eides statt, dass ich nach bestem Wissen die reine Wahrheit erklärt und nichts verschwiegen habe. / I affirm that the above is the absolute truth to the best of my knowledge and that I have not concealed anything.

……. ……..

Ort und Datum / Place and date Unterschrift / Signature

[1)] Nicht Zutreffendes streichen. Bei Bejahung sind anzugeben: der Titel der andernorts vorgelegten Arbeit, die Hochschule, das Jahr der Vorlage und die Art der Prüfungs- oder Qualifikationsleistung. / Please cross out what is not applicable. If applicable, please provide: the title of the thesis that was presented elsewhere, the name of the university, the year of presentation and the type of examination or degree.

Summary

Streptococcus suis is an important opportunistic zoonotic pathogen, of which serotype 2 (ST2) is considered to be the most virulent for its natural host, the pig, as well as for humans. The most common clinical manifestations for pigs and humans are septicemia and meningitis. Previous *in vivo* observations in *S. suis*-infected pigs, revealed lesions at the choroid plexus (CP), which forms the interface at the blood-cerebrospinal fluid barrier to the central nervous system. *In vitro* experiments with primary porcine CP epithelial cells (PCPEC) and immortal human CP epithelial (HIBCPP) cells demonstrated that *S. suis* can invade and traverse the CP epithelial cells, and that the CP contributes to the immunological response via cytokine expression and secretion. In this study, a comparative approach to investigate the global transcriptome profile via RNA-seq of *in vitro* and *in vivo S. suis* ST2 challenged PCPEC/HIBCPP cells and pigs, respectively, was performed.

In a first step to process the RNA-seq generated data, significant differentially expressed genes (DEGs) were identified. The highest amount of DEGs was observed for the dataset obtained from the CP isolated from *in vivo S. suis* ST2 infected pigs which suffered from meningitis. The primary PCPEC, which were infected *in vitro* with *S. suis* ST2, exhibited a strong inflammatory response 6 h post-infection, with a maximal differential regulation of 134-fold, whereas HIBCPP cells exhibited a predominant differential gene regulation of genes related to hypoxia, where a maximum of an 8-fold change was observed. In the Gene Set Enrichment Analysis (GSEA), which interpreted the data based on gene groups performing a common biological function, a significant enrichment of 18, 28, and 21 hallmark gene sets (GSs) for infected HIBCPP cells, PCPEC, and in the CP of pigs suffering from *S. suis* ST2 meningitis, respectively, were identified. Of these significantly enriched GSs, 8 GSs overlapped between the three different sample sets. The majority of these GSs are involved in in cellular signaling (e.g. TNFα via NFκB) and pathways (e.g. hypoxia), immune response (e.g. inflammatory response), and development (e.g. epithelial-mesenchymal transition). In contrast, suppressed GSs observed during *in vitro* and *in vivo S. suis* ST2 infections included those, which were involved in cellular proliferation and metabolic processes. Furthermore, the RNA-seq method was validated via quantitative PCR.

In a further comparative analysis using the CP samples obtained from the *in vivo* infection experiments, the conventional RNA-sequencing method was compared to the Massive Analysis of cDNA Ends (MACE) sequencing method. A concordance of approximately 50 % was observed for the significant DEGs, and the GSEA revealed an enrichment of the same 17 GSs.

This study suggests that similar cellular processes occur in human and porcine infected CP (epithelial) cells, especially in terms of inflammatory response. However, further follow-up investigations need to be performed to gain specific insights to the cellular response at the CP during a *S. suis* infection.

Zusammenfassung

Streptococcus suis ist ein wichtiger opportunistischer zoonotischer Krankheitserreger, wobei der Serotyp 2 (ST2) die stärkste Virulenz im natürlichem Wirt, dem Schwein, sowie bei Menschen aufweist. Am häufigsten äußert sich die Infektion im Schwein und Mensch als Septikämie und Meningitis. Bisherige Beobachtungen aus *in vivo S. suis*-erkrankten Schweinen wiesen Läsionen am Choroid Plexus (CP) auf, welcher die Blut-Liquor-Schranke zum zentralen Nervensystem bildet. Durch den Einsatz von primären porzinen CP Epithelzellen (PCPEC) und humanen CP Papillom-Epithelzellen (HIBCPP) in *in vitro* Versuchen mit *S. suis* konnte gezeigt werden, dass der Erreger in der Lage ist die CP Epithelzellen zu invadieren und zu überqueren, und dass der CP sich an der Immunabwehr beteiligt indem er Zyktokine exprimiert und in die Umgebung ausschüttet. Ziel dieser Arbeit war es mittels Gesamt-Transkriptom-Shotgun-Sequenzierung (RNA-seq) die zelluläre Antwort von *in vitro* mit *S. suis*-infizierten HIBCPP Zellen und PCPEC, sowie die Antwort des CP aus experimentell mit *S suis*-infizierten Schweinen, zu ermitteln und miteinander zu vergleichen.

Im ersten Schritt der Auswertung der RNA-seq generierten Daten wurde eine Auflistung der signifikanten differenziell-exprimierten Gene (DEG) ermittelt. Die Daten, die aus den Gewebeproben von *in vivo* mit *S. suis* infizierten Schweinen mit einer Meningitis erworben wurden, wiesen die höchste Anzahl von DEG auf. Die primären PCPEC zeigten nach einer 6-stündigen Infektion mit *S. suis in vitro* eine starke Entzündungsreaktion, mit einer maximal 134-fachen differenziellen Genregulierung, während die infizierten HIBCPP Zellen hauptsächlich signifikante DEGs aufwiesen, die an der hypoxischen Stressantwort beteiligt sind, mit einer maximalen differenziellen Genregulierung von 8-fach. Durch eine „Gene Set Enrichment Analysis“ (GSEA), welche die differenziell exprimierten Gene anhand von gemeinsamen biologischen Funktionen in Gruppen zuordnet, wurden 18 signifikante Gen-Sets (GSs) bei *S. suis*-infizierten HIBCPP Zellen, sowie 28 GS für PCPEC und 21 bei den CPs von Schweinen, die an einer Meningitis erkrankt waren, identifiziert. Bei diesen signifikanten GSs gab es eine Überlappung von 8 GSs zwischen den 3 Versuchsansätzen. Der größte Anteil der signifikanten GSs spielt eine Rolle bei Zellsignaltransduktionwegen (zum Beispiel TNFα durch NFκB) und Zellsignalwegen (zum Beispiel Hypoxie), aber auch bei der Immunabwehr (zum Beispiel Entzündungsreaktion) und Zellentwicklung (zum Beispiel Epithel-Mesenchym Übergang). Zusätzlich zu den in den infizierten Proben angereicherten GSs wurde auch analysiert, welche biologischen Prozesse während einer *S. suis* Infektion unterdrückt wurden. Hier wurden GSs, die bei der Zellvermehrung und beim Zellmetabolismus eine Rolle spielen, identifiziert. Letztlich wurde die RNA-seq Methode mittels einer quantitativen PCR validiert.

In einer weiteren Vergleichsanalyse wurden zusätzlich anhand der CP Proben aus den *in vivo* Tierversuchen die konventionelle RNA-seq Methode mit der „Massive Analysis of cDNA Ends“ (MACE) Sequenziermethode verglichen. Eine Übereinstimmung von ungefähr 50 % der mithilfe der

beiden Methoden ermittelten signifikanten DEGs wurde gefunden, und bei der GSEA wurde für beide Methoden eine Anreicherung der identischen 17 signifikanten GSs aus beiden Sequenziermethoden beobachtet.

Durch diese Arbeit wurde aufgedeckt, dass viele zelluläre Antworten im humanen und porzinen CP vergleichbar sind, vor allem bei den zellulären Prozessen der Immunabwehr. Jedoch müssen in der Zukunft ausführlichere nachverfolgende Untersuchungen durchgeführt werden, um spezifische Abläufe am CP bei einer *S. suis* Infektion aufzuklären.

Table of Contents

Abbreviations

A	ATP	adenosine triphosphate
	ANOVA	analysis of variance
	AS RNA	anti-sense RNA
B	BCSFB	blood-cerebrospinal fluid barrier
	bp	base pairs
C	°C	degree Celsius
	Ca^{2+}	calcium
	cDNA	copy deoxyribonucleic acid
	CFU	colony forming units
	CNS	central nervous system
	CO_2	carbon dioxide
	CP	choroid plexus
	CPS	polysaccharide capsule
	CSF	cerebrospinal fluid
	C_T	threshold cycle
	CXCL	(CXC-motif) ligand
D	DEG	differentially expressed gene(s)
	DMSO	dimethylsulfoxide
	DNA	deoxyribonucleic acid
	DNase	deoxyribonuclease
	DPBS	Dulbecco's phosphate buffered solution
	DUSP2	Dual specificity phosphatase 2
E	e.g.	*exempli gratia*
	EDTA	ethylenediaminetetraacetic acid
	EF	extracellular factor
	EMT	epithelial-mesenchymal transition

F	FCS	fetal calf serum
	FC	fold change
	FDR	false discovery rate
	FITC	fluorescein isothiocyanate
G	GAPDH	glyceraldehyde-3-phosphate dehydrogenase
	GO	Gene Ontology
	GSEA	Gene Set Enrichment Analysis
	GSs	Gene Sets
	x g	relative centrifugal force
H	h	hour
	H_2O	water
	HIBCPP	human choroid plexus epithelial papilloma cells
	HIF	hypoxia-inducible factor
I	i.e.	*id est*
	IL	interleukin
K	KRAS	Kirsten rat sarcoma viral oncogene homolog
L	LINC	long intergenic non-coding RNA
M	MACE	massive analysis of cDNA ends
	Mg^{2+}	magnesium
	µl	microliter
	min	minute(s)
	MIR	microRNA
	ml	milliliter
	MOI	multiplicity of infection
	mRNA	messenger RNA
	MRP	muramidase-released protein
	MSigDB	Molecular Signature Database
	MXI1	MAX interactor 1
	Myc	myelocytomatosis

N	NGS	Next-Generation Sequencing
	NES	normalized enrichment score
	NET	neutrophil extracellular trap
	NFκBIA	NFκB inhibitor alpha
	nm	nano meter
O	Ω	ohm
	OD_{600}	optical density at 600 nm
	ORF	open reading frame
P	PartekGS	Partek Genomics Suite
	P/S	penicillin-streptomycin
	PCPEC	porcine choroid plexus epithelial cells
	PCR	polymerase chain reaction
	poly(A)	polyadenylated
Q	qPCR	quantitative polymerase chain reaction
R	RIN	RNA Integrity Number
	RNA	ribonucleic acid
	RNase	ribonuclease
	RNA-seq	RNA-sequencing
	RND1	Rho family GTPase 1
	RPKM	reads per kilobase of exon model per million reads
	rRNA	ribosomal RNA
	RT-PCR	reverse transcriptase polymerase chain reaction
S	*S. suis*	*Streptococcus suis*
	S.D.	standard deviation
	SAS	subarachnoid space
	sec	seconds
	SFM	serum-free medium
	SLY	suilysin
	SNP	single nucleotide polymorphism

	SRA	sequence read archive
	ST	serotype
T	TAE	tris-acetic acid-EDTA buffer
	Taq	*Thermus aquaticus*
	TCIM	transcriptional and immune response regulator
	TEER	transepithelial electrical resistance
	TGFβ	transforming growth factor beta
	THB	Todd-Hewitt Broth
	TNFα	tumor necrosis factor alpha
U	U	Units
V	V	Volt
	v/v	volume per volume
	VEGFA	vascular endothelial growth factor a
Z	ZO	zonula occludens
	ZC3H12A	zinc finger CCCH-type containing 12A

1. Introduction

1.1. *Streptococcus suis* (*S. suis*)

1.1.1. Characterization

S. suis is a Gram-positive, opportunistic, and zoonotic pathogen. As a Gram-positive bacterium, it is surrounded by a thick polysaccharide capsule (CPS). The CPS is used to divide *S. suis* into different serotypes (STs) (Smith et al., 1999). Currently, 35 different *S. suis* STs have been characterized based on the antigen presence on the bacterial CPS (Dutkiewicz et al., 2017). Furthermore, these various STs are further divided into different sequence types based on the Multilocus Sequence Typing method, which compares the nucleotide sequence of selected house-keeping genes and therefore can also determine the evolutionary relationship (Goyette-Desjardins et al., 2014; King et al., 2002). 616 sequence types have been identified for *S. suis*, with approximately half of them being allocated to specific STs (Haas and Grenier, 2018). Furthermore, different sequence types were found to be associated with disease to a different degree. For example, sequence type 1 was strongly associated with meningitis and sepsis, and is most often isolated in cases of disease in Europe, whereas sequence types 27 and 87 are less likely to be associated with disease (Goyette-Desjardins et al., 2014; King et al., 2002).

Additionally, the predominance of specific *S. suis* STs tends to vary depending on the geographic location. The predominant STs isolated from diseased pigs in Europe are 2, 9, and 7, whereas in Asia these include STs 2, 3, and 4 (Haas and Grenier, 2018). Worldwide though, ST 2 is most frequently isolated in disease incidences (Haas and Grenier, 2018).

Although vaccine development is of high importance and a few products exist on the market for specific *S. suis* ST2 and ST9 strains, due to the high antigen variance of the *S. suis* CPS, development of a single universal vaccine has remained a challenge (Baums et al., 2009; Haas and Grenier, 2018). However, continuous research to understand the role of potential virulence-associated and virulence factors of *S. suis* remains a main focus for vaccine development (Segura, 2015).

1.1.2. Virulence factors and virulence-associated factors

Virulence factors are required for a pathogen to successfully aid in establishing an infection in the host. Approximately 200 virulence factors have been described in recent years, which contribute to *S. suis* establishing disease in the host (Dutkiewicz et al., 2018; Segura et al., 2017). The majority of

the described factors are considered being associated with disease development, whereas the bacterial CPS is the only "true" virulence factor required to establish disease (Smith et al., 1999).

The polysaccharide bacterial CPS is considered the only essential virulence factor for *S. suis*, since *in vivo* porcine experiments demonstrated that CPS deletion resulted in complete loss of pathogenicity (Smith et al., 1999). Studies have shown that the CPS protects *S. suis* from immune recognition in the blood by masking its surface antigens, therefore preventing the up-take by phagocytic immune cells (Fittipaldi et al., 2012). However, the absence of the CPS allows for better adhesion, e.g. to epithelial cells, suggesting that *S. suis* can regulate the CPS expression depending on the niche it is colonizing (Fittipaldi et al., 2012).

Besides the CPS, the most important virulence factors which are found in the majority of virulent *S. suis* STs include suilysin (SLY), extracellular factor (EF), and muramidase-released protein (MRP), therefore making them candidates for a universal *S. suis* vaccine development (Haas and Grenier, 2018). The factor SLY is a known pore-forming toxin, thereby inducing host cell lysis and aiding *S. suis* during invasion (Gottschalk et al., 1995). Furthermore, EF is a secreted protein and MRP is a protein found anchored to the bacterial cell wall, both of which were found associated with *S. suis*-induced disease (Vecht et al., 1991).

The presence of these numerous virulence-associated factors supports, but is not essential, for the successful *S. suis* pathogenesis in the porcine or human host.

1.1.3. Pathogenesis in swine

By being the natural host, pigs are often found colonized with *S. suis*. *S. suis* usually asymptomatically colonizes pigs tonsils, nasal cavities, intestinal tract, and genital tract (Wertheim et al., 2009). During birth, the offspring are exposed to, and colonized by, the mother's vaginal flora, and protected by the maternal antibodies from birth and during weaning (Cloutier et al., 2003; Dutkiewicz et al., 2017). *S. suis* disease primarily affects young piglets (4 to 10 weeks of age), often in the post-weaning phase when maternal antibodies decline (Rieckmann et al., 2018). However, with advancing age following weaning, growing pigs showed an increase of antibody production, concurrent with reduced bacterial survival in blood-bactericidal assays (Rieckmann et al., 2018). Furthermore, aerosol transmission between experimentally colonized and *S. suis*-free piglets was also demonstrated (Berthelot-Herault et al., 2001).

The most common clinical manifestations observed in the field include sepsis and meningitis, but endocarditis, arthritis, pneumonia, and peritonitis are also reported (Dutkiewicz et al., 2017). Much

research is dedicated to understanding the pathogenic mechanisms which elicit disease, in order to develop vaccines, improve treatment options with rising antibiotic resistance, and reduce economic losses (Haas and Grenier, 2018). Animal suffering is not only an ethical down-side of this pathogen, but from the human industrious aspect, *S. suis* also affects the pork industry and can lead to major economic losses. For example, in the United States alone, a loss of US$ 300 million in the pork industry was estimated (Staats et al., 1997).

Since *S. suis* is a known zoonotic pathogen, it does not only affect pigs, but it can also have a detrimental impact on humans.

1.1.4. Pathogenesis in humans

The first human-associated *S. suis* meningitis and septicemia cases were described in 1968 in the Netherlands (Perch et al., 1968). Over the past 20 years, the number of *S. suis* afflicted humans has increased, and between the years of 2002 and 2013, 1,642 *S. suis* infections in humans were reported (Dutkiewicz et al., 2017; Goyette-Desjardins et al., 2014). Furthermore, one minor and one major outbreak have occurred in 1998 in Jiangsu, China (Hu et al., 2000) and during the summer of 2005 in Sichuan, China (Yu et al., 2006), respectively. The morbidity during these outbreaks was 25 and 215 cases, with a mortality rate of 56 % and 18 % in Jiangsu and Sichuan, respectively, and these human cases were concurrent to outbreaks in the pig populations, which affected 80,000 animals (Du et al., 2017; Dutkiewicz et al., 2017).

The primary risk factor for disease development in humans has been associated with working in the swine industry as a butcher or abattoir worker, and *S. suis* infection in humans is therefore considered an occupation-associated disease (Rayanakorn et al., 2018). Furthermore, disease development has also been linked to the consumption of undercooked or raw pork products and blood, which are part of cultural dishes in countries like Thailand, Vietnam, and China (e.g. Hong Kong) (Rayanakorn et al., 2018). This, together with the fact that Asia has a major swine-rearing industry for producing the majority of the global pork products for consumption, provides an explanation as to why *S. suis* is one of the leading causes for adult bacterial meningitis in southeastern Asian countries (Dutkiewicz et al., 2017; Pappas, 2013). For example, Ho Dang Trung and colleagues found that *S. suis* was the number one leading cause for CNS infection in Vietnam (Ho Dang Trung et al., 2012). However, Asian countries are not the only ones affected. In Europe, approximately 71 % of the reported *S. suis* cases came from The Netherlands, The United Kingdom, Spain, and France, which are countries also home to major swine husbandry (Dutkiewicz et al., 2017).

Approximately 75 % of human *S. suis* infections have been attributed to ST2, with the second most common being ST14, making up 2 % (Goyette-Desjardins et al., 2014). As also seen in pigs, the most common and severe clinical manifestations include meningitis, sepsis, and streptococcal toxic shock syndrome, while endocarditis, arthritis, and spondylodiscitis have also been reported (Huong et al., 2014; Tang et al., 2006).

The recovery of *S. suis*-induced meningitis is often accompanied by long-term impairments, such as vestibular dysfunction, visual impairment, or complete or partial auditory loss, with the latter being the most common implication from *S. suis* infection (Huong et al., 2014). In a retrospective meta-analysis study focusing on *S. suis* meningitis in humans, it was found that 53 % of survivors suffered from hearing loss (van Samkar et al., 2015). These long-term sequelae are not only a hindrance for the patient, but can also have an economic impact. For example, a study carried out in Vietnam, where *S. suis* is the leading cause for bacterial meningitis, found that individuals suffering from hearing loss or other vestibular dysfunction, following the recovery of *S. suis* meningitis, either were unlikely to continue in their line of work or had a 2.6 times higher risk of being unemployed (Huong et al., 2019).

1.2. The central nervous system (CNS)

Two major barriers are described in separating our CNS from the rest of our body. These barriers are known as the blood-brain barrier (BBB) and the blood-cerebrospinal fluid barrier (BCSFB). During his exploration for the human soul in the early 16th century, Leonardo da Vinci was the first to illustrate the ventricular system (Del Maestro, 1998), which is known today as the site of the BCSFB. Later, during the turn of the 20th century, observations made by Ehrlich and Goldmann provided the first evidence that the CNS is compartmentalized from the rest of the body (Ehrlich, 1885; Goldmann, 1913). This was demonstrated by the injection of dye into the vascular system, thereby staining all organs with the exception of the brain, and vice versa following the dye injected into the cerebrospinal fluid (CSF) (Ehrlich, 1885; Goldmann, 1913). These barrier interfaces are in place in order to regulate metabolite influx and waste efflux, thereby maintaining a strict homeostatic and sterile environment.

1.2.1. The blood-brain barrier (BBB)

The main property of the BBB is constituted by tightly connected endothelial cells lining the capillaries of the vascular system in the brain, thereby making up the largest barrier between the blood and CNS (Abbott et al., 2010). The tight connection between the endothelial cells is created by

the presence of the tight junction proteins, namely zonula occludens 1, 2, and 3 (ZO1-3), as well as adherens junctions, such as cadherin proteins (Wolburg and Lippoldt, 2002). Additional cells found in close association with the BBB endothelial cells are pericytes and astrocytes, which provide further main support in the BBB maintenance and function (Abbott et al., 2006). Pericytes are most closely associated with BBB endothelial cells, and together they are found within the basal lamina (Abbott et al., 2006). This basal membrane structure is surrounded by the endfeet of astrocytes, which are located in an extracellular matrix space where additional cell types, such as microglial immune cells and nerve terminals are found, which further provide support to the BBB (Abbott et al., 2006). In addition to the physical barrier property, the BBB is described to be equipped with specialized adenosine triphosphate (ATP)-binding cassette (ABC) transporters, as well as transcytosis mechanisms for the influx of macromolecules to support the in- and efflux between the blood and CNS, thereby creating a chemical and metabolic barrier (Abbott et al., 2010).

1.2.2. The blood-cerebrospinal fluid barrier (BCSFB) at the choroid plexus (CP)

The second vascular barrier is the BCSFB. The BSCFB is located in the four brain ventricles at the choroid plexus (CP) structure, which forms an interface between the vascular system and the cerebrospinal fluid (CSF) (Wolburg and Paulus, 2010). The main difference of the BCSFB to the BBB is that the barrier at the BCSFB is constituted by the tight junctions connecting the CP epithelial cells and the endothelial cells exhibit fenestration (Wolburg and Paulus, 2010).

In the ventricular system, a total of four BCSFB sites exist, which can be located at the two CP present in each of the lateral ventricles of the two brain hemispheres, and one CP in each of the third and fourth ventricle of the CNS (Figure 1 A) (Liddelow, 2015). Figure 1 B depicts the overall cell arrangement found at the CP, making up an interface of the BCSFB, which is the second largest, highly-vascularized, barrier to the CNS. The main barrier property at the CP results from the polarized epithelial cells, which are connected via tight junctions and tight junction-associated proteins, such as ZO1 and occludin (Figure 1 B) (Wolburg et al., 2001). These tightly connected epithelial cells rest on a basement membrane with an underlying stroma (Figure 1 B). Fenestrated endothelial cells are found lining the vasculature and allow for the passage of water, nutrients, and immune cells from the blood to the CNS (Figure 1 B) (Wolburg and Paulus, 2010).

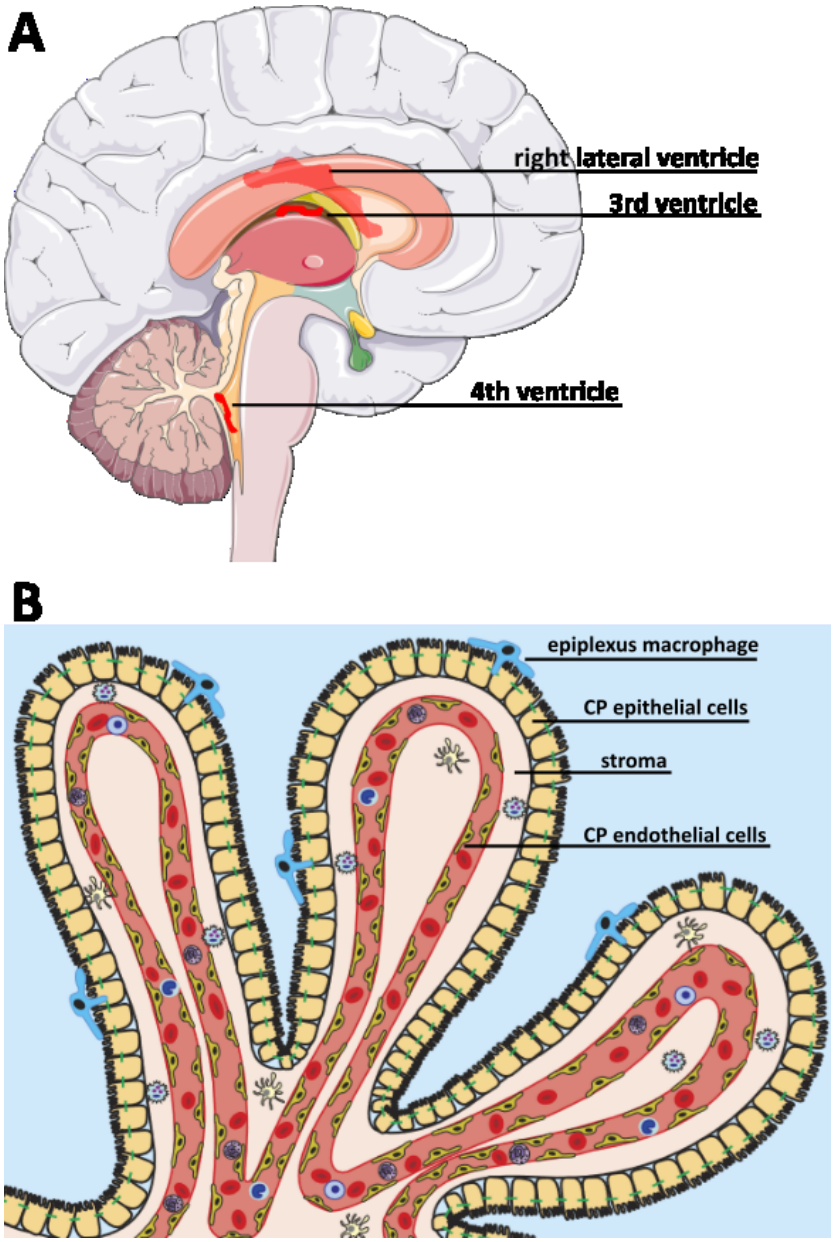

Figure 1. The choroid plexus (CP) localization and cellular arrangement. The red-labelled marks are indicative of the two CP located in the lateral ventricles of the left and right brain hemispheres, as well as the CP in the 3rd and the 4th ventricles (A). The CP epithelial cells are tightly connected and form the barrier to the CNS, and fenestrated CP endothelial cells allow immune cells to migrate into the stroma, but also water and nutrient exchange from the blood to the CNS (B). Image A was modified from Servier Medical Art, licensed under a Creative Commons Attribution 3.0 Unported License (http://smart.servier.com/). Image B was modified from Lauer et al. (2018).

The BCSFB barrier does not only present a physical barrier to keep the CNS a sterile environment from potential pathogens or other blood-borne threats to the CNS, but has also been described to act as a chemical barrier (Ghersi-Egea et al., 2018; Liddelow, 2015). The epithelial cells of the CP are known to be equipped with an array of efflux transmembrane transporters, for e.g. family members of ABC transporters, and metabolizing enzymes in order to aid in the removal of neurotoxic substances (Ghersi-Egea et al., 2018). Furthermore, a neuroprotective role is enabled via other

passive and active transporters, for e.g. members of the solute carrier family, for the movement of substrates across the barrier, thereby preventing the free diffusion from the bloodstream (Liddelow, 2015). However, this chemical specificity makes drug-delivery into the CNS challenging and is, therefore, a subject of pharmaceutical research (Strazielle and Ghersi-Egea, 2016).

The CP is not only an essential physical and biochemical barrier to the CNS, but also has the important function of producing the majority of the CSF in our CNS, which, amongst other things, acts as a shock-absorber to prevent harm to the brain (Liddelow, 2015). A physiological feature which allows for optimal CSF secretion is the apically located microvilli of the CP epithelial cells, which form a brush border, thereby increasing the surface area (Ghersi-Egea et al., 2018). Through the flux of sodium, chloride, and bicarbonate across the cell membrane, an osmotic gradient is created, which results in the sodium / potassium - ATPase and carbonic anhydrase enzyme activity. Via the enzymatic activities, water from the vascular system is then subsequently driven through aquaporin-1 channels into the CNS, thereby generating the CSF (Ghersi-Egea et al., 2018; Liddelow, 2015). It is estimated that the CP produces approximately 500 ml CSF per day, thereby replacing the CSF three to five times daily (Ransohoff and Engelhardt, 2012).

The CP has an important function in maintaining the BCSFB and producing the CSF for the homeostasis of the CNS. However, due to its location at the interface between the blood and CNS, barrier disruption caused by, for e.g., inflammation has been implicated with debilitating diseases, such as multiple sclerosis (Vercellino et al., 2008). Furthermore, the CP has also been implicated in cancer metastasis to the CNS, schizophrenia, as well as an invasion route of pathogenic microorganisms (Kim et al., 2016; Lauer et al., 2018; Schwerk et al., 2015; Vandenhaute et al., 2015).

1.2.3. The arachnoid barrier

Finally, a third, non-vascular, arachnoid barrier is described. The brain and spinal cord are fully surrounded by the meninges membranes depicted in Figure 2, which is comprised by the dura mater, arachnoid mater, and pia mater (Ransohoff and Engelhardt, 2012; Weller et al., 2018). The dura mater is found directly underneath the skull bone, followed by the arachnoid mater, which forms the outer layer of the subarachnoid space (SAS). The bottom layer of the SAS is composed of the pia mater, which surrounds the cerebral cortex - the gray matter of the brain (Weller et al., 2018). The SAS is the location of CSF circulation, but also the site where blood vessels run through with perpendicular arteries reaching into the cerebral cortex (Weller et al., 2018). Parts of the arachnoid membrane protrude outward through the dura, creating villi which allow for the reabsorption of CSF into the vascular system (Ransohoff and Engelhardt, 2012).

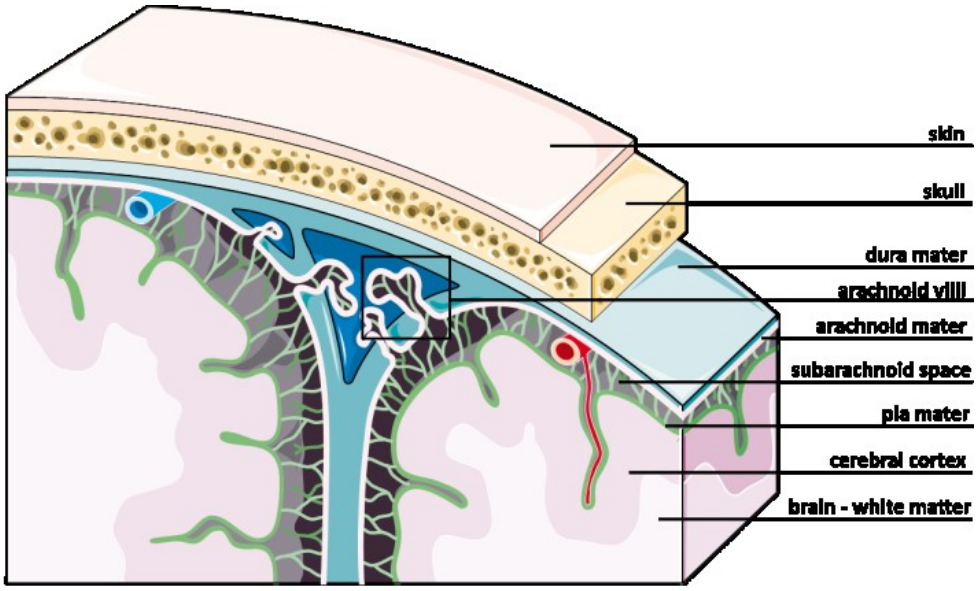

Figure 2. The meninges in the CNS. The meninges are comprised by the dura, arachnoid, and pia matter, which lie between the skull bone and the gray matter (cerebral cortex) of the brain. This image was modified from Servier Medical Art, licensed under a Creative Commons Attribution 3.0 Unported License (http://smart.servier.com/).

The CNS barriers are essential in maintaining a homeostatic environment via selective influx and efflux mechanisms, but also by providing a physical barrier. The physical and biochemical barriers are not only in place to prevent entry of blood-borne microorganisms or neurotoxic substances, but strictly regulate immune cell activity, too.

1.3. Infection of the CNS

Although the CNS is compartmentalized from the rest of the body, it is not immune to infection. Different types of inflammation can occur due to infection with a pathogenic agent. These are divided into meningitis, encephalitis, or meningoencephalitis (Dando et al., 2014). During meningitis, the meninges membranes (Figure 2) covering the brain and spinal cord becomes inflamed, and clinically presents itself with neck stiffness, fever, headache, and a change in the mental state (Dando et al., 2014). During encephalitis, the brain parenchyma (gray and white matter) is affected and inflamed, with symptoms similar to meningitis, including the possible presentation with seizures (Dando et al., 2014). Lastly, meningoencephalitis is when not just the brain, nor just the meningitis, but both are inflamed, often resulting in a lethal outcome, especially when induced by amoeba (Dando et al., 2014).

Many different pathogens, which are classified into viral, bacterial, fungal, and parasitic classes, are capable of inducing meningitis. The most common cause of meningitis are viral pathogenic agents, which can provoke aseptic meningitis, but are also a frequent cause of encephalitis (Glaser et al.,

2006; Wright et al., 2019). The optimal therapy of viral meningitis is prevention via vaccination; however, viral meningitis normally results in a positive prognosis for a full recovery with supportive care provided in a hospital (Wright et al., 2019). Fungal and parasite-induced meningitis tend to occur at a much lower rate, with clinical manifestation commonly linked to the immune status of the patient, but are often associated with a high mortality rate or long-term sequelae (Goralska et al., 2018; Graeff-Teixeira et al., 2009). The second most common cause of infection of the CNS are bacterial agents, which, unlike viral pathogens, tend to cause more detrimental outcomes in terms of recovery, and are not uncommon to result in death despite the availability of antibacterial treatment agents (Doran et al., 2016).

1.3.1. Bacterial meningitis

Meningitis caused by bacterial microorganisms tends to be more severe than viral meningitis, and can lead to death if no prompt treatment actions are taken. The age group plays an important factor for an individual to develop bacterial meningitis, and includes newborn, infants, adolescents, and elderly people (Dando et al., 2014). Studies examining the long-term sequelae of children who suffered from bacterial meningitis found that the most common long-term ailments included a low intelligence quotient, seizures, auditory impairment, and problems with their fine motor skills (Chandran et al., 2011; Grimwood et al., 1995). However, in addition to age, an individual's immune status is also considered an important factor in susceptibility (Dando et al., 2014).

In theory, most microorganisms infecting humans are capable of causing meningitis. However, the most common bacterial agents include *Neisseria meningitidis*, *Streptococcus pneumoniae*, *Listeria monocytogenes*, *Haemophilus influenzae* type b, *Streptococcus agalactiae*, and *Escherichia coli* K1 strains (Kim, 2010; van Ettekoven et al., 2017). Furthermore, the neglected zoonotic pathogen *Streptococcus suis* (*S. suis*) has been one of the leading causes of adult bacterial meningitis in recent years, especially in southeast Asian countries (Dutkiewicz et al., 2017).

Although vaccines for the most common bacterial meningitis-causative agents exist and are effectively applied in the western world, incidences still occur which require a speedy diagnosis and adequate treatment plans for the best outcome. The use of antibiotics in combination with the application of corticosteroids, but only for infections with selected bacteria, have been suggested for the treatment during bacterial meningitis (van Ettekoven et al., 2017). Compared to western countries, incidences are much higher in non-industrial countries such as along the "meningitis belt" in Africa, where seasonal epidemics of meningitis occur and mortality is high (Agier et al., 2017).

In order for bacteria to induce meningitis in the host, a series of steps must occur. Bacterial meningitis isolates are commonly found as part of the mucosal membrane of the nasopharynx (Doran et al., 2016). In a next step, the pathogen must penetrate the tissue in order to reach the bloodstream. Here, the successful meningitis-inducing microorganisms are known to possess an array of virulence factors and defense mechanisms, which allows them to evade or overcome the recognition by the immune system (Doran et al., 2016). Once the pathogen reaches either the BBB or BCSFB, it must adhere to the endothelial (BBB) or epithelial (BCSFB) cells before it can breach the barriers to the CNS. Three main pathogen invasion mechanisms have been described, which involve the traversing of the BBB or BCSFB via transcellular (through the cell) or paracellular (between adjacent cells) mechanisms, but also a "Trojan horse" mechanism has been characterized, which commonly utilizes phagocytic immune cells traveling to the site of infection (Doran et al., 2016; Kim, 2008; Schwerk et al., 2015).

During bacterial invasion and replication, damage to the host's cells occurs in many different ways. However, while fighting the infection, a badly orchestrated immune response as well as factors released by the host can also cause cellular damage to the host's own cells, which can have long-term consequences for recovery or can result in death.

1.3.2. The host response during bacterial CNS infection

Upon the successful establishment of infection, a tug-of-war between the host defense and invading pathogens occurs. As mentioned above, evolved human pathogens are equipped with an array of virulence factors to help them survive against the host's primary defense mechanisms, which occur via the innate immune response (Ransohoff and Engelhardt, 2012).

Various immune cells are found residing in the CNS, such as microglia cells in the brain parenchyma and Kolmer's epiplexus cells associated with the apical microvilli surface of the CP at the BCSFB, which are both a type of phagocytic cell (Ransohoff and Engelhardt, 2012). Furthermore, dendritic cells and macrophages are found patrolling the stroma of the BCSFB (Ransohoff and Engelhardt, 2012). However, immune cells found circulating in the blood stream are also known to patrol the CNS, despite the physical barriers present at the BBB and BCSFB (Engelhardt et al., 2017). The CNS has even been described as an "immune privileged" site, since a much lower number of immune cells are found to be monitoring this environment in comparison to circulating immune cells in the bloodstream (Engelhardt et al., 2017; Meeker et al., 2012). In a healthy state, the composition of immune cells found in the CNS consists of approximately 1 white blood cell per µl of CSF, which gives a ratio of immune cells in the CNS to the blood of approximately 1 to 2,500 for T and B cells and 1 to

2,000 for monocytes (Meeker et al., 2012). However, during infection, the immune cell profile was found to vary depending on the causative agent. For example, viral meningitis is associated with a higher number of T cells in the CNS, whereas bacterial meningitis is associated with a higher presence of neutrophils (Egelund et al., 2017; Meeker et al., 2012).

In addition to the host's immune cells, epithelial cells, for example, have been shown to contribute to the immune response by releasing inflammatory signaling molecules, e.g. cytokines, to recruit immune cells to the site of infection for effective clearance, or other components, e.g. matrix metalloprotease 9, which aid in the degradation of pathogen-released factors (Grandgirard et al., 2013; Lauer et al., 2018). These factors, however, not only have the function of clearing the pathogen, but in some instances can result in damage to the host itself. A study investigating the early inflammatory response via cytokine presence in the CSF of patients suffering from meningitis found that the presence of, e.g., interleukins 1 beta and 6 (IL1β and IL6), as well as tumor necrosis factor alpha (TNFα) was significantly enriched in patients who died or suffered long-term sequelae (Grandgirard et al., 2013).

Furthermore, tissues infected with bacterial agents were found to be in a hypoxic state (Schaffer and Taylor, 2015). Hypoxia describes the limited presence of oxygen molecules in a given environment, and results in the dimerization of, most commonly, the transcription factor hypoxia-inducible factor (HIF), which transcribes genes regulating anoxic metabolism and increased vascularization (i.e. angiogenesis) in order to promote cell survival in the hypoxic tissue (Taylor and Colgan, 2017). However, hypoxia can also modulate the host's immune cell function and response (Taylor and Colgan, 2017). A pathological hypoxic environment can have different sources, which include the replication of cancer cells, immune cells consuming oxygen in a microenvironment due to increased immune cell presence or as a defense mechanism during infection, and bacterial replication and metabolism (Schaffer and Taylor, 2015; Taylor and Colgan, 2017). Furthermore, hypoxia has been linked to the breakdown of the BBB (Al Ahmad et al., 2012).

1.3.3. The BCSFB and *S. suis*

It has been demonstrated that pathogens can overcome the barriers to the CNS. Since the BBB provides the largest interface between the blood and CNS, the main research focus is dedicated to this area. However, the BCSFB was also demonstrated to play an important role for pathogen invasion into the CNS (Lauer et al., 2018; Schwerk et al., 2015). Importantly, substantial evidence exists between the interplay of the BSCFB and the zoonotic pathogen *S. suis*, hinting at the utilization of the BCSFB as a main route to the CNS. One common observation is that *S. suis* infections are

associated with lesions at the CP, which was first observed in natural and experimentally *in vivo* infected pigs described by Sanford, as well as Williams and Blakemore (Sanford, 1987; Williams and Blakemore, 1990). Consequently, an increase of *in vivo* and *in vitro* research has been dedicated to investigating *S. suis* virulence.

Many *in vitro* models of the BCSFB exist from a variety of organisms. For example, cultivated human papilloma (HIBCPP) (Ishiwata et al., 2005), primary porcine (PCPEC) (Haselbach et al., 2001), immortal porcine (PCP-R) (Schroten et al., 2012), immortal rat (Z310) (Zheng and Zhao, 2002), and primary rat (Tsutsumi et al., 1989) CP epithelial cells are used. Furthermore, many *in vivo* models used for studying *S. suis* pathology exist, including pigs, mice, and adult and larval zebrafish (Segura et al., 2017). However, the porcine *in vivo* model is the most essential, given that pigs are the natural host organisms of *S. suis*, and experimental induction *in vivo* has been well established with piglets (Seele et al., 2018; Segura et al., 2017).

Additionally, *S. suis* investigations utilizing *in vitro* BCSFB models with human and porcine CP epithelial cells have been conducted (Schwerk et al., 2012; Tenenbaum et al., 2009). These *in vitro* BCSFB models allow for the cell cultivation in a standard model, which cultivates the polar CP epithelial cells with the apical surface facing upwards (*in vivo* reflecting the CSF compartment), and an inverted culture, where the CP epithelial cells are cultivated with the basolateral cell side facing upwards (*in vivo* reflecting the blood compartment) (Tenenbaum et al., 2009).

By employing PCPEC and HIBCPP cells, it was observed that *S. suis* can invade the CP epithelial cells and traverse the BCSFB *in vitro* when applied to the basolateral cell side (Schwerk et al., 2012; Tenenbaum et al., 2009). Furthermore, from the aspect of the host response, it was observed that the primary PCPEC contribute to inflammatory response *in vitro* via cytokine expression (Schwerk et al., 2011). In a further study, the *in vitro* BCSFB composed of PCPEC was used in order to investigate and characterize the transmigration of granulocytes following the infection of *S. suis* (Wewer et al., 2011). In an advanced set-up of the human *in vitro* human BCSFB model, which also applied granulocytes, the formation of neutrophil extracellular traps (NETs) was observed following the infection with *S. suis* of HIBCPP cells from the basolateral cell side (de Buhr et al., 2017).

Despite growing evidence of the important role the BCSFB plays as an entry gate for, e.g., pathogens into the CNS, the CP remains to be an understudied area of research.

1.4. Transcriptome studies via Next-Generation Sequencing (NGS)

For nearly two decades, the Sanger-sequencing method, also known as the first generation sequencing, provided break-through scientific advancements, such as sequencing the human genome (International Human Genome Sequencing, 2004; Sanger et al., 1977). However, this method of DNA-sequencing was time consuming and costly, and advancements to this method did not provide much improvement (Metzker, 2005). NGS technology has become increasingly popular over the past decade, and encompasses the expedited high through- and output of data acquired with the help of informatics, in order to apply it in a biological setting (Metzker, 2010).

NGS can be applied in a variety of ways, including for the single-cell analysis, where the transcriptome of a single cell is analyzed, or dual sequencing, which, in the case of studying host-pathogen interaction, examines the transcriptome of both organisms simultaneously (Saliba et al., 2017). Additionally, various forms of RNA-sequencing (RNA-seq) exist which allow for the investigation of not only the polyadenylated (poly(A)) mRNA, but also include non-coding RNA (e.g. micro RNA and long non-coding RNA), total RNA, and pre-mRNA (Hrdlickova et al., 2017; Kukurba and Montgomery, 2015).

1.4.1. RNA-seq

RNA-seq, which uses NGS technology, has become a popular method to evaluate the global transcriptional response of a defined cell sample exposed to different stimuli, and over the past years has become the preferred method for transcriptome studies. Due to its numerous advantages, it has quickly become the preferential method over microarray analysis for studying the transcriptional response in a cell (Wilhelm and Landry, 2009). The major advantage is that RNA-seq quantifies transcripts, without the requirement of prior knowledge of a gene sequence (Kukurba and Montgomery, 2015). Furthermore, uncharacterized genes can be identified though RNA-seq, as well as alternatively spliced or rare transcripts (Metzker, 2010).

However, a few drawbacks to this advanced method exist. Factors can be the costs for maintaining the technology, having the capacity to store the large amounts of generated data, but also sequencing experiments with complex aims (Wilhelm and Landry, 2009). As an example for the latter, in order to identify and determine a reliable number of alternatively spliced transcripts, a higher number of transcripts out of the sample have to be sequenced (termed “high sequence depth”) (Kukurba and Montgomery, 2015). Furthermore, the assembly and reliable analysis of the generated data can present a challenge, with many software programs available in order to

normalize and compute sequencing-generated data, which can sometimes lead to differential results (Martin and Wang, 2011; Soneson and Delorenzi, 2013).

The RNA-seq work-flow encompasses a series of basic steps. Following the RNA isolation from the biological sample, the transcripts have to be prepared to a library, which consists of fragmented transcripts, since the sequencing machine is limited in capacity to produce long reads (Hrdlickova et al., 2017). The transcripts in the library are ligated with adapter regions on both ends, which contain predefined sequences for barcoding the samples and sequences complementary to the flow cell utilized for sequencing (Hrdlickova et al., 2017). Figure 3 depicts the sequence of events via the Illumina sequencing method, following the preparation of the RNA-seq library. The samples are applied to a flow cell (Figure 3 C), where transcript clusters are generated through bridge amplification (Figure 3 A) (Metzker, 2010). Once the clusters are generated, the flow cell is flooded with fluorescent-labelled nucleotides (Fig. 3 B), which allows the computer to generate the transcript sequence based of the different emitting colors, which are uniquely assigned to the specific nucleotides (Figure 3 C) (Metzker, 2010).

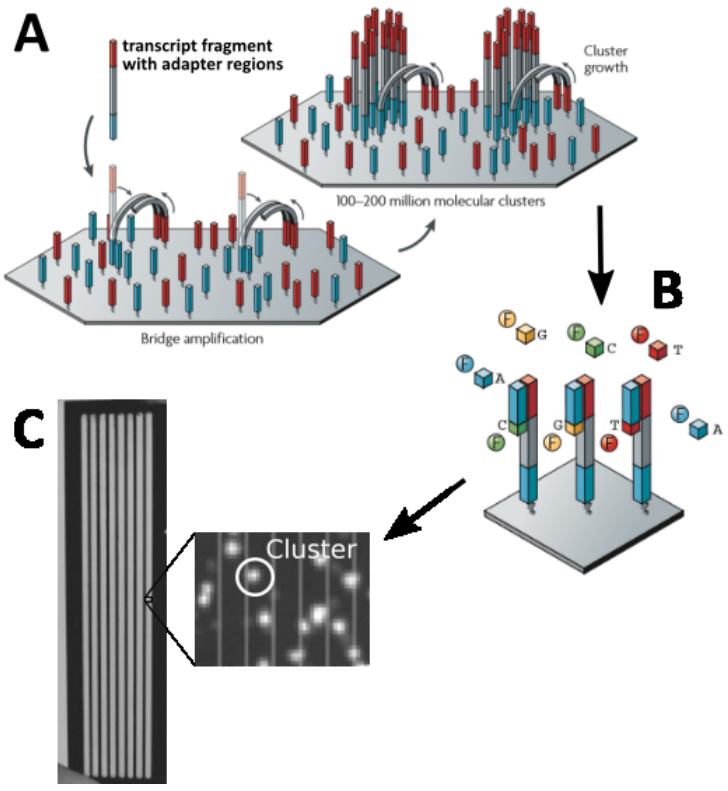

Figure 3. Illumina's sequencing method. In an initial step, the prepared RNA-seq library consisting of the fragmented transcripts containing adapter regions are applied to the flow cell for bridge amplification (A). Following the bridge amplification and cluster formation, the flow cell is flooded with fluorescent-labelled nucleotides (B). Following the binding of the compliment nucleotide, the computer tracks the sequence of each cluster on the flow cell based on the fluorescent color being emitted at a defined wavelength (C). This image was modified from Metzker (2010) and Whiteford et al. (2009).

Furthermore, samples can be sequenced via single- or paired-end reads. In the single-end sequencing mode, the transcript is sequenced only from a single direction, and this mode has the advantage of being cheaper, but still works well for thoroughly annotated organisms (Conesa et al., 2016). The paired-end sequencing mode sequences the transcript from both directions, which aids in the confidence of a sequenced read being aligned to the correct transcript, especially when working with an organism whose transcriptome has not been well annotated (Conesa et al., 2016; Wang et al., 2009).

An additional aspect to take into consideration when undertaking a transcriptome study is the sequencing depth. The depth of sequencing reflects the amount of transcripts in a sample, which are covered and detected during sequencing (Tarazona et al., 2011). Normally, the sequencing depth is dependent on the experimental aim, where more complex aims are encouraged to generate a higher number of sequence reads, i.e. deeper sequencing (Conesa et al., 2016). For example, in order to evaluate alternatively spliced transcripts or wanting to generate data on rare expressed transcripts, the samples must be sequenced deeper (Conesa et al., 2016). However, there is no uniform consensus for an appropriate number of reads required for an adequate biological interpretation of the given experimental set-up (Conesa et al., 2016; Tarazona et al., 2011).

1.4.2. Massive Analysis of cDNA Ends (MACE)

Conventional RNA-seq sequences randomly fragmented transcripts (Figure 4). However, various sequencing techniques exist, one of which is a newly developed sequencing method named MACE. Unlike in the conventional RNA-seq method, MACE sequences transcripts specifically from the 3' transcript end (Figure 4) (Rotter et al., 2017).

Figure 4. Conventional RNA-seq versus MACE sequencing. A higher sequencing depth can be achieved with the MACE sequencing method, due to each sequenced read accounting for a single transcript in the analyzed sample, whereas conventional RNA-seq results in possibly more than one sequenced read of a single transcript. This image was modified from Rotter et al. (2017).

The MACE sequencing method brings many advantages with it. The main advantage in comparison to the conventional RNA-seq method is that the investigated sample set can be sequenced at a deeper level without increased costs or number of reads, due to each read accounting for a single transcript (Rotter et al., 2017). Figure 4 depicts the distribution of reads along a transcript from conventional generated RNA-seq and MACE. During conventional RNA-seq, the transcripts are randomly fragmented and sequenced, which can result in different fragments from a single transcript flowing into the final data quantification, and may result in an overrepresentation of longer transcripts (Rotter et al., 2017). During MACE library preparation the transcripts are also fragmented. However, only the fragments from the 3' transcript end are used as input for sequencing, which results in each sequence read accounting for a single transcript in the sample, thereby eliminating the bias of longer versus shorter transcript expression in a sample (Rotter et al., 2017). Furthermore, MACE is advantageous for studies investigating single nucleotide polymorphisms (SNPs), since SNPs are found to primarily occur in the untranslated region at the 3' end of a transcript, which is covered by MACE (Rotter et al., 2017).

1.5. Aim of this study

Since the CP at the BCSFB was previously observed to be utilized by *S. suis* to gain entry into the CNS, the aim of this study was to evaluate the transcriptional response of human and porcine CP epithelial cells. Furthermore, the response of *in vitro* infected porcine CP cells was compared to the CP from pigs infected with *S. suis* ST2 *in vivo*, which were suffering from meningitis. Especially gaining insight into the *in vivo* aspect is of high interest and value, since the CP transcriptome of pigs suffering from meningitis has never been investigated. From this study, new cellular mechanisms should be elucidated, which take place during the pathogenesis of infection, and will allow further insight into the host's cellular processes and, specifically, the contribution of the CP during a potentially fatal *S. suis* infection of the CNS. For the transcriptome analysis, NGS technology was applied in order to sequence mRNA transcripts from the host cells.

Additionally, two sequencing methods which utilize NGS technology were compared to each other. The CP tissue samples obtained from the porcine *in vivo* infection experiments were subject to sequencing via the conventional RNA-seq method, as well as the MACE sequencing method, both of which were carried out with the Illumina system. Although the same sample analysis should theoretically produce the same results, different sequencing techniques could have the potential of introducing variation, therefore making it subject to investigation as part of this work.

2. Materials

2.1. *Streptococcus suis* (*S. suis*)

2.1.1. *S. suis* strains

S. suis ST2, strain 10, wild type ("H4") and a *S. suis* ST2, strain 10, capsule-deficient mutant ("H5") used in this study were kindly provided by Dr. Maren Seitz from the Institute of Microbiology at the University for Veterinary Medicine Hannover, Germany. These strains were previously characterized in an *in vivo* porcine model, where the H5 strain was characterized to be avirulent (Smith et al., 1999).

2.1.2. *S. suis* cultivation and preservation medium

S. suis H4 and H5 were cultivated in liquid Todd Hewitt Broth (THB; Oxoid, Wesel, Germany) in order to prepare bacteria stocks for long-term storage and infection experiments. Columbia agar plates with sheep blood (Oxoid, Wesel, Germany) were used as solid medium for bacterial cultivation and determining the colony forming units (CFU). The medium for long-term preservation at -80 °C was composed of bacteria suspended in DMEM/F-12 (1x) medium (containing L-Glutamine, 15 mM HEPES, without phenol red; Gibco/Life Technologies™, Paisley, UK) with an optical density at 600 nm (OD_{600}) of 0.65, containing 20 % glycerol (Sigma-Aldrich, Steinheim, Germany).

2.2. Host cells and *in vivo* experiments

2.2.1. Human papilloma choroid plexus epithelial (HIBCPP) cells

In this study, HIBCPP cells were used as a human *in vitro* BCSFB model. These cells were originally isolated from a 29-year-old woman diagnosed with a malignant choroid plexus papilloma, and characterized as a cell line by Ishiwata and colleagues (Ishiwata et al., 2005). They have been described by Schwerk and colleagues to be a suitable *in vitro* BCSFB model due to their nature of forming tight junctions, which in turn resulted in low permeability towards macromolecules and a high transepithelial electrical resistance (TEER) (Schwerk et al., 2012). Furthermore, in concordance of their nature to maintain a homeostatic niche in the CNS, HIBCPP cells have been characterized to possess transporter proteins essential for xenobiotic restriction (Bernd et al., 2015). Additionally, HIBCPP cells exhibit cellular polarity, with the presence of microvilli on the apical cell side (Schwerk et al., 2012). This cellular polarity is a further essential point when utilizing HIBCPP cells for *in vitro* investigations, since the cultivation in a standard model allows for the investigation of cellular responses from the apical epithelial cell side, which *in vivo* would reflect the CSF compartment. In

contrast, an inverted BCSFB model utilizing HIBCPP cells has been established, which allows for the *in vitro* investigation of these cells when applying the substance or subject of interest to the epithelial's basolateral surface, which *in vivo* would reflect the blood side of the barrier (Dinner et al., 2016; Schwerk et al., 2012).

2.2.2. Primary porcine choroid plexus epithelial cells (PCPEC)

The isolation and characterization of primary PCPEC was first described by Gath and colleagues and Haselbach and colleagues (Gath et al., 1997; Haselbach et al., 2001). These primary cells were characterized to have maintained their ability to form tight junctions, exhibited phenotypic polarization with the presence of microvilli on their apical surface, and displayed the ability to secrete fluid from the basolateral to the apical side when they were cultivated *ex vivo* (Gath et al., 1997; Haselbach et al., 2001). These characteristics have made PCPEC ideal for *in vitro* investigations involving the BCSFB. Tenenbaum and colleagues later applied the primary PCPEC in the inverted cell culture BCSFB model, which allows for *in vitro* cellular investigations from the epithelia's basolateral cell side (Tenenbaum et al., 2009).

For each cell batch utilized for an infection experiment in this present work, the CP of freshly slaughtered pigs was collected at the meat-processing center in Mannheim (Fleischversorgungszentrum GmbH Mannheim).

2.2.3. Porcine *in vivo* experiments

The CP tissue samples used for the transcriptome analysis were collected from two independent *in vivo* porcine infection experiments. Both experiments were carried out in collaboration with the research group of Prof. Christoph G. Baums, head of the Institute for Bacteriology and Mycology at the Veterinary Faculty of the University of Leipzig. Additionally, the same pig breed (German Landrace Pig from the Bundes Hybrid Zucht Programm (BHZP) GmbH, Dahlenburg-Ellringen, Germany, Line 01), which were approximately 8 weeks old, was used in both animal experiments.

The *in vivo* porcine infection experiment, from which our "meningitis-free" samples were obtained, was carried out at the Institute for Bacteriology and Mycology at the Veterinary Faculty of the University of Leipzig. The animals from which the samples were obtained were part of a published study performed by Rieckmann and colleagues (Rieckmann et al., 2018).

The *in vivo* porcine infection experiment, from which our "meningitis" samples were obtained, was carried out at an animal experiment facility at the Veterinary University of Hannover. The animals from which the samples were obtained were part of the published study carried out by Rungelrath and colleagues (Rungelrath et al., 2018).

2.3. Cell media, their composition and constituents required for cell culture maintenance

All incubation and cell maintenance steps took place in a humidified incubator (Thermo Fisher Scientific, Dreieich, Germany) at 37 °C and 5 % CO_2, unless otherwise noted.

2.3.1. HIBCPP cells

HIBCPP cells were cultivated on ThinCert™ cell culture filter membranes, with a 3 µm pore diameter, in the inverted BCSFB model and maintained as previously described by Schwerk and colleagues (Schwerk et al., 2012). Table 1 summarizes the cell medium composition required for HIBCPP cell cultivation, infection experiments, and long-term storage.

In addition, Trypsin-EDTA (0.25 %; Gibco/Life Technologies, Paisley, Germany) was used to detach cells from the cell culture flask and trypan blue solution (Sigma-Aldrich, Steinheim, Germany) was used diluted at a ratio of 1:10 with the HIBCPP cell suspension, in order to determine cell density.

Table 1. HIBCPP cell medium required for cell cultivation and long-term storage.

10 % HIBCPP cell cultivation medium composition	Final concentration	Manufacturer
DMEM/F-12 (1x) with L-Glutamine, 15 mM HEPES, and phenol red		Gibco/Life Technologies™, Paisley, UK
Fetal calf serum (FCS)	10 % (v/v)	Gibco/Life Technologies™, Paisley, UK
Penicillin/Streptomycin (5000 U ml^{-1})	100 U/ml/ 100 µg/ml	Gibco/Life Technologies™, Paisley, UK
Human recombinant insulin solution (10 mg ml^{-1})	0.05 % (v/v)	Sigma-Aldrich, Steinheim, Germany
1 % HIBCPP infection medium composition		
DMEM/F-12 (1x) with L-Glutamine, 15 mM HEPES, without phenol red		Gibco/Life Technologies™, Paisley, UK
FCS	1 % (v/v)	Gibco/Life Technologies™, Paisley, UK
Human recombinant insulin solution	0.05 % (v/v)	Sigma-Aldrich, Steinheim, Germany
Long-term storage medium composition		
HIBCPP cells suspended in 10 % HIBCPP cell culture medium	70 % (v/v)	See above
FCS	20 % (v/v)	Gibco/Life Technologies™, Paisley, UK
DMSO (dimethylsulfoxide)	10 % (v/v)	Sigma-Aldrich, Steinheim, Germany

2.3.2. Primary PCPEC

Primary PCPEC were cultivated on ThinCert™ cell culture filter membranes, with a 3 µm pore diameter, in the inverted BCSFB model and were cultivated and maintained as previously described (Tenenbaum et al., 2009).

Mouse laminin (50 µg ml^{-1}; Becton, Dickinson & Co., Franklin Lakes, NJ, USA), which is an important glycoprotein part of the basement membrane, was used to facilitate epithelial adherence to the cell culture filter membrane.

Table 2 summarizes the media and individual medium components required for the primary PCPEC isolation and maintenance.

Table 2. Media composition for the cultivation of primary porcine choroid plexus epithelial cells.

	Final concentration	Manufacturer
1. For meat-processing center		
HBSS with Ca^{2+} and Mg^{2+}		Gibco/Life Technologies™, Paisley, UK
HEPES Buffer (1 M)	2 % (v/v)	Lonza, Basel, Switzerland
Penicillin-Streptomycin (P/S; 5000 U ml^{-1})	2.4 % (v/v)	Gibco/Life Technologies™, Paisley, UK
2. For meat-processing center		
DMEM/F-12 (1x) with L-Glutamine, 15 mM HEPES, and phenol red		Gibco/Life Technologies™, Paisley, UK
P/S	2 % (v/v)	Gibco/Life Technologies™, Paisley, UK
3. For washing the CP after collection ("wash medium")		
HBSS without Ca^{2+} and Mg^{2+}		Gibco/Life Technologies™, Paisley, UK
HEPES Buffer (1 M)	2 % (v/v)	Lonza, Basel, Switzerland
P/S	2.4 % (v/v)	Gibco/Life Technologies™, Paisley, UK
4. Medium for trypsin treatment ("trypsin medium")		
HBSS without Ca^{2+} and Mg^{2+}		Gibco/Life Technologies™, Paisley, UK
P/S	2.4 % (v/v)	Gibco/Life Technologies™, Paisley, UK
Trypsin	0.2 % (w/v)	Belger Biochemie, Kleinmachnow, Germany
5. Medium for seeding cells ("AraC medium")		
DMEM (1x) with GlutaMAX™ with 4.5 g L^{-1} D-Glucose, pyruvate, and phenol red		Gibco/Life Technologies™, Paisley, UK
Fetal calf serum (FCS)	10 % (v/v)	Gibco/Life Technologies™, Paisley, UK
P/S	2 % (v/v)	Gibco/Life Technologies™, Paisley, UK
Human recombinant insulin solution	0.05 % (v/v)	Sigma-Aldrich, Steinheim, Germany
Cytosine Arabinoside (AraC; 40 mg)	20 µM	Cell Pharm GmbH, Hannover, Germany
6. Cell-cultivation medium without AraC ("AraC-free medium")		
As described for "5. AraC medium", but without AraC		
7. Serum-free medium ("SFM – with P/S")		
DMEM (1x) with GlutaMAX™ with 4.5 g/L D-Glucose and without phenol red		Gibco/Life Technologies™, Paisley, UK
P/S	2 % (v/v)	Gibco/Life Technologies™, Paisley, UK
HEPES Buffer (1 M)	2.4 % (v/v)	Lonza, Basel, Switzerland
L-Glutamine (200 mM)	2 % (v/v)	Invitrogen, Carlsbad, CA, USA
Sodium Pyruvate (100 mM)	1.2 % (v/v)	Invitrogen, Carlsbad, CA, USA
Human recombinant insulin solution	0.05 % (v/v)	Sigma-Aldrich, Steinheim, Germany
8. Serum-free medium for infection experiment ("PCPEC infection medium")		
As described for "7. SFM – with P/S", but without P/S		

2.4. Oligonucleotide primers and DNA Size Ladder

The oligonucleotide primers were designed with the help of Primer3 software (Rozen and Skaletsky, 2000), were synthesized by Sigma-Aldrich (Steinheim, Germany), and delivered in lypophilic form. The oligonucleotide primers were reconstituted with double-distilled H_2O (Gibco/Life Technologies™, Paisley, UK), to a concentration of 100 pmol μl^{-1}, as recommended by the manufacturer. Furthermore, the primers were designed to overlap the exon-exon regions of a gene, therefore yielding PCR products of mature mRNA transcripts.

For evaluating the reverse transcriptase polymerase chain reaction (RT-PCR) products during the agarose gel electrophoresis, the GeneRuler 100 bp DNA Ladder (Thermo Fisher Scientific, Dreieich, Germany) was run along with the samples as an amplicon size indicator.

Table 3 summarizes the oligonucleotides used to perform the semi-quantitative RT-PCR.

Table 3. Oligonucleotide primers used for the RT-PCR.

Gene	Oligonucleotide primer for RT-PCR	Annealing Temp. (°C)	Amplicon size (bp)	Reference
Human				
gapdh	Forward 5'-TGTTGCCATCAATGACCCCTT-3' Reverse 5'-CTCCACGACGTACTCAGCG-3'	60	202	Borkowski et al. (2014)
nfkbiz	Forward 5'-CAGTTCAAGTTAGCTGGCTGA-3' Reverse 5'-TCTGTGGAGAATACTGGTACAGG-3'	60	177	Borkowski et al. (2014)
il8	Forward 5'-CAAGAGCCAGGAAGAAACCA-3' Reverse 5'-GTCCACTCTCAATCACTCTCAG-3'	60	225	Borkowski et al. (2014)
tnf-α	Forward 5'-GAGCACTGAAAGCATGATCC-3' Reverse 5'-CGAGAAGATGATCTGACTGCC-3'	60	234	Borkowski et al. (2014)
cxcl1	Forward 5'-CTCTTCCGCTCCTCTCACAG-3' Reverse 5'-GGGGACTTCACGTTCACACT-3'	60	239	van Sorge et al. (2008)
cxcl2	Forward 5'-CTCAAGAATGGGCAGAAAGC-3' Reverse 5'-AAACACATTAGGCGCAATCC-3'	60	213	van Sorge et al. (2008)
Porcine				
gapdh	Forward 5'-CAGCCTCAAGATCATCAGCA-3' Reverse 5'-TCCAGGGGCTCTTACTCCTT-3'	55	594	Tenenbaum et al. (2008)
il8	Forward 5'-GATGCCAACACAACTTCAATCA-3' Reverse 5'-GCCAAAACAGGATTTCCAGC-3'	60	221	This study
il1ß	Forward 5'-ATGCCAACGTGCAGTCTATG-3' Reverse 5'-GAAGACGGGCTTTTGTTCTG-3'	55	400	This study
cxcl2	Forward 5'-ACTGCTCTTGTTTAGCATCTTCTC-3' Reverse 5'-TGACCAAACGGAAGTCATAGC-3'	55	109	This study
Bacteria – *S. suis*				
ORF E&F of capsule	Forward 5'-ATTGGAGATATGAGTCTAGTCGGTA-3' Reverse 5'-CATGACCGTCTGGGTTTACG-3'	60	695	This study & Lakkitjaroen et al. (2011)

bp, base pairs; *cxcl*, (C-X-C motif) ligand; *gapdh*, glyceraldehyde-3-phosphate dehydrogenase; *il*, interleukin; *nfkbiz*, NF-kappa-B inhibitor zeta; ORF, open reading frame; *tnf-α*, tumor necrosis factor alpha

Table 4 summarizes the oligonucleotides utilized for the quantitative PCR (qPCR) in order to verify single genes from the RNA-seq data.

The human oligonucleotide primers used for the qPCR, which encode for the genes *gapdh*, *tnfα*, *il8*, and *cxcl2*, and the porcine oligonucleotide primers used for the qPCR, which encode for the genes *il8* and *cxcl2*, were the same primers as described in Table 3.

Table 4. Oligonucleotide primers used for the qPCR.

Gene	Oligonucleotide primer for qPCR	Annealing Temp. (°C)	Amplicon size (bp)	Reference
Human				
il1β	Forward 5'-AGCTACGAATCTCCGACCAC-3' Reverse 5'-CGTTATCCCATGTGTCGAAGAA-3'	60 °C	186	This study
zc3h12a	Forward 5'-GGCAGTGAACTGGTTTCTGGA-3' Reverse 5'-GATCCCGTCAGACTCGTAGG-3'	60 °C	232	Borkowski et al. (2014)
tcim	Forward 5'-AGAAGAGCCTGGACAGATGT-3' Reverse 5'-TTTTCTCTCCCTGTCCTCCC-3'	58 °C	175	This study
nfkbia	Forward 5'-CTCCGAGACTTTCGAGGAAATAC-3' Reverse 5'-GCCATTGTAGTTGGTAGCCTTCA-3'	60 °C	135	This study
hif1α	Forward 5'-GAACCCATTCCTCACCCATC-3' Reverse 5'-GCATCCTGTACTGTCCTGTG-3'	58 °C	250	This study
vegfa	Forward 5'-TCTTCAAGCCATCCTGTGTG-3' Reverse 5'-CCCTTTCCCTTTCCTCGAAC-3'	58 °C	235	This study
mxi1	Forward 5'-CTCTCTTCCTCACAGTCCCA-3' Reverse 5'-CAGGGGTAAGGTCTCCAAGA-3'	58 °C	194	This study
dusp2	Forward 5'-ATCTTGCCCTACCTGTTCCT-3' Reverse 5'-GCTGTTCTTCACCCAGTCAA-3'	58 °C	222	This study
Porcine				
gapdh	Forward 5'-TGGTGCTACGTATGTTGTGG-3' Reverse 5'-ATTGCTGACGATCTTGAGGG-3'	58 °C	177	This study
tnfα	Forward 5'-ACGTTTTCCTCACTCACACC-3' Reverse 5'-TCGATCATCCTTCTCCAGCT-3'	58 °C	176	This study
il1β	Forward 5'-GAGTGCAAACTCCAGGACAA-3' Reverse 5'-GGTGGGCGTGTTATCTTTCA-3'	58 °C	218	This study
zc3h12a	Forward 5'-CTGTAGGATTGGTTCTGGCC-3' Reverse 5'-CGAGAGAAAGGAGGGTTTGG-3'	58 °C	156	This study
tcim	Forward 5'-CCGATCAACTTCACGTCTGT-3' Reverse 5'-CTGCAATTCTTCTCCAGCCT-3'	58 °C	181	This study
nfkbia	Forward 5'-TGTCGCTCTTGTTGAAGTGT-3' Reverse 5'-TCTGTGAACTCTGACTCCGT-3'	58 °C	193	This study
hif1α	Forward 5'-TGTAATGCTCCCCTCATCCA-3' Reverse 5'-GGCTGATCTTGAATCTGGGG-3'	58 °C	198	This study
vegfa	Forward 5'-CGAGTACATCTTCAAGCCGT-3' Reverse 5'- CATCTCTCCTATGTGCTGGC-3'	58 °C	154	This study
mxi1	Forward 5'- GCAGAGTATTGGGAGTGACG-3' Reverse 5'-GAGACTGCAACATGAACCCA-3'	58 °C	155	This study
dusp2	Forward 5'-CAGATGGTGGAGATCAGTGC-3' Reverse 5'-CTGCCCCATGAAACTGAAGT-3'	58 °C	228	This study

dusp2, dual specificity phosphatase 2; *hif1α*, hypoxia-inducible factor 1 alpaha; *mxi*, MAX interactor 1; *nfkbia*, NFαB inhibitor alpha; *tcim*, transcriptional and immune response regulator; *vegfα*, vascular endothelial growth factor alpha; *zc3h12a*, zinc finger CCCH-type containing 12A

2.5. RNA-seq

RNA-seq was carried out in collaboration in the Biochip Laboratory of PD Dr. Ludger Klein-Hitpass, at the University Hospital in Essen, Germany.

In order to prepare the RNA library for conventional RNA-seq of the HIBCPP cells, the Ovation Human FFPE RNA-Seq Multiplex System Kit (NuGen, Illumina, San Diego, CA, USA) was used. For the PCPEC and the porcine CP tissue from the *in vivo* infection experiments, the Universal Plus mRNA-Seq kit (NuGen, Illumina, San Diego, CA, USA) was used for the RNA library preparation. Furthermore, a second RNA library was prepared using the RNA from the CP tissue samples obtained from the *in vivo* porcine infection experiments with the MACE Library Preparation Kit (6x) for Mi-Seq (Illumina), Single End Sequencing, (GenXPro, Frankfurt am Main, Germany). The latter RNA library was prepared in order to explore an alternative RNA-seq method called MACE.

The sequencing of the pooled HIBCPP cell sample set library was performed using HiSeq 2500 flow cell system (Illumina®, San Diego, CA, USA) in the high-output and paired-end mode. The sequencing of the pooled RNA libraries of the PCPEC samples and the *in vivo* CP samples was carried out on the HiSeq 2500 flow cell system (Illumina®, San Diego, CA, USA) in the rapid-run and paired-end mode. Lastly, the RNA library, also generated from the *in vivo* CP samples, for MACE was sequenced using the MiSeq v3 flow cell system (Illumina®, San Diego, CA, USA) in the single-end mode.

2.6. Laboratory Equipment

The following laboratory equipment was utilized to carry out the work in this thesis.

Description and Model	Manufacturer
Agilent 2100 Bioanalyzer	Agilent Technologies, Waldbronn, Germany
Analog Vortex Mixer	VWR, Darmstadt, Germany
Autoclave 5075 ELV	Systec, Linden, Germany
Cell culture/CO_2 incubator Hera Cell 240	Thermo Fisher Scientific, Dreieich, Germany
Centrifuge – Micro 200R with 242A Rotor	Hettich, Kirchlengern, Germany
Centrifuge – Rotana 460R with Rotor 5624	Hettich, Kirchlengern, Germany
Centrifuge – Picofuge® II Microfuge	Stratagene, San Diego, CA, USA
Clean Bench Hera Save	Thermo Fisher Scientific, Dreieich, Germany
Geldocumentation Biovision-3026WL/26MX	Vilber Lourmat, Eberhardzell, Germany
Hemocytometer (Neubauer Chamber); 0.1 mm depth; 0.0025 mm^2	NeoLab, Heidelberg, Germany
HiSeq 2500 Sequencing System	Illumina®, San Diego, CA, USA
Light microscope Axiovert 40C	Zeiss, Oberkochen, Germany
Magnetic Stand – 96	Thermo Fisher Scientific, Dreieich, Germany
Micro pestle	Eppendorf, Hamburg, Germany
MiSeq Benchtop Sequencer	Illumina®, San Diego, CA, USA
Multiwell plate Reader Infinite M200	Tecan, Männedorf, Germany
Pipetboy Comfort	IBS Integra Biosciences, Zizers, Switzerland
Pipette Reference (10 µl / 2.5 µl)	Eppendorf, Hamburg, Germany
Pipette Research (1000 / 200 / 100 / 20 µl)	Eppendorf, Hamburg, Germany
Qubit® 2.0 Fluorometer	Thermo Fisher Scientific, Dreieich, Germany
S220 Focused-ultrasonicator with Adaptive Focused Acoustics®	Covaris®, Woburn, MA, USA
Spectrophotometer NanoDrop® ND1000	Peqlab, Erlangen, Germany
Spectrophotometer WPA Biowave Co 8000	Biochrom, Berlin, Germany
Thermocycler 2720	Applied Biosystems, Waltham, MA, USA
Thermomixer compact	Eppendorf, Hamburg, Germany
Voltohmmeter Millicell® -ERS	Millipore, Billerica, MA, USA
Voltohmmeter-Electrode MERSSTX 01	Millipore, Billerica, MA, USA
Waterbath SW22	Julabo, Seelbach, Germany

2.7. Chemicals and Buffers

The following chemicals and buffers (and their composition) were used in this study. For the preparation buffers, media, and agarose gels, water from the MilliQ® ultrapure water filtering system was used (Millipore; Billerica, MA, USA).

Description	Composition	Manufacturer
Dimethylsulfoxide (DMSO)		Sigma-Aldrich, Steinheim, Germany
TAE Buffer (1x)	40 mM Tris	Carl Roth, Karlsruhe, Germany
	20 mM Acetic acid	Merck, Darmstadt, Germany
	1 mM EDTA pH 0.3	Carl Roth, Karlsruhe, Germany
RLT Lysis Buffer	RLT-Lysis Buffer	Qiagen, Hilden, Germany
	10 mM ß-mercaptoethanol	Sigma-Aldrich, Steinheim, Germany
Agarose NEEO Ultra Quality		Carl Roth, Karlsruhe, Germany
Ethidium Bromide		AppliChem, Darmstadt, Germany
Ethanol (absolute 99.9 %)		Mallinckrodt, Baker, Devender, Netherlands
Dulbecco's phosphate buffered solution (DPBS) with Ca^{2+} and Mg^{2+}		Gibco/Life Technologies, Paisley, UK
DPBS without Ca^{2+} & Mg^{2+}		Gibco/Life Technologies, Paisley, UK

2.8. Consumables

The following consumables were used to carry out this project.

Description	Manufacturer
Mx3000P Optical Strip Caps	Agilent Technologies, Waldbronn, Germany
Mx3000P Strip Tubes	Agilent Technologies, Waldbronn, Germany
Agilent Bioanalyzer HS DNA chip	Agilent Technologies, Waldbronn, Germany
Agilent Bioanalyzer RNA Nano chip	Agilent Technologies, Waldbronn, Germany
qPCR 96-well non-skirted plate	Agilent Technologies, Waldbronn, Germany
Agencourt AMPure XP SPRI Beads	Beckman Coulter Life Sciences, Brea, CA, USA
Serological Pipette (5 ml/10 ml/25 ml)	Becton, Dickinson & Co., Franklin Lakes, NJ, USA
Covaris microTUBE	Covaris®, Woburn, MA, USA
Safe-lock Centrifuge Tubes (0.5 ml/1.5 ml/2ml)	Eppendorf, Hamburg, Germany
96-well plate, black and uncoated	Nunc, Roskilde, Denmark
Cryo.s™, cryogenic vial with screw cap, PP, 1 ml	Greiner Bio-One, Frickenhausen, Germany
Conical Tubes (15 ml / 50 ml)	Greiner Bio-One, Frickenhausen, Germany
Cuvette	Greiner Bio-One, Frickenhausen, Germany
ThinCert™ Cell Culture Filter Membrane for 24-well plates; 3 µm pore diameter, 2 x 10^6 pores	Greiner Bio-One, Frickenhausen, Germany
Tissue Culture flask, 75 cm^2, 250 ml, PS, red filter	Greiner Bio-One, Frickenhausen, Germany
6-well Cell Culture Plate	Starlab, Hamburg, Germany
12-well Cell culture Plate	Starlab, Hamburg, Germany
24-well Cell Culture Plate	Starlab, Hamburg, Germany
TipOne® (100 µl / 200 µl / 1000 µl XL) Graduated Filter Tip (sterile)	Starlab, Hamburg, Germany
TipOne® 10 µl XL Graduated Filter Tip Max. Vol. 20 µl (sterile)	Starlab, Hamburg, Germany
TipOne® RPT (100 µl / 200 µl / 1000 µl XL) Graduated Filter Tip (sterile)	Starlab, Hamburg, Germany
TipOne® RPT 10 µl XL Graduated Filter Tip Max. Vol. 20 µl (sterile)	Starlab, Hamburg, Germany

2.9. Kits

The following kits were used to carry out parts of this project.

Kit	Manufacturer
AffinityScript QPCR cDNA Synthesis Kit	Agilent Technologies, Waldbronn, Germany
Brilliant II SYBR® Green QPCR Master Mix	Agilent Technologies, Waldbronn, Germany
MACE Library Preparation Kit (6x) for Mi-Seq (Illumina), Single End Sequencing	GenXPro, Frankfurt am Main, Germany
LIVE/DEAD Viability/Cytotoxicity Kit for mammalian cells	Molecular Probes, Eugene, Oregon, USA
NEBNext® Library Quant Kit for Illumina®	New England Biolabs Inc., Ipswich, MA, USA
Ovation Human FFPE RNA-Seq Multiplex System Kit	NuGen, Illumina, San Diego, CA, USA
Universal Plus mRNA-Seq	NuGen, Illumina, San Diego, CA, USA
QIAShredder	Qiagen, Hilden, Germany
QIAquick PCR Purification kit, up to 10 µg PCR products; 100 bp to 10 kbp	Qiagen, Hilden, Germany
RNase-free DNase Set	Qiagen, Hilden, Germany
RNeasy Micro Kit	Qiagen, Hilden, Germany
RNeasy Mini Kit	Qiagen, Hilden, Germany
Taq DNA Polymerase Kit (1000 U)	Qiagen, Hilden, Germany
Qubit™ double stranded DNA high sensitivity assay	Thermo Fisher Scientific, Dreieich, Germany

2.10. Software

The following software programs were utilized in order to acquire data presented in this study.

Differing versions of the Molecular Signature Database (MSigDB) were used due to the extended time frame in between sequencing analysis of the different samples.

Software	Developer
MXPro	Agilent Technologies, Waldbronn, Germany
Trimmomatic-0.30	Bolger et al. (2014)
Spliced Transcripts Alignment to a Reference (STAR) RNA aligner	Dobin et al. (2013)
InkScape version 0.92	General Public License Version 2
CASAVA 1.8.2	Illumina®, San Diego, CA, USA
Illumina® Sequencing Analysis Viewer (SAV)	Illumina®, San Diego, CA, USA
Partek Genomics Suite	Partek Inc., St. Louis, MO, USA
Integrative Genomics Viewer (IGV)	Robinson et al. (2011)
Primer3	Rozen and Skaletsky (2000)
StrandNGS	Strand Life Sciences Pvt. Ltd., Bangalore, India
i-control™	Tecan, Männedorf, Switzerland
Vision-Capt	Vilber Lourmat, Eberhardzell, Germany
Zeiss ZEN Imaging Software	Zeiss, Oberkochen, Germany
Gene Set Enrichment Analysis (GSEA) V 2.0.14	Mootha et al. (2003); Subramanian et al. (2005)

• MSigDB
  ○ HIBCPP: Version 5.2
  ○ PCPEC and *in vivo* CP: Version 6.1
	Liberzon et al. (2015); Liberzon et al. (2011); Subramanian et al. (2005)

3. Methods

3.1. *S. suis*

3.1.1. Bacteria cultivation and preparation for *in vitro* infection experiments

In order to cultivate bacteria for the infection experiments, an aliquot of the *S. suis* strain long-term storage stock (from – 80°C) was added to 10 ml Todd Hewitt Broth (THB) in a 15 ml conical tube. The lid of the test tube was kept loose and the test tube was placed at an angle in the water bath, where the bacteria were incubated at 37 °C for 6 h, where the bacteria were grown to mid-log phase. Following the incubation, the bacterial culture was washed twice. First, the bacterial cell suspension was centrifuged at 2680 x g for 10 min. The supernatant was discarded and the bacteria pellet was re-suspend in 10 ml on the respective HIBCPP cell or PCPEC infection medium (see Table 1 and Table 2). The centrifugation step was repeated and the supernatant was discarded before the bacterial pellet was re-suspended in 1 ml medium used during the infection experiment (see above). A 1:10 dilution of the bacteria suspension was made, and the OD_{600}, using a photometer, was determined. The bacterial cell suspension was then adjusted to an OD_{600} of 0.65, which resulted in approximately $2x10^8$ CFU ml^{-1}. Again, the bacterial cell density was adjusted in the respective HIBCPP cell or PCPEC infection medium. The bacterial cell suspension adjusted to an OD_{600} of 0.65 will be referred to as the inoculum.

In order to determine the bacterial CFU, which was used for infection of host cells *in vitro*, as well as the CSF throughout the infection time points, the inoculum and an amount, which equaled a multiplicity of infection (MOI) 10, was serial diluted up to 10^6, and 10 µl of the last 3 dilutions were plated in duplicate onto Colombia sheep blood agar plates. The sheep blood agar plates were incubated inverted in a humidified incubator at 37 °C and 5 % CO_2 overnight, and the CFU were counted the following day.

3.1.2. Strain-confirmation PCR

The bacteria primers listed in Table 3 were used in order to confirm the strain containing the open reading frames (ORFs) E and F in the *S. suis* wildtype (H4) and to assure the absence of the bacterial capsule (H5).

S. suis was prepared as described above (section 3.1.1) by being cultivated in THB, washed twice with DPBS (with Ca^{2+} and Mg^{2+}), and the OD_{600} was adjusted to 0.65. The bacterial inoculum was incubated

at 99°C for 10 min in order to lyse the bacterial cell membranes and to release the genomic content into the suspension.

The composition of the PCR reaction mixture is summarized in Table 7 and the PCR program is described in Table 8 was set. The cDNA synthesis step was not performed preceding the PCR, since the bacterial cell lysis released its DNA.

Figure 5 depicts the positive confirmation of the presence of the bacterial cell wall in the *S. suis* ST2 wildtype (H4) strain. The PCR product is indicative of the presence of the bacterial ORFs E and F, which is expressed by the gene *cpsE* and *cpsF*. Smith and colleagues previously described that the ORFs E and F are essential in order for the proper formation of the bacterial capsule (Smith et al., 1999). In contrast, the absence of a PCR product for the non-encapsulated H5 *S. suis* ST2 strain confirms the deletion of ORFs E and F.

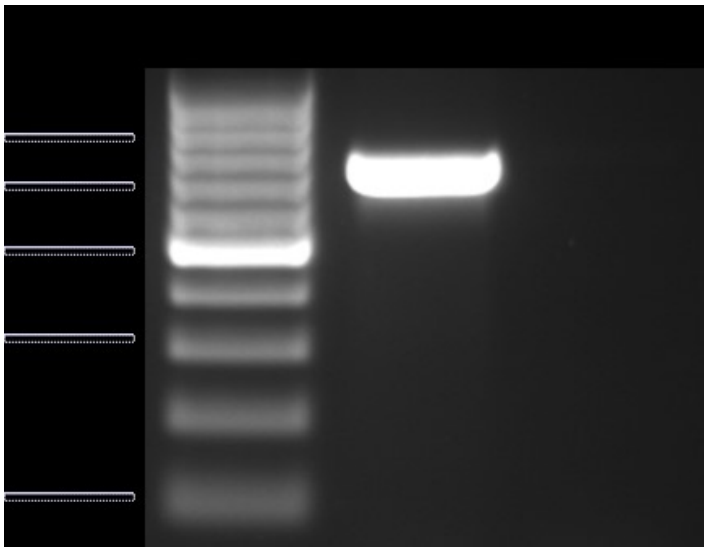

Figure 5. *S. suis* ST2 strain 10 bacterial capsule verification via PCR. A size marker ranging from 100 to 1000 base pairs (bp) is indicated on the left. The band at approximately 700 bp for the H4 strain is indicative for the genes encoding for the bacterial cell well formation. The absence of a product band for the H5 strain confirms the absence of the bacterial capsule on a transcriptome level. The PCR products were run on a 1.5 % agarose gel at 120 V for 40 min and the image was captured using the VisionCapt software.

3.1.3. Long term storage

The *S. suis* strains were cultivated and washed twice with DPBS (with Ca^{2+} and Mg^{2+}) as described above (3.1.1). Subsequently to the second DPBS wash, the OD_{600} of the bacterial cell suspension was adjusted to 0.65 in DMEM/F-12 medium containing 20 % glycerol. The bacterial suspension was aliquoted into cryo tubes and stored at -80 °C.

3.2. Cell culture

3.2.1. HIBCPP cell cultivation

3.2.1.1. Splitting and seeding the cells onto ThinCert™ cell culture filter membranes

To split the HIBCPP cells from a T75 cell culture flask, the cells were rinsed twice with 10 ml DPBS (without Ca^{2+} and Mg^{2+}) in order to remove free Ca^{2+} and Mg^{2+} ions, which can prevent the proper enzymatic activity of 0.25 % Trypsin-EDTA, which was subsequently added. The cells were incubated with trypsin-EDTA for up to 20 min at 37 °C in order to detach them from the cell culture flask. To stop the trypsin digestion, 1 volume of the 10 % HIBCPP cell medium was added.

The cell suspension was transferred to a 50 ml conical tube and a 1:2 dilution was made with trypan blue in order to count the cells. Trypan blue is an azo dye, which is taken up by dead or dying cells and thereby stains them blue due to their permeable membranes; living cells remain unstained. The diluted cell suspension was counted while the HIBCPP cell suspension was centrifuged at 55 x g for 10 min at room temperature. Following the centrifugation, the supernatant was discarded and the cell density was adjusted to 1 x 10^6 cells ml^{-1}.

The cells were cultivated as previously described by Schwerk and colleagues in the inverted cell culture method of the human *in vitro* BCSFB model (Schwerk et al., 2012), with some modifications. For this, 24-well cell culture membrane filters, with a pore diameter of 3 µm, were placed inverted into a 12-well cell culture plate, thereby exposing the basolateral filter side upwards. Pre-warmed 10 % FCS HIBCPP cell culture medium was used to fill the well along with the inverted apical filter side, before the HIBCPP cell suspension was applied to the basolateral side of the filter membrane. A maximum of 100,000 cells were seeded per cell culture filter insert, which, when confluent, resulted in approximately 400,000 cells per filter. As a general rule, for HIBCPP with a lower cell passage number, fewer cells were seeded onto the filter membrane. HIBCPP cells up to passage 38 were used for experiments, since these exhibited the most continuity based on previous experiences in the laboratory.

One day after the cells were seeded onto the basolateral cell culture filter membrane side, the filter membranes were flipped, and placed hanging into a 24-well cell culture plate. The cells were supplied with 10 % FCS HIBCPP cell culture medium – 1 ml medium on the apical cell side (well) and 500 µl on the basolateral cell side (inside the filter compartment). Cell culture medium was exchanged every second day.

Approximately three to four days post-seeding, the barrier-forming property (TEER) of the HIBCPP cells was monitored via a voltohmmeter (section 3.3.1.1.1). Once the HIBCPP cells reached a TEER of at least 70 Ω x cm^2, they were transferred to 1 % HIBCPP cell medium. The exposure to serum-starvation induced the formation of a higher TEER usually by the following day, a phenomenon previously observed during the cultivation of PCPEC (Gath et al., 1997). It has been suggested, that FCS inhibits proper tight junction formation, but also an improved cell polarity *in vitro*, likely due to serum-containing growth factors (Chang et al., 1997; Hakvoort et al., 1998). Confluent HIBCPP cell filters with a TEER of at least 240 Ω x cm^2 and a maximum of 740 Ω x cm^2 were used in the infection experiments.

3.2.1.2. Long-term storage

The HIBCPP cells were treated with trypsin and washed twice as described above (3.2.1.1). Subsequently to the final wash, the HIBCPP cells were suspended in medium composed of 70 % of the 10 % FCS HIBCPP cell medium (Table 1), 20 % (v/v) FCS, and 10 % (v/v) DMSO.

The cells were slowly cooled in increments by starting with placing them on ice, storage at – 20 °C for a few hours, then being placed in – 80 °C overnight, followed by the transfer into liquid nitrogen the following day.

3.2.2. PCPEC: collection, isolation, and maintenance

The day before the CP were collected at the meat-processing center of Mannheim (Fleischversorgungszentrum Mannheim GmbH), the basolateral side of the 24-well ThinCert™ cell culture filter membranes (3 µm pore diameter; pore density of 2 x 10^6 pores cm^{-1}) was coated with 5 µg $cm^{2\ -1}$ mouse laminin (50 µg/ml stock; Becton, Dickinson & Co., Franklin Lakes, NJ, USA). The laminin-coated filters were left to dry overnight.

All the cell culture media and their components, utilized for the CP collection, primary CP epithelial cell selection, and cell cultivation, are summarized in Table 2.

The following day, the CP was collected from the lateral ventricle from freshly slaughtered pigs at the meat-processing center. Upon the removal from the carcass, the CP was immediately placed into medium 1 “for the meat-processing center”. Before leaving the facility, the collected CP were transferred to medium 2 “for the meat-processing center” (Table 2).

The collected CP were subsequently processed in an aseptic setting under laboratory conditions. In the first step, the CP tissue was transferred to pre-warmed “wash medium” in a petri dish. In order to remove excess blood and wash the CP, the thin end of the CP was held with sterile tweezers while the thick end of the CP was cut off with dissection scissors. Subsequently, the CP was pulled across the edge of the petri dish. This process was repeated until the CP had a light pink-white appearance.

In order to remove the CP epithelial cells from the CP tissue strands, the “trypsin medium” was freshly prepared. 11 washed and bled-out CP strands were added to the trypsin medium and incubated for 45 min at 4 °C. This was followed by a 17 min incubation step in a 37 °C water bath with slight agitation. In order to stop the trypsin digestion, one volume of pre-warmed FCS was added to the 20 ml CP-trypsin solution. The CP strands were further agitated using a serological pipette, in order to remove remaining CP epithelial cells from the stroma, and subsequently discarded.

The cell suspension was transferred to a 50 ml conical tube and centrifuged for 10 min at 55 x g at room temperature. Following centrifugation, the supernatant was removed, including the red blood cells, layered on top of the white cell pellet. The pellet was suspended in a total of 10 ml “AraC medium”, before 100 µl of the cell suspension was applied to the laminin pre-coated basolateral ThinCert™ cell culture filter membrane side, which contained pre-warmed AraC medium on the apical side.

In addition to seeding the cells onto the cell culture filter membranes, PCPEC were also seeded in a 6-well cell culture plate, in duplicate, in order to monitor cell adherence and potential fibroblast contamination. For this, 1 ml of the PCPEC cell suspension was added to 2 ml AraC medium. These cells were supplied with the same cell medium as the cells cultivated on the cell culture filter membranes, and were discarded once the PCPEC developed a TEER high enough to be used in infection experiments.

One day after the cells were seeded, the filters were washed once by flipping and hanging the cell culture filter membranes into a 24-well cell culture plate containing pre-warmed DPBS (containing Ca^{2+} and Mg^{2+}) in order to remove non-adherent cells. The AraC medium from the 12-well cell culture plate, in which the PCPEC were seeded in the day before, was transferred to a new 24-well cell culture plate, to which the filters were transferred to after the DPBS wash.

The PCPEC were left undisturbed until day 4 post-seeding. After 4 days in AraC medium, the cell medium was changed every 2 days using “AraC-free” medium. Starting 6 days post-seeding, the TEER development was monitored with a voltohmmeter (section 3.3.1.1.1). Once the TEER reached approximately 100 Ω x cm^2, the cells were transferred to SFM – with P/S.

Once a TEER of approximately 170 Ω x cm^2 was reached, the cells were cultivated in SFM – without P/S. A confluent primary PCPEC layer on the 24-well cell culture filter membrane consisted of approximately 60,000 cells.

3.3. Sample generation: infection experiments

Transcriptome analysis was carried out on samples obtained from three different sources. The first sample set was generated by infecting immortal HIBCPP cells in the established human *in vitro* model of the BCSFB. The second sample set was generated by infecting *ex vivo* cultivated primary PCPEC cells in a porcine *in vitro* BCSFB model. The third sample set was obtained by isolating the CP from piglets, which were experimentally infected *in vivo*. These piglets were diagnosed as suffering from meningitis or were diagnosed as meningitis-free.

3.3.1. *In vitro* infection experiments

HIBCPP cells and PCPEC were infected *in vitro* with *S. suis* ST2, strain 10, wildtype (H4) and a non-encapsulated mutant strain (H5) once the TEER values reached at least 250 Ω x cm^2. The infection was performed with a MOI of 10, meaning 10 bacterial cells were added per 1 host cell. Therefore, 4 x 10^6 and 6 x 10^5 bacterial cells were added to the confluent HIBCPP cells and PCPEC, respectively.

The HIBCPP cells were infected up to 10 h, with time points being in 2 h increments. The primary PCPEC were infected up to 6 h, again, with time increments being in 2 h. Throughout the infection time points, multiple parameters were measured and examined to evaluate the barrier intactness.

3.3.1.1. Barrier Integrity of the in vitro BCSFB models

One main characteristic of CP epithelial cells is the formation of tight junctions, thereby producing a barrier. The ability of HIBCPP cells and primary PCPEC to form tight junctions *in vitro* has previously been demonstrated, which makes these cells ideal as an *in vitro* BCSFB model (Schwerk et al., 2012; Tenenbaum et al., 2009).

3.3.1.1.1. Transepithelial Electrical Resistance (TEER)

In order to evaluate the barrier development and barrier integrity of HIBCPP cells and PCPEC, the TEER was measured by utilizing a voltohmmeter coupled with a chopstick STX01 electrode (Millipore, Schwalbach, Germany). Before each TEER measurement, the electrode was incubated in 80 % ethanol for 10 min. Subsequently, the residual ethanol traces were rinsed off of the electrode and calibrated in the cell culture medium in which the host cells were in. In order to measure the TEER, the longer arm of the chopstick electrode was placed into the well, whereas the shorter arm was placed inside the compartment of the cell culture membrane filter insert. The resulting measurement was presented in units of resistance Ohm (Ω).

In order to calculate the resistance across the cell culture filter membrane area (Ω x cm^2), the measured Ω, from which the blank value was subtracted (cell culture membrane filter not containing any cells) was multiplied by the surface area of the 24-well cell culture filter membrane (approximately 0.336 cm^2).

For the *in vitro* infection experiments of HIBCPP cells and PCPEC, the TEER was measured before starting the infection and following the infection time point, in order to monitor the barrier intactness of the epithelial cells.

3.3.1.1.2. Inulin-flux

In order to monitor the paracellular permeability of the confluent CP epithelial cell layer throughout the infection intervals, fluorescein isothiocyanate (FITC)-inulin solution was utilized. FITC-inulin is a flurecein-labelled sugar molecule, with a molecular weight ranging from 2000 to 5000. By utilizing the Tecan Infinite M200 multiwell reader, FITC-inulin was excited at 490 nm and a fluorescence measurement was obtained at 520 nm.

At the start of each *in vitro* infection experiment, 10 µl of a 50 µg ml^{-1} FITC-inulin stock solution was added to the filter compartment of each filter (basolateral cell side), in order to evaluate paracellular permeability from the basolateral to the apical cell side.

Following the infection time point, the medium in the 24-well (apical CP epithelial cell side) was removed, and 200 µl was added per well in duplicate of a black 96-well plate per condition, and measured at 490 nm excitation and 520 nm emission. Based on a standard curve, which was run in parallel during each infection experiment, the percentage of the FITC-inulin flux was calculated.

3.3.1.2. Cell viability – live/dead assay

Following the infection time point, the filters were washed once with phenol red- and serum-free DMEM/F-12 cell medium, referred to as "SFM", before being placed into a fluorescent dye mixture, provided in the Live/Dead Viability/Cytotoxicity kit for mammalian cells, composed of ethidium homodimer (2 mM stock) and calceine green (4 mM stock) diluted 1:500 and 1:8000, respectively, in SFM. The cells were incubated in a humidified incubator at 37 °C and 5 % CO_2 for 15 min. Following the incubation, the filters were washed three times in SFM, and were subsequently placed into a new well containing SFM. The filters were analyzed using the fluorescence microscope with the 10x objective in conjunction with the ZEN software and representative pictures were captured. Cells which emitted green (excitation 490 nm and emission 515 nm) are indicative of viable cells, whereas red-emitting (excitation 535 nm and emission 617 nm) cells are identified as dead.

3.3.2. *In vivo* porcine infection experiments

3.3.2.1. Animal ethics statement

In vivo piglet infection experiments, and the subsequent necropsy, were carried out by veterinarians, in compliance with the principles outlined in the European Convention for the Protection of Vertebrate Animals Used for Experimental and Other Scientific Purposes, as well as the German Animal Protection Law (Tierschutzgesetz). The CP tissue samples analyzed in this study originated from two different *in vivo* infection studies. The CP tissue samples from the meningitis-free animals were part of a study, which was approved by the Landesdirektion Sachsen, with the permit number TVV26/15, which includes approval through the registered committee for animals experiments (Rieckmann et al., 2018). The experiment analyzing the CP from animals suffering from meningitis were approved by the Committee on Animal Experiments of the Lower Saxonian State Office for Consumer Protection and Food Safety under the permit number 33.12-42,502-04-16/2305A (Rungelrath et al., 2018).

3.3.2.2. Experimental set-up and CP collection

In the study, from which the CP tissue samples were collected from the meningitis-free animals, 8-week old male piglets were intravenously infected with a bacterial density of 2 x 10^8 CFU ml^{-1} *S. suis* ST7 (Rieckmann et al., 2018).

In the study, from which the CP tissue samples from piglets suffering from meningitis were taken, sedated, 8-week old male piglets, which were same breed as the meningitis-free pigs, were infected via intranasal application with a bacterial density of 1.5 x 10^9 CFU ml^{-1} *S. suis* ST2 following a

treatment with 1 % acetic acid of the mucosal surface of the nasal cavity (Baums et al., 2006; Rungelrath et al., 2018). In a previous investigation of the piglet model used to study *in vivo* experimentally induced *S. suis* infections, Pallares and colleagues found that an experimental set-up, which included the pre-treatment of the mucosal nasopharynx area with acetic acid prior to intranasal infection, resulted in effective disease induction, which reflected disease observations made in the field (Pallares et al., 2003).

In both experiments, the animals were monitored and examined every 8 h post-infection for the onset of disease and were given a clinical score, based on their body temperature, food uptake, and overall behavior (alertness, breathing pattern, mobility). An animal was considered morbid if it presented with a fever of at least 40.2 °C. If a high fever persisted (at least 40.5 °C), along with apathy and/or anorexia over a 36 h time period, the piglet was euthanized for predefined animal welfare reasons. Additionally, if the piglet presented severe symptoms, such as body tremors, convulsions, or polyarthritis, the animal was subject for immediate euthanasia.

Onset of severe disease usually occurred 3 to 5 days post-infection. Once a predefined humane endpoint was reached, the animal was sedated and subsequently euthanized via the intravenous administration of T61® (200 mg ml^{-1} embutramide, 50 mg ml^{-1} mebezonium, and 5 mg ml^{-1} tetracain; Intervet, Merck, Sharp & Dohme).

Immediately following the euthanasia of each animal, a necropsy was performed, which has been previously described by Baums and colleagues (Baums et al., 2006). Additionally, the brain was promptly removed and cut between the two brain hemispheres in order to gain access to the lateral ventricles. One of the two CP from the lateral ventricles was removed, briefly rinsed in sterile DPBS, and flash-frozen in liquid nitrogen for subsequent RNA isolation and transcriptome analysis.

When working with RNA, time in fixating the samples is of the essence to maintain RNA integrity for reliable downstream analyses (Kukurba and Montgomery, 2015). Due to RNase enzymatic activities, mRNA turnover is a strictly regulated process in living cells. However, once death sets in, RNA degradation is not part of normal cellular function and could skew the transcriptome profile at a given physiological state (Gallego Romero et al., 2014; Kukurba and Montgomery, 2015). In order to aim at the most accurate snap-shot of the transcriptome profile being investigated, the time between the death of the animal and freezing the CP was kept to a minimum and averaged approximately 20 min.

3.4. Molecular techniques

3.4.1. RNA isolation

For isolating RNA from the infection experiments, the RNeasy technology from Qiagen was used. In this method of RNA isolation, a buffer is utilized in order to inactivate RNase activity. Ethanol is employed to enhance RNA-binding to a silica-based membrane of a spin column, and a series of the manufacturer's buffers are provided in the RNA isolation kits in order to wash away any contaminants resulting from the cell lysis process in order to obtain pure RNA post-isolation.

The RNeasy Mini Kit was used for total RNA isolation from HIBCPP cells and the CP tissue from the *in vivo* porcine experiments. For the HIBCPP cell infection experiments, the filters were briefly rinsed with DPBS (with Ca^{2+} and Mg^{2+}), before the filter was placed inverted into a 12-well cell culture plate. 150 µl of the RLT cell lysis buffer (section 2.7) was applied to the cells, and using a pipette, the cells were gently scratched off while applying the lysis buffer. The cell lysate was collected in a 1.5 ml centrifuge tube and at a later point further processed following the Qiagen RNeasy Mini kit protocol "purification of total RNA from animal cells using spin technology". Additionally, one cell culture transmembrane filter containing a confluent layer of approximately 400,000 cells was used for RNA isolation.

For the CP tissue collected from the *in vivo* porcine infection experiments, 30 mg of the fresh-frozen tissue was suspended in 600 µl RLT cell lysis buffer (section 2.7) and a micro pestle was used to homogenize the tissue. To further process the samples, the homogenized tissue suspension was applied to a QiaShredder before the total RNA was isolated according to the manufacturer's protocol "purification of total RNA from animal tissues".

RNA was isolated from PCPEC using the RNeasy Micro Kit, due to the low starting material requirement defined by the manufacturer. As with the HIBCPP cell samples, 150 µl of the RLT cell lysis buffer (section 2.7) was used per filter for the RNA isolation and four cell culture membranes containing a confluent layer of PCPEC, with approximately 60,000 cells, were pooled. The manufacturer's protocol "purification of total RNA from animal and human cells" was followed.

All isolated RNA samples underwent an on-column DNase I treatment, which was integrated during the RNA isolation protocols (15 min incubation at room temperature), as described by the manufacturer. Following the isolation, RNA samples were eluted in RNase-free H_2O and stored at -80 °C. The RNA concentration was determined with the spectrophotometer NanoDrop.

3.4.2. cDNA synthesis

In order to perform the RT-PCR or qPCR with RNA isolated from the infection experiments, 0.5 µg RNA from HIBCPP and the *in vivo* experiments was reverse transcribed to generate the complementary strand to the isolated RNA transcripts called copy DNA (cDNA). For PCPEC, due to the low RNA yield following the isolation, 0.125 µg RNA was reverse transcribed to generate cDNA. Table 5 summarizes the individual components for 1 cDNA synthesis reaction mixture for a total volume of 20 µl, as was described in the AffinityScript QPCR cDNA Synthesis Kit.

Table 5. Composition for 1 cDNA synthesis reaction mixture.

10 µl	First Strand Master Mix
3 µl	Random Primers
1 µl	AffinityScript Reverse Transciptase/RNase Block Enzyme Mixture
X* µl	RNA
X** µl	RNase-free H_2O

* amount equal to 0.125 µg PCPEC RNA or 0.5 µg HIBCPP and CP tissue RNA
** amount to equal the total volume of the reaction to 20 µl

Table 6 summarizes the program used for the cDNA synthesis. The cDNA was synthesized with the help of the Thermocycler 2720.

Table 6. cDNA synthesis program used with the thermocycler 2720.

cDNA synthesis step	Program temperature	Program length
primer annealing	25 °C	5 min
cDNA synthesis	42 °C	15 min
cDNA synthesis termination	95 °C	5 min

All cDNA samples were prepared according to manufacturer's instructions and the subsequent resulting cDNA was stored at -20 °C.

3.4.3. Semi-quantitative RT-PCR and gel electrophoresis

Following the double-strand cDNA synthesis, a semi-quantitative RT-PCR was performed in order to evaluate the expression of specific genes. The PCR allows for the exponential amplification, enabled by thermal cycling, which facilitates DNA melting and enzyme-driven replication of a desired region or gene of interest with the use of oligonucleotide primers. In this study, the expression of mature mRNA transcripts, which do not include intron regions, was investigated.

In this study, the gene expression was evaluated semi-quantitatively in order to compare and detect changes in expression levels before amplification resulted in a fully saturated band on the gel

electrophoresis. In order to achieve this, the thermocycler was paused after either the 26th, 28th, or 32nd cycle of amplification, depending on the evaluated sample, and the remainder of the sample was amplified for four more cycles.

With the use of Qiagen's Taq DNA Polymerase kit, the reaction mixture was prepared as described in Table 7.

Table 7. The composition for one PCR reaction mixture, with the total volume of 25 µl.

Compositions for 1 PCR Reaction Mixture	
2.5 µl	CoralLoad PCR Buffer, 10x
1 µl	dNTP mixture, 10 mM of each nucleotide
1 µl	Forward and Reverse Oligonucleotide Primer mixture, 1:10 diluted
0.125 µl	Taq polymerase, 250 units
0.5 µl	cDNA
19.88 µl	distilled H_2O

Table 8 was the program setting of the Thermocycler 2720 in order to perform the RT-PCR reaction.

Table 8. PCR program for the RT-PCR reaction.

PCR step	Temperature (°C)	Time	Number of Cycles
Initial denaturing	94	2 min	1
Denaturation	94	30 sec	30**
Annealing	58-60*	30 sec	30**
Extension	72	1 min	30**
Final Extension	72	7 min	1
Hold	8	∞	

*Annealing temperature was dependent on primer. See Table 3 for exact annealing temperature.
**Number of cycles varied on the PCR type and samples used. See figure legends for specification.

The PCR products were run on a 1.5 % agarose-ethidium bromide gel in 1 x TAE buffer and 120 V for approximately 40 min. Images were captured using the gel documentation system in conjunction with the VisionCapt software.

3.4.4. qPCR

Quantitative PCR (qPCR) allows for the numerical assessment of gene expression either via absolute or relative quantification. The qPCR detection format in this study applied the use of SYBR® Green I Dye. SYBR® green is a fluorescent dye, which binds to the minor groove of the double-stranded DNA generated during amplification. Once SYBR green is bound, a maximum excitation at 497 nm and maximum emission at 520 nm can be used to detect product amplification.

Additionally, a reference dye is included during the qPCR reaction which acts as a baseline since its fluorescence does not change, and can therefore be used to normalize any non-PCR related fluorescence variations which may arise. It can be detected with an excitation at 584 nm and emission at 612 nm.

To quantitatively evaluate the expression of selected genes, the Brilliant II SYBR® Green QPCR Master Mix kit was used to prepare the reaction mixture for the qPCR, which is summarized in Table 9.

Table 9. The composition of one qPCR reaction mixture.

Compositions for 1 qPCR Reaction Mixture	
12.5 µl	2 x Brilliant II SYBR Green Master Mix
0.375 µl	30 nM diluted reference dye (ROX)
6.925 µl	distilled H_2O
0.5 µl	cDNA
5 µl	forward and reverse oligonucleotide primer mixture with a final concentration of 250 nM

The qPCR was run using the Stratagene Mx3005P system with the MX software using the 1 plateau pre-melt / RT segment and normal 2-step amplification setting, as described in Table 10. A third segment was included to determine the dissociation curve and to ensure amplification of only the amplicon product of interest, since SYBR green binds to all available double stranded DNA, including primer dimers. To generate the dissociation/melting curve, the sample is initially heated to 95 °C in order to melt the DNA, then cooled to 55 °C, followed by a temperature ramp up to 95 °C. During the temperature ramp-up, the increasing fluorescence measurements are collected, resulting in a peak. A drop can be observed when the double-stranded DNA melts, thereby releasing the intercalated SYBR green molecules. Based on the resulting dissociation/melting curve, an interpretation to the amplified product and number of amplicons can be made.

Table 10. The MxPro software setting for the qPCR.

PCR step	Temperature (°C)	Time	Number of Cycles
Segment 1:			
Initial denaturing	95	10 min	1
Segment 2:			
Denaturation	95	30 sec	40
Combined Annealing and Extension	58	1 min	40
Segment 3:			
Dissociation/Melting curve	95	1 min	1
	55	30 sec	1
	95	30 sec	1

During the qPCR run, the threshold cycle (C_T) was determined, which was used to calculate the fold-change between phenotype A versus phenotype B (infected versus uninfected). The C_T ensures that the gene of interest is being expressed in the exponential phase during the PCR amplification step, and is inversely correlated to the number of amplicons in the sample (Schmittgen and Livak, 2008).

The gene fold-change was calculated based on the method for relative quantification called the $2^{-\Delta\Delta Ct}$ method (Livak and Schmittgen, 2001). The formula which is applied in order to determine the $2^{-\Delta\Delta Ct}$ is as follows:

$$2^{-\Delta\Delta CT} = \frac{C_T\ gene\ of\ interest - C_T\ internal\ control\ of\ phenotype\ A}{C_T\ gene\ of\ interetst - C_T\ internal\ control\ of\ phenotype\ B}$$

The house-keeping gene (internal control) *gapdh* was used to calculate the fold-change $2^{-\Delta\Delta Ct}$ of the gene of interest between the infected versus uninfected phenotypes.

Furthermore, the significance of the gene fold change from infected samples in comparison to uninfected samples was calculated using the unpaired student's t-test. A result was considered significant if $p \leq 0.05$.

3.5. Conventional RNA-seq and MACE sequencing – an external collaboration

A conventional RNA-seq was carried out in collaboration with PD Dr. Ludger Klein-Hitpass at the Institute for Cell Biology at the University Hospital Essen with all samples obtained during the infection experiments (section 3.3).

In addition to the conventional RNA-seq, a sequencing method called MACE was perform. The MACE-sequencing method was carried out on the samples, which were obtained from the *in vivo* porcine infection experiments.

3.5.1. RNA integrity

Before the RNA libraries were prepared for sequencing, the RNA integrity was evaluated using the Agilent 2100 Bioanalyzer System in combination with the Agilent Bioanalyzer RNA Nano Chip. The Agilent 2100 Bioanalyzer system utilizes an automated electrophoresis solution in order to score the ratio between the 18S and 28S ribosomal RNA (rRNA) subunits. A score ranging from 1 – 10 is given based on the ratio, and this score is termed the "RNA Integrity Number" (RIN). A RIN of 10 is given to non-degraded RNA, with a 2-to-1 ratio between the 28S and 18S rRNA, and, therefore, the best RNA

quality. RNA used in NGS studies should have a RIN of at least 6 in order to retrieve reliable data (Kukurba and Montgomery, 2015).

3.5.2. Library preparation and library sequencing

For this study, different RNA-seq library preparation kits were utilized and the preparation was carried out in strict accordance to the manufacturer's protocols for the respective kits. The RNA-seq library preparation involves a sequence of the same steps, which include poly(A) mRNA selection, RNA fragmentation, cDNA synthesis, blunt end repair, adaptor ligation, strand selection, and the final library amplification via PCR. However, the sequence of these steps may vary depending on the sequencing design or sample input. Since the main aim of this study was to investigate the transcriptional response during infection, the RNA-seq library preparation focused on selecting the poly(A) mRNA transcripts and depleting the samples of rRNA in order to achieve a proper coverage of the changing transcriptome to gain a better insight into the biological processes. The rRNA transcripts make up approximately 80 to 90 % of the total RNA profile, and do not provide much biologically relevant information when investigating the global transcriptional profile of infected and uninfected samples (O'Neil et al., 2013). The main difference for the use of two different library preparation kits in this study was the rRNA elimination step.

The Ovation® Human FFPE RNA-Seq Library system was utilized for the library preparation of 100 ng total RNA from the HIBCPP cells for conventional RNA-seq. In the initial step of this library preparation method, the total isolated RNA was reverse transcribed with random priming. The rRNA depletion step was performed later during the library preparation with the help of AnyDeplete Technology, which is also known as Insert-Dependent Adaptor Cleavage (InDA-C), and was part of the library preparation kit protocol. AnyDeplete technology involves the use of a library of oligonucleotide primers which anneal to the known human rRNA (12S, 16S, 18S, and 28S) sequences. Following the annealing, the sequences are extended and then cleaved with an unknown reagent, provided in the manufacturer's kit, in order to eliminate sequencing of these transcripts.

The Universal Plus mRNA-Seq library kit was used for the preparation of 100 ng total RNA from the porcine samples sequenced via conventional RNA-seq. The main reason for the use of this kit to prepare the porcine samples was the unavailability of a porcine AnyDeplete oligonucleotide library. With this kit, the poly(A) mRNA transcripts are selected with polydT Beads at the beginning of the library preparation, therefore eliminating the need for further rRNA elimination.

A third library preparation kit was utilized in order to prepare 500 ng total RNA from the *in vivo* samples for the alternative MACE sequencing method. This method of library preparation consisted

of the cDNA synthesis, a step which directly involved the selection of poly(A) mRNA transcripts, purification, fragmentation, end repair, adaptor ligation, and a library amplification via PCR. The rRNA was depleted via poly(A) mRNA selection, in a first step of the library preparation.

Further steps of the library preparation include the fragmentation of the transcripts. The desired fragment length is dependent on the instrument used for sequencing, since length can have an influence during the cluster generation on the flow cell (Head et al., 2014). The Covaris S220 Focused-ultrasonicator, with the Covaris microTUBE, set to 10 % duration, 200 cycles per burst, and 140 sec was used to generate fragment sizes of approximately 250 bp long. Fragment lengths were analyzed on the Agilent 2100 Bioanalyzer System using the Agilent Bioanalyzer HS DNA chip.

Bead-purification steps were carried out with the help of Agencourt AMPure XP SPRI beads in order to remove adapter or primer dimers throughout the various cDNA synthesis, adaptor ligation, or PCR amplification steps.

The Qubit system was used in combination with the double stranded DNA high sensitivity assay kit in order to determine the DNA concentration of the prepared libraries before these were pooled.

Adaptor ligation introduces specific 8 bp long barcode sequence to each of the individual biological replicates of infected and uninfected samples. With the use of the barcodes, one library pool containing all the biological replicates for each phenotype (infected and uninfected) was generated for sequencing. The library pool was quantified utilizing the NEBNext® Library Quant kit, which is a SYBR Green based qPCR method essential in order to achieve the optimal cluster density on the sequencing flow cell required for an optimal sequencing output.

The final prepared transcript for sequencing is depicted in Figure 6. It includes adapters which recognize the corresponding sequence on the sequencing flow cell. Adapters are located on both ends of the transcript (library insert), due to the bridge amplification step for cluster generation preceding the sequencing. Additionally, a barcode sequence is included in the adapter region to allow pooling of different samples into a single lane of the flow cell. Furthermore, the final library structure also includes a “read primer” for the cluster generation on the flow cell preceding sequencing.

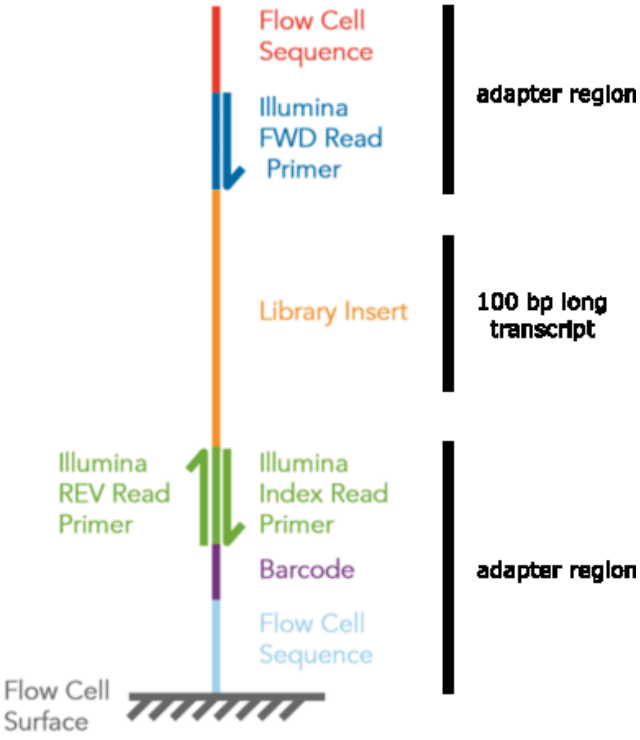

Figure 6. The general library structure following the RNA-seq library preparation. The library structure consists of two adapter regions, which contain a barcode sequence, primers for cluster generation on the flow cell, and the corresponding flow cell sequence for attachment. The sequence of interest is the "library insert". This image was modified from the Illumina RNA-seq library preparation instruction manual.

The pooled libraries were sequenced using Illumina's HiSeq 2500 or MiSeq flow cell system in the paired-end mode for the epithelial cells (HIBCPP cells and PCPEC) and the CP samples obtained *in vivo,* and single-end mode for the samples obtained *in vivo* sequenced via MACE. For details, please refer to section 2.5.

3.5.3. Bioinformatic data processing post-sequencing

In order to analyze the sequenced fragments, also termed "reads", in terms of differential gene expression and utilizing transcriptome analysis platforms, the data had to be bioinformatically processed. The data processing for all sequenced samples included the trimming of the adapter sequences, alignment and quantification of the fragments post-sequencing.

The first step was to remove the adapter sequences in order to ensure accuracy during further downstream processing and preventing the loss of valid sequence data. This was carried out with the help of the Trimmomatic-0.30 software tool, which was designed to identify full and partial adapter sequences from single- and paired-end Illumina NGS data (Bolger et al., 2014).

The trimmed sequences were subject to alignment by utilizing the RNA aligner STAR software (Dobin et al., 2013). The sequences generated from the HIBCPP cells were aligned to the human genome 19 and the sequences generated from the porcine samples (PCPEC and CP from the *in vivo* infection experiments) were aligned to the *Sus scrofa* genome 11.1. The aligned sequences of the HIBCPP cell and PCPEC samples were imported into the StrandNGS software and filtered on quality metrics, which included the removal of reads that had more than one match, an alignment score of below 95, mapping quality below 40, and lengths less than 20. This additional filtering step was not carried out on the sequences aligned from the *in vivo* experiment. Instead, these sequences were subject to Universal Molecular Identifiers filtering, which resulted in less than 5 % of reads removed. These aligned and filtered reads can be imported to the Integrative Genomics Viewer, which allows visualization of the NGS datasets (Robinson et al., 2011).

Lastly, for the quantification of the RNA sequences, the aligned and filtered reads were imported to the Partek Genomics Suite (PartekGS) software. This software reports the reads per kilobase of exon model per million reads (RPKM), which is a scaling method applied in order to normalize the RNA abundancies (Mortazavi et al., 2008). The formula employed in order to calculate the RPKM is as follows:

$$RPKM = \frac{raw\ number\ of\ reads}{exon\ length}\ x\ \frac{1{,}000{,}000}{number\ of\ mapped\ reads\ in\ sample}$$

The RPKM normalizes the transcript length in relation to the total number of reads of the transcript in the sequencing measurement.

In order to evaluate the differential gene expression and to utilize data analysis platforms for downstream analysis, the resulting RPKM values and/or the raw reads were used to generate the Differentially Expressed Genes (DEGs) list and to perform a Gene Set Enrichment Analysis (GSEA).

3.5.4. RNA-Seq statistical data analysis: DEGs and GSEA

In order to evaluate the differential expression of individual genes, DEGs were identified using the PartekGS software implementing the one-way analysis of variance (ANOVA) test. A step-up method to correct for multiple testing was applied to generate corrected *p*-values, but due to the low number of replicates, the correction for multiple testing eliminated many potential true-positive targets. For this reason, the identification of DEGs was based on uncorrected p-values. The resulting *p*-values were exported and further manual filtering steps were carried out in Excel from Microsoft Office. Filters, which were applied in order to generate the final DEG list, included at least 10 (for the

PCPEC and *in vivo* samples) or 20 (for the HIBCPP cell samples) raw reads of the transcript in the biological triplicates of one class (uninfected versus infected) and an uncorrected *p*-value of ≤ 0.05. Additionally, a more stringent list was created which only displayed a list of significant DEGs with a corrected (step-up method) *p*-value ≤ 0.05. The genes resulting in the final DEG list with an uncorrected and corrected *p*-value ≤ 0.05 were taken into consideration.

A second statistical analysis was applied using the RPKM values, by utilizing the GSEA software, which allows the user to interpret the data on a biological relevant gene set level, and not on individual genes, when comparing different biological states (Mootha et al., 2003; Subramanian et al., 2005). The GSEA makes use of the Molecular Signature Database (MSigDB), which contains approximately 18,000 gene sets (GSs), categorized into eight major groups (Liberzon et al., 2015; Liberzon et al., 2011; Subramanian et al., 2005). The GSEA was run with the standard settings in the gene set permutation mode, set to 1000 permutations. In order to select potential interesting candidates, GSs which presented a false discovery rate (FDR) *q*-value ≤ 0.25 were considered to be of interest, along with a normalized enrichment score (NES) of approximately ± 2.

3.5.5. Accession numbers

The data generated during RNA-seq was deposited in the Sequence Read Archive (SRA) on the National Center for Biotechnology Information (NCBI) platform. The BioProject accession number for the HIBCPP cell data is PRJNA533919. The BioProject accession number for the PCPEC data is PRJNA533792. The BioProject accession numbers for the data acquired from the in CP tissue which was isolated following the *in vivo* infection experiments can and sequenced via conventional RNA-seq and MACE are PRJNA534398 and PRJNA534382, respectively.

4. Results

4.1. *In vitro* infected HIBCPP cells show an inflammatory response 6 h post-infection from the basolateral cell side with *S. suis* ST2

An infection with the zoonotic pathogen *S. suis* ST2, whose natural host is the pig, is known to result in the same clinical manifestations, such as septicemia and meningitis, in humans. Its interaction with the immortal HIBCPP cells line in the *in vitro* BCSFB model was previously investigated. Observations showed that *S. suis* ST2 and the non-encapsulated mutant display strong invasion rates into the HIBCPP cells when applied to the basolateral host cell side (Schwerk et al., 2012). To date, no transcriptome analysis has been performed with HIBCPP cells infected from the basolateral cell side *in vitro* with *S. suis*. Therefore, the first aim of this thesis was to determine the time point of the strongest transcriptional inflammatory response when the HIBCPP cells were infected from the basolateral cell side, which *in vivo* would demonstrate the blood side.

The *in vitro* infection study parameters, which were collected included the epithelial barrier integrity via TEER measurement and the determination of the FITC-inulin flux across the barrier. Additionally, a live/dead assay was performed in order to assess cell viability throughout infection time points. Lastly, the cells were fixed and lysed following each infection time point, and the RNA was isolated in order to evaluate the expression of inflammatory genes for each time point. HIBCPP cells were infected for a total of up to 10 h with a bacterial MOI of 10, and samples were collected in an increment of 2 h. Due to the HIBCPP cells exhibiting the strongest inflammatory response 6 h post-infection (data not shown), the data for this time point will be presented.

Figure 7 A depicts the TEER values of HIBCPP cells before the infection (0 h) and infected with *S. suis* ST2 for 6 h, either with the wildtype (H4) or the non-encapsulated mutant (H5). The TEER remained stable, with only a slight decrease after the 6 h infection time point. Before the infection experiment, the TEER values displayed an average of 475 Ω x cm^2 (± 130), 510 Ω x cm^2 (± 106), and 508 Ω x cm^2 (± 136) for uninfected, H4 infected, and H5 infected, respectively. Following the 6 h infection time point, the TEER showed a slight decrease for all conditions, with the average TEERs being 415 Ω x cm^2 (± 95) for uninfected HIBCPP cells, 460 Ω x cm^2 (± 109) for H4 infected cells, and 382 Ω x cm^2 (± 128) for H5 infected cells.

Additionally, Figure 7 B depicts that the average FITC-inulin flux remained very low after 6 h of infection, with values of below 1.7 % (± 1.9), 0.7 % (± 0.8), and 1.6 % (± 1.4) for uninfected, H4 infected, and H5 infected cells, respectively. By relying on an educated guess, a value was determined based on previous experiences in our laboratory, which accepts a 1 % FITC-inulin flux per

hour of infection. These low FITC-inulin flux values therefore reflect an intact barrier 6 h post-infection.

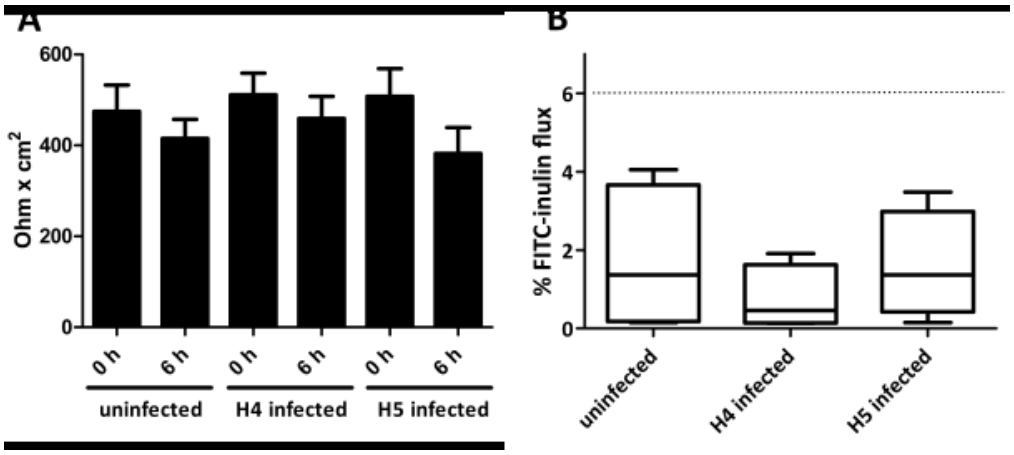

Figure 7. The HIBCPP barrier integrity remained intact 6 h post-infection with *S. suis* ST2. The average TEER (Ω x cm^2) and standard deviation values of the measurements before (0 h) and after (6 h) the infection time period of the HIBCPP cells is presented (A). The average percentage with the standard deviation of the FITC-inulin flux following the 6 h infection time point is presented in a box-plot (B). The HIBCPP cell infection experiments were carried out at least three times and in triplicates for each condition.

Analysis of cell viability, via the live/dead assay, after the 6 h infection time point is depicted in Figure 8. The majority of the HIBCPP cells remained viable (indicated in green), with very few dead cells (indicated in red) present for uninfected, *S. suis* H4 and *S. suis* H5 infected cells (Figure 8).

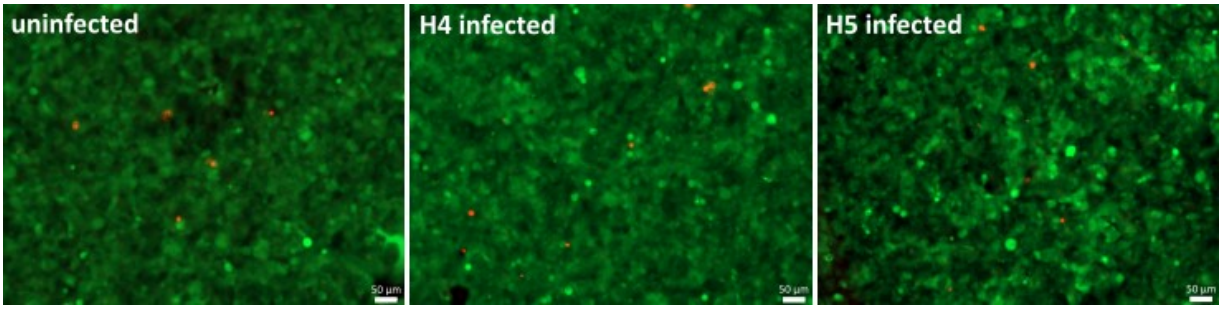

Figure 8. The live/dead assay of HIBCPP cells infected with *S. suis* ST2 H4 and H5 strains for 6 h reveals a majority of viable cells. A representative image for each condition was chosen, and the live/dead assay was performed in duplicate. The images were captured with the 10x magnification using a fluorescent microscope, and the white bar in the bottom right corner represents 50 µm.

Lastly, Figure 9 depicts the analysis of inflammatory genes via a semi-quantitative RT-PCR, demonstrating that HIBCPP cells exhibit a strong inflammatory response 6 h post-infection with *S. suis* ST2. When comparing the uninfected cells to HIBCPP cells infected with the H4 and H5 *S. suis* ST2 strains, the expression levels indicated by the band intensity increased for genes encoding for the cytokines and chemokines TNFα, IL8, CXCL1, CXCL2, as well as for IκBζ, which encodes for a regulator of the transcription factor NFκB, while the expression of the house-keeping gene encoding

for GAPDH remained coherently expressed. For the uninfected cells, it appears that a basal level of expression exists for the evaluate genes. However, when comparing the band intensities, it is apparent that a stronger expression occurs during infection. Furthermore, the *S. suis* ST2 H5 strain appears to clearly induce a stronger response in all of the evaluated inflammatory genes, especially when comparing the band intensities after 26 cycles to those of the *S. suis* ST2 H4 infected cells, since some 30 cycle amplicons appeared to have reached saturation. Following the 6 h time point, the inflammatory response diminished (data not shown).

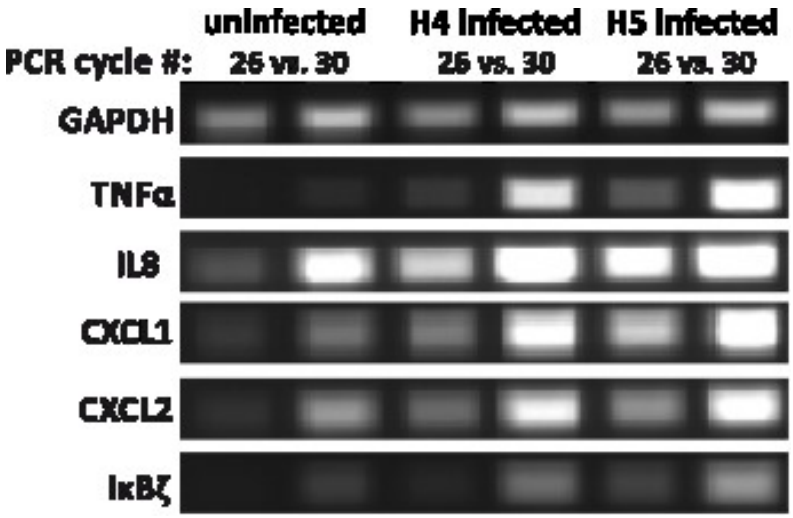

Figure 9. Semi-quantitative RT-PCR of 6 h *in vitro* infected HIBCPP cells reveals a strong inflammatory response on the transcriptome level. The gene expression of the genes indicated on the left hand side were semi-quantitatively assessed after 26 and 30 PCR cycles (indicated at the top) of uninfected HIBCPP cells in comparison to HIBCPP cells infected for 6 h with *S. suis* ST2 strains H4 and H5. A representative image is depicted. The samples were run on a 1.5 % agarose-ethidium bromide gel and the image was captured using the Vision-Capt software.

Due to the strong transcriptional response following the 6 h infection period (Figure 9), during which the CP epithelial barrier was maintained, as was demonstrated by a high TEER and a low flux of FITC-inulin (Figure 7), as well as a viable cell population (Figure 8), these cell samples were selected for the global transcriptome analysis via RNA-seq. The *S. suis* ST2 H5 infections were included in the preliminary analysis, since this mutant had previously shown to induce gene regulation with some variation in CP epithelial cells in comparison to the *S. suis* H4 wildtype (Schwerk et al. (2011) and unpublished data). However, these samples were excluded from further analysis due to the higher relevance of *S. suis* ST2 wildtype causing infection in the field.

4.2. Primary PCPEC show a strong inflammatory response 6 h post - *in vitro* infection from the basolateral cell side with *S. suis* ST2

As a zoonotic pathogen, not only is the interaction of *S. suis* ST2 with human cells is of interest, but also understanding the pathogenesis during the interactions with cells of its natural host is of high importance. A few *in vitro* studies have previously been conducted, in order to study the interaction of *S. suis* ST2 with primary PCEPC. It was demonstrated, that *S. suis* ST2 can effectively invade host cells, when applied to the basolateral epithelial cell side, and translocate to the apical cell side (Tenenbaum et al., 2009). It was further found to induce apoptosis and necrosis when PCPEC were infected from the apical cell side (Tenenbaum et al., 2006). Furthermore, PCPEC cells were observed to contribute to the inflammatory response by producing cytokines and chemokines (Schwerk et al., 2011). However, in the latter experimental set-up, PCPEC were infected from the apical cell side, which *in vivo* reflects the CSF compartment. So far, no transcriptional response had been investigated, when PCPEC were infected from the basolateral cell side. The aim of this experiment was to investigate the time point at which PCPEC exhibited the strongest inflammatory response at the transcriptional level, when infected from the basolateral side with S*. suis* ST2 at a MOI of 10.

In this study, PCPEC were infected *in vitro* up to 6 h from the basolateral cell side with *S. suis* ST2 H4 and the non-encapsulated H5 strains. As was done with the HIBCPP cells, different experimental parameters were evaluated every 2 h, including the cell barrier integrity via TEER measurement and the passage of the fluorescent-labelled macromolecule, FITC-inulin, since it had previously been described that *S. suis* ST2 infecting PCPEC from the apical cell side induced a barrier break-down (Tenenbaum et al., 2005). Additionally a live/dead assay was performed to examine cell viability throughout the infection period. Lastly, the RNA was isolated and a semi-quantitative RT-PCR was performed as a pre-assessment for determining the time point of the strongest inflammation, and the RNA was subsequently subject for RNA-seq. These experiments were carried out at least three times and were performed in quadruplicates for each condition. Due to the PCPEC exhibiting the strongest inflammatory response 6 h post-infection (data not shown), the data for this time point will be presented.

The PCPEC barrier displayed an intact barrier, with the average TEER before of 277 Ω x cm^2 (± 44), 289 Ω x cm^2 (± 17), and 277 Ω x cm^2 (± 37) for uninfected, H4 infected, and H5 infected primary PCPEC, respectively, before the start of infection (Figure 10 A). The barrier property of the epithelial cells remained intact throughout the 6 h infection period, with the average TEER values being 275 Ω x cm^2 (± 67) for uninfected cells, 274 Ω x cm^2 (± 32) for H4 infected cells, and 297 Ω x cm^2 (± 76) for H5 infected PCPEC.

Additionally, the FITC-inulin flux through the barrier remained very low 6 h post-infection, with the average percentages depicted in Figure 10 B as being 2.2 (± 1.9) for uninfected cells, 1.9 (± 1.3) for H4 infected cells, and 1.1 (± 0.9) for H5 infected cells. By relying on an educated guess, a value was determined based on previous experiences in our laboratory, which accepts a 1 % FITC-inulin flux per h of infection. Since the TEER values remained stable and the flux of the FITC-inulin remained below 6 %, it was deduced that the *in vitro* barrier remained intact throughout the 6 h infection time period.

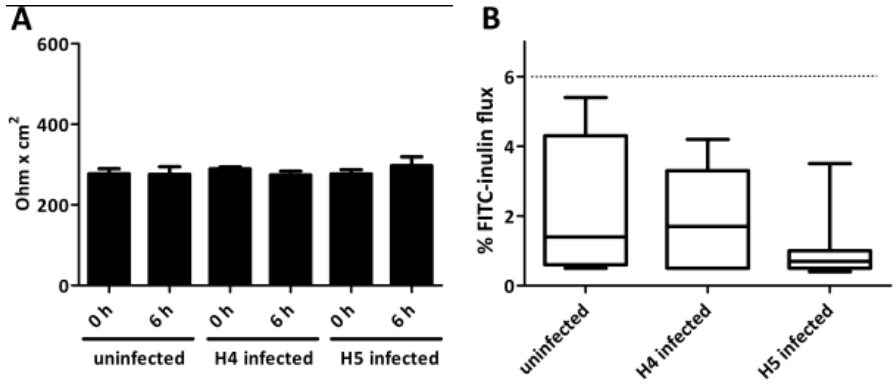

Figure 10. The PCPEC *in vitro* barrier remained intact 6 hours post-infection with *S. suis* ST2. The average TEER (Ω x cm^2) before (0 h) and after a 6 h infection time point remained stable (A). The average FITC-inulin flux remained below 6 % following the infection time point, indicating a low permeability for macromolecules through the *in vitro* barrier property, and is presented in a box-plot (B). The PCPEC infection experiment was carried out at least three times, for each condition performed in quadruplicate.

The live/dead assay revealed that the majority of cells remained viable (green cells), with a minority being dead (red), following the 6 h period (Figure 11). However, in comparison to the live/dead assay of the HIBCPP cells which displayed a green layer of cells (Figure 8), the presence of black spots was observed. This may be due to PCPEC forming a true monolayer of epithelial cells, whereas HIBCPP cells have been observed to form papilloma-like multi-cell layers (Ishiwata et al., 2005).

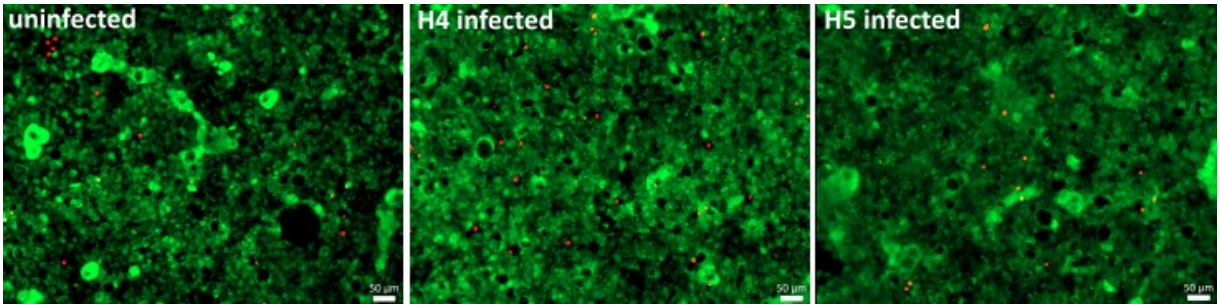

Figure 11. The live/dead assay of uninfected primary PCPEC and PCPEC infected with *S. suis* ST2 H4 and H5 strains for 6 h reveals a majority of viable cells. A representative image for each condition was chosen and the live/dead assay was performed in duplicate. The images were capture with the 10x magnification using a fluorescent microscope, and the white bar in the bottom right corner represents 50 µm.

Lastly, following the RNA isolation, the expression levels of the inflammatory response genes were evaluated, with a representative image depicted in Figure 12. The inflammatory response genes selected for evaluation were previously shown to be regulated by CP epithelial cells during infection experiments in our laboratory (Schwerk et al., 2011). As was observed with the HIBCPP cells, the PCPEC also displayed strong expression levels of inflammatory cytokines 6 h post-infection with *S. suis* ST2. Again, basal levels of expression were observed for genes encoding for IL8 and CXCL2 in the uninfected PCPEC. However, no expression could be detected for IL1β in uninfected cells. The expression of the house-keeping gene GAPDH showed a coherent expression level.

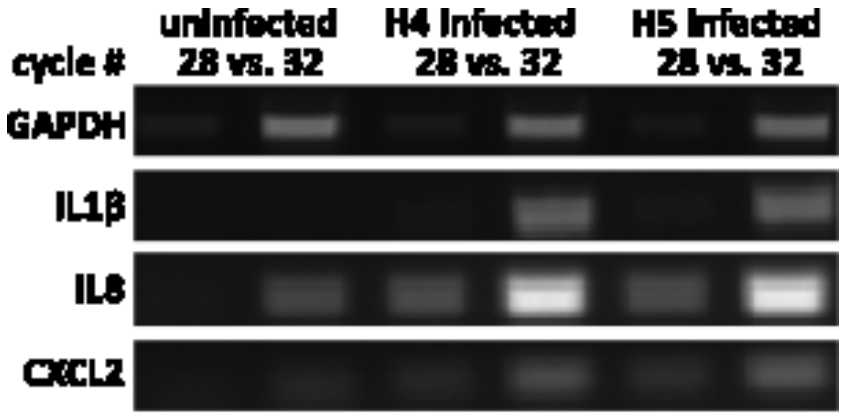

Figure 12. Semi-quantitative RT-PCR of infected PCPEC displays an inflammatory response 6 h post-infection with *S. suis* ST2. The gene expression of the genes indicated on the left hand side were semi-quantitatively assessed after 26 and 30 PCR cycles (indicated at the top) of uninfected PCPEC in comparison to 6 h infected PCPEC with *S. suis* ST2 strains H4 and H5. A representative image is depicted. The samples were run on a 1.5 % agarose-ethidium bromide gel and the image was captured with the Visio-Capt software.

Since the primary PCPEC demonstrated the strongest inflammatory response on a transcriptional level 6 h post-infection, along with an intact barrier and a viable cell population, these samples were selected for the global transcriptome analysis via RNA-seq. As was the case with the HIBCPP cells, the PCPEC infected with *S. suis* H5 strain were only included in the preliminary analysis due to their previous implication of inducing a strong inflammatory response, but were excluded from the sequencing analysis due to the higher relevance of *S. suis* ST2 wildtype causing infection in the field.

4.3. The CP of *in vivo* infected piglets suffering from meningitis exhibited an inflammatory response

Previous observations made by Sanford and colleagues, and later by Williams and Blakemore, from naturally and experimentally infected pigs, first implicated the CP during *S. suis* – induced meningitis (Sanford, 1987; Williams and Blakemore, 1990). Lesions were observed at the CP in animals suffering from meningitis. In association with these lesions was the loss of the microvilli of the apical CP epithelial cell side, a reduction of CP-associated epiplexus macrophages, as well as an increased presence of immune cells and fibrinous exudate in the ventricles (Sanford, 1987; Williams and Blakemore, 1990). To date, no global transcriptome analysis has been performed of the CP during *S. suis*-induced bacterial meningitis. In collaboration with the group of Prof. Baums, at the Institute for Bacteriology and Mycology, Faculty of Veterinary Medicine, University of Leipzig, *S. suis* ST2 *in vivo* infection experiments with 8-week old piglets were carried out.

The meningitis-free animals were part of a study, which included being experimentally infected with *S. suis* ST7 (Rieckmann et al., 2018). These animals exhibited minor symptoms post-infection, including fever, which cleared within 48 h. For the remaining 14 days of the experiment, the animals did not show any symptoms of disease. Following the conclusion of the experiment, the animals were euthanized and a necropsy was performed subsequently to euthanasia. Part of the necropsy consisted of CSF collection and preserving the organs, known to be colonized by *S. suis*, in formalin for histopathological evaluation by the veterinary pathologist at the Institute for Veterinary Pathology, Faculty of Veterinary Medicine, University of Leipzig. No bacterial growth occurred from the collected CSF and the veterinary pathologists confirmed the absence of histopathological abnormalities, for the three animals included in this study, at the brain and the CP. These results are summarized in Table 11.

The CP tissues from the animals suffering from meningitis were part of a study, which included being experimentally infected with the wildtype *S. suis* ST2 strain 10 (Rungelrath et al., 2018). The onset of clinical symptoms occurred approximately 3 to 5 days post-infection, and included high fever, body tremors, convulsions, and ataxia. The onset of these symptoms resulted in the humane endpoint, and the animals were euthanized. Again, part of the necropsy consisted of CSF collection and preserving the organs, known to be colonized by *S. suis*, in formalin for histopathological evaluation by the veterinary pathologist at the Department of Pathology, University of Veterinary Medicine Hannover. The CSF of all animals showed a high amount of bacterial CFUs per ml of CSF, which were confirmed via PCR to be *S. suis* ST2 (data not shown). Additionally, all of the piglets which exhibited symptoms of meningitis were also confirmed post-mortem, via histopathological evaluation of the brain and CP, to be suffering from meningitis. These results are summarized in Table 11.

Table 11. Summary of the symptoms post-infection with *S. suis* ST2: bacterial CFU in the CSF and the histopathological findings of the CP from the *in vivo* infected piglets used in this study.

Meningitis-free animals			
Animal Number	**Symptoms post-infection**	**Bacterial CFU per ml of CSF**	**Histopathological findings**
17	Day 1: 40.7 °C fever Day 2: no fever	None	No indication of infection of the brain or CP
24	Day 1: 41.1 °C then 40.4 °C fever Day 2: 40.7 °C fever, which cleared by the end of the day	None	No indication of infection of the brain or CP
43	Day 1: 41.1 °C then 41.3 °C Day 2: 41.3 °C, which cleared by the end of the day	None	No indication of infection of the brain or CP
Animals suffering from meningitis			
4	42.1 °C fever, ataxia, kyphosis, body tremors, abdominally reinforced breathing	3.33×10^7	Moderate multifocal fibro-purulent meningitis and moderate multifocal plexus chorioiditis
5	41 °C fever, ataxia, body tremors, convulsions	5.43×10^7	High grade multifocal fibro-purulent meningitis and moderate multifocal plexus chorioiditis
34	41.7 °C fever, body tremors, abdominal reinforced breathing, nystagmus, opisthotonus	3.03×10^7	Moderate multifocal fibro-purulent meningitis (no comment on the state of the CP)

Before the brain was preserved in formalin, one CP was removed from one lateral ventricle and flash frozen in liquid nitrogen. Following the RNA isolation, a semi-quantitative RT-PCR was performed in order to confirm an inflammatory response at the CP of *in vivo S. suis* ST2 infected piglets. The same inflammatory genes encoding for the cytokines and chemokines, IL1β, IL8, and CXCL2, used to evaluate the PCPEC, were also used for this sample set. As depicted in Figure 13, the CP isolated from piglets suffering from meningitis shows a clear inflammatory response by the increased expression (enhanced signal when referencing the GAPDH signal) of the genes encoding IL1β and IL8, as compared to the meningitis-free piglets. The signal for the CXCL2 expression, in contrast, was only enhanced for some piglets suffering from meningitis. Again, as was observed in the semi-quantitative RT-PCR performed with the PCPEC (Figure 12), a basal level of expression was present for IL8 and CXCL2 in all three piglets. However, IL1β was found to be basally expressed in two out of the three meningitis-free piglets. GAPDH was used as a house-keeping gene, which displayed a non-coherent expression likely due to either the heterogeneous cell population found in the CP tissue or lower RNA integrities compared to RNA from the *in vitro* infection experiments (Figure 14).

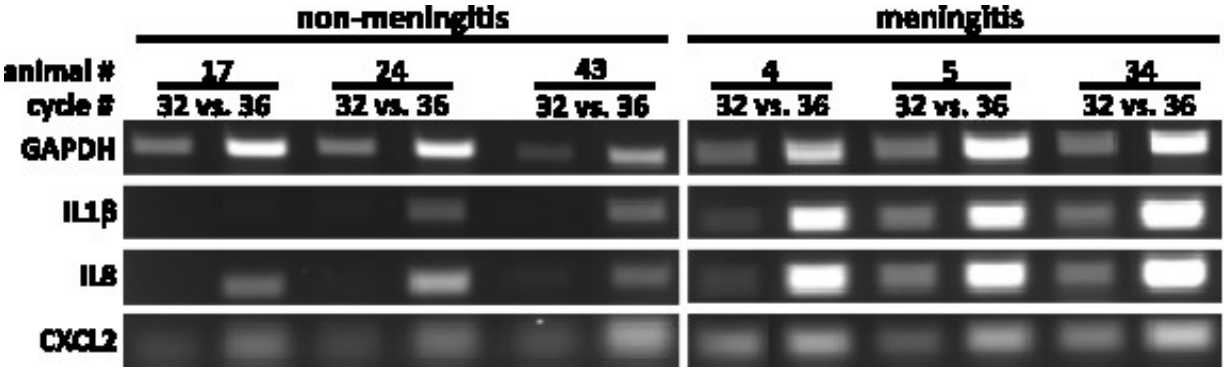

Figure 13. The choroid plexus of *S. suis* ST2 *in vivo* infected piglets shows an inflammatory response in comparison to piglets not suffering from meningitis. The samples were run on a 1.5 % agarose-ethidium bromide gel and the image was captured using the Vision-Capt software.

Following the confirmation of an inflammatory response at the CP of pigs suffering from meningitis in comparison to meningitis-free animals, the samples from these six animals were selected for further global transcriptome analysis via RNA-seq.

4.4. RNA-sequencing quality controls and sequencing alignment analysis

Preceding the RNA-seq analysis, two quality controls were performed to ensure reliable input for a proper downstream analysis. The first quality control consisted of evaluating the RNA integrity. Following the confirmation of high quality RNA as input, the RNA-seq library was prepared and a second quality control of the library was performed to ensure the correct fragment sizes and determine the concentration.

Following the RNA-seq, the quantity and the transcript alignment of the reads to the reference genome were analyzed.

For each sample set (HIBCPP cells, PCPEC, CP from *in vivo* studies), biological triplicates for each condition (uninfected versus *S. suis* ST2 H4 infected / meningitis-free versus meningitis) were selected for a global transcriptome analysis via RNA-seq.

4.4.1. RNA samples were of high integrity for RNA-seq analysis

The first control step, before the RNA samples were prepared for RNA-seq, was to perform a quality control of the RNA. For this, the RIN was determined by evaluating the ratio of the 28S and 18S rRNA. A score of 10 is given when the ratio of 28S to 18S rRNA is 2:1, indicating no degradation, and a score below 10 indicating various levels or rRNA degradation (Schroeder et al., 2006).

A good RNA integrity is an important factor during sequencing analysis for a reliable down-stream analysis. Previous studies examined the correlation between RNA integrity and accurate transcript quantification, and it has been suggested that utilizing RNA with a RIN of at least 6 yielded the most reliable results in down-stream analysis for data interpretation (Gallego Romero et al., 2014; Kukurba and Montgomery, 2015).

Figure 14 summarizes the electropherograms produced by the Agilent 2100 Bioanalyzer, which was used to evaluate the RNA integrity. Based on the surface area of each peak, the ratio between the 28S and 18S rRNA is determined, and a score is given by the software of the Agilent 2100 Bioanalyzer. Each biological replicate underwent this quality control preceding the RNA-seq.

All biological replicates of the uninfected (Figure 14 A) and *S. suis* ST2 H4 infected (Figure 14 B) HIBCPP cells displayed a very high RIN, with the lowest RIN being 9.5. Additionally, all biological samples for uninfected (Figure 14 C) and infected (Figure 14 D) PCPEC exhibited a high RIN, with the lowest RINs being 8.9. These high RIN values are indicated by the two large, distinct peaks at 42 sec and 49 sec, indicative of the 18S and 28S rRNA, respectively.

The RNA quality of the RNA isolated from the CP tissue isolated following the *in vivo* infection experiments generally displayed lower, but overall good, RINs. The RINs from the meningitis-free animals (Figure 14 E) and animals suffering from meningitis (Figure 14 F) were above 8.5, with exception of one sample, the CP from pig number 34 suffering from meningitis, having a RIN of 7.4.

The RNA samples isolated following the infection experiments displayed good quality, and were therefore processed further via RNA-seq library preparation, as described in section 3.5.2. Subsequently to the library preparation, the library was evaluated for fragment sizes and profile on the Agilent 2100 Bioanalyzer, which were approximately 300 bp for the HIBCPP library and 350 bp for the porcine (*in vitro* and *in vivo* samples) libraries (data not shown).

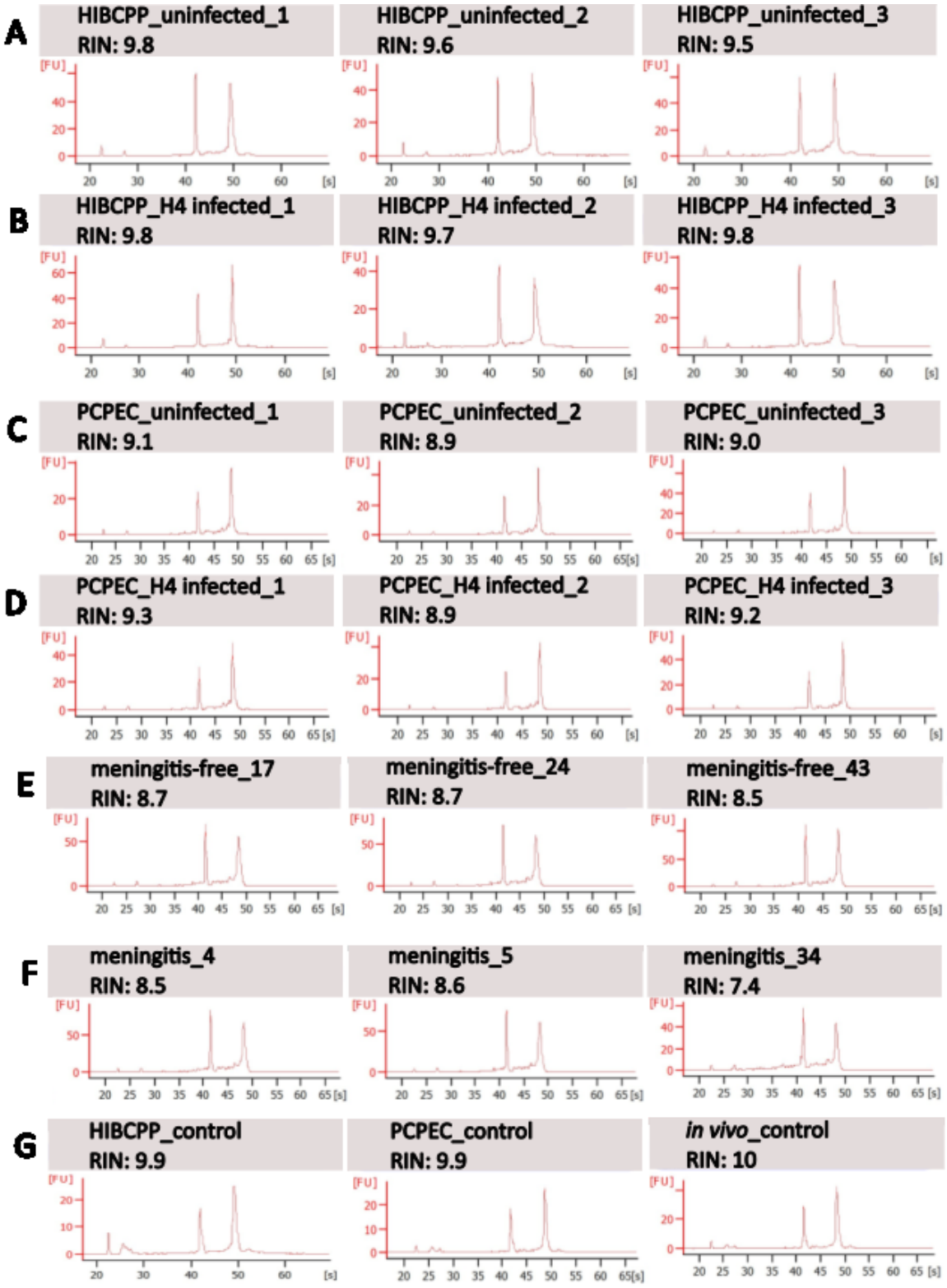

Figure 14. Summary of the Agilent 2100 Bioanalyzer electropherogram depicts RNA with high integrity used as starting material for RNA-seq. The label for each electropherogram lists the sample origin, phenotype, and biological replicate or animal number, along with the RIN for each sample. The distinct peaks at approximately 42 sec and 49 sec are indicative of the 18S and 28S rRNA, respectively, whereas the small peak appearing at approximately 28 sec is indicative of the 5S rRNA subunit. The small peak appearing at approximately 22 sec is indicative of the marker.

4.4.2. Bioinformatic processing post-sequencing revealed efficient mapping to exon gene regions

Following the sequence run, the generated reads were aligned to either the human or the porcine reference genome with the RNA aligner STAR (Dobin et al., 2013), which was part of the PartekGS software (2.10). Subsequently, the aligned reads were mapped and assigned to corresponding host transcripts, thereby simultaneously quantifying them. Evaluation of the alignment and mapping efficiency to the reference genome is an important aspect before proceeding with the data interpretation, in order to determine sequencing accuracy and DNA contamination (Conesa et al., 2016). Since we want to investigate the transcriptional profile change of protein-coding genes during the state of *S. suis* ST2 infection, efficient mapping to exon regions of mRNA transcripts is necessary.

Table 12 summarizes the output generated following the read alignment to the human or porcine reference genomes. No pre-defined ranges exist for acceptable values for the various parameters. Instead, suggestions exist based on experimental aim or set-up (Conesa et al., 2016).

The total number of reads reflects the sequencing depth achieved for each sample. Approximately 20 million reads were generated per sample of the HIBCPP cell sample set and for the samples originating from the *in vivo* infection experiments, and approximately 10 million reads were generated for the PCPEC samples. For the PCPEC, less reads were generated for the samples due to the sequencing mode, which was set to rapid-run, in contrast to high-output sequencing mode selected for HIBCPP cells. However, neither of the two sequence modes have an effect on the data output.

For the HIBCPP cell samples, approximately 62 - 74 % of the aligned reads fully overlapped to an exon region, and up to approximately 15 % fully overlapped an intron region of the reference genome. The aligned reads obtained from the samples of porcine origin (*in vitro* and *in vivo* samples) displayed a higher full exon overlap, of approximately 80 %, and only approximately 4 % fully overlapping to an intron region.

Approximately 8 % human and 5 % of porcine paired-end reads had one aligned read, which displayed an overlap with an exon region, but was not compatible with any transcript due to no compatible alignment of the second read and, therefore, did not contribute to transcript read count.

All samples displayed a very low percentage of transcripts which partially overlapped an exon region (2 % or less), and approximately 10 % of reads which were located between genes.

Additionally, about 70 % of transcripts in the models (62,083 for human and 49,447 for pigs) had reads aligned to them. Lastly, the majority of reads which aligned to an intron-exon junction were compatible with a transcript.

The alignment and mapping summary post-sequencing displayed values within acceptable ranges for all samples which underwent sequencing and alignment, and therefore, were statistically analyzed in the next step.

Sample ID	Number of Alignments	Total Number of Reads	% of reads which fully overlap exon	% of PE reads where one alignment fully overlaps an exonic region but the reads is not compatible with any transcript	% of reads which partially overlap exon	% of reads within an intron	% of reads between genes	Total number of transcripts in the model	% of transcripts with reads	Total reads with junctions	Reads with junctions that are compatible with a transcript
HIBCPP											
uninfected 1	418129980	215888301	74.0	8.5	0.97	5.85	10.27	62083	68.61	8743330	7671827
uninfected 2	44089136	22735231	70.1	8.6	1.10	9.16	11.05	62083	68.43	8653330	7607078
uninfected 3	50319995	25851941	62.2	8.5	1.51	1.65	11.61	62083	68.83	8872975	7742916
H4_1	45962652	23703216	70.4	8.5	1.05	8.44	11.78	62083	68.45	8945455	7848024
H4_2	45420281	23418693	68.7	8.4	1.31	10.04	11.31	62083	68.39	8652365	7574587
H4_3	43455157	22366536	68.0	7.8	1.50	15.80	11.91	62083	68.89	7547908	6601683
PCPEC											
uninfected 1	24567537	12320165	79.9	5.7	1.78	3.92	8.68	49447	71.73	5451784	4755696
uninfected 2	24811641	12443572	80.7	5.8	1.77	3.56	8.20	49447	72.19	5584892	4876506
uninfected 3	21868765	11030540	79.6	7.0	1.82	3.46	8.08	49447	71.45	4983861	4200845
H4_1	24639006	12356225	80.5	5.8	1.81	3.58	8.31	49447	69.70	5475811	4767420
H4_2	23250548	11668472	80.8	5.8	1.79	3.55	8.00	49447	71.78	5166339	4511482
H4_3	26909456	13497069	80.6	5.8	1.76	3.60	8.26	49447	72.07	5931923	5183824
In vivo											
meningitis-free_17	391043280	195993634	80.4	5.8	1.85	3.65	8.25	49447	73.42	8886653	7723674
meningitis-free_24	472100006	236855559	80.1	5.8	1.96	3.96	8.24	49447	74.39	10540261	9200179
meningitis-free_43	413645431	207286556	80.5	5.9	1.88	3.56	8.14	49447	73.67	9427844	8193555
meningitis_4	320240006	160651805	78.8	5.7	2.03	4.46	8.93	49447	74.45	11259045	9811894
meningitis_5	403871285	202455568	78.4	5.7	2.10	4.91	8.82	49447	73.59	8621131	7496964
meningitis_34	304484850	152175887	80.1	5.7	1.93	3.80	8.49	49447	72.90	6568586	5722822

ped and aligned reads generated by the PartekGS software.

4.5. The statistical analysis of the sequenced samples via DEG and GSEA

Multiple data analysis tools exist today, which allow for the interpretation of the data generated during the high-throughput NGS analysis. The RNA-seq-generated data was statistically analyzed on two different levels in order to gain thorough insight, but to also gain a biological overview. The first evaluation included the generation of DEGs lists, which evaluate the differential gene expression of individual genes following different treatment conditions. The second evaluation was performed with the GSEA utilizing the MSigDB in order to give a biological interpretation of the samples during infection and uninfected states.

4.5.1. DEGs

The first aim to interpret the data was to determine the magnitude of statistically significant DEGs based on the number of reads detected during the alignment and mapping process by the PartekGS software. This software applied a one-way ANOVA test in order to generate lists of significantly DEGs (uncorrected $p \leq 0.05$) for the samples which were infected with *S. suis* ST2 in relation to uninfected host cells or meningitis-free animals. An additional DEG list was generated with a corrected *p*-value, in order to correct for multiple testing (De and Baron, 2012). As an additional filtering step, only genes which displayed at least 10 raw reads of a transcript in all three biological replicates for one class (uninfected versus infected) were taken into consideration for the final DEG list.

A total of 1,479 significant ($p \leq 0.05$) DEGs were identified following the analysis of *S. suis* ST2 infected versus uninfected HIBCPP cells. However, only a total of 63 DEGs were identified, which exhibited at least a 2-fold up- or down-regulation, of which 32 genes displayed an up-regulation and 31 genes displayed a down-regulation. The results of the uncorrected *p*-values are presented in Table 13, since the correction of the *p*-value yielded no significantly DEGs (data not shown). Table 13 summarizes the significant DEGs for infected versus uninfected HIBCPP cells, which showed a fold change of at least 2 (up- and down-regulated) and had an uncorrected *p*-value of ≤ 0.05.

The highest significant up-regulation observed was a 3.6 fold change for the gene encoding for ZFPL36L1. The strongest down-regulation was observed for the microRNA3648 with an 8-fold change. Interestingly, the majority of the genes only exhibited a 2- to 3-fold differential expression following the 6 h infection period with *S. suis* ST2.

Table 13. A total of 63 genes were significantly differentially expressed in *S. suis* ST2 infected versus uninfected HIBCPP cells. The significance and gene fold change were determined with the PartekGS software implementing the one-way ANOVA test. Significant DEGs with a ±2 fold change and an uncorrected *p*-value ≤ 0.05 are presented.

Gene Symbol	Gene Name	*p*-value	Fold Change
ZFP36L1	ZFP36 ring finger protein like 1	0.0427	3.5
PCK1	Phosphoenolpyruvate carboxykinase 1	0.0254	3.3
TCIM	Transcriptional and immune response regulator	0.0249	3.1
LOC100996419	uncharacterized ncRNA	0.0247	3.0
C8orf44-SGK3	Chromosome 8 open reading frame 44 - Serum/glucocorticoid regulated kinase family member 3 readthrough	0.0415	2.9
HLA-F-AS1	Major histocompatibility complex, class I, F antisense RNA 1	0.0059	2.7
ARIH2OS	Ariadne RBR E3 ubiquitin protein ligase 2 opposite strand	0.0420	2.7
FSBP	Fibrinogen alancer binding protein	0.0223	2.6
FBXL8	F-box and leucine rich repeat protein 8	0.0137	2.6
LIFR-AS1	Leukemia inhibitory factor receptor antisense RNA1	0.0879	2.5
RASA4	RAS p21 protein activator 4	0.0090	2.5
MXI1	MAX interactor 1, dimerization protein	0.0430	2.5
LINC00887	Long intergenic non-protein coding RNA 887	0.0136	2.5
MHENCR	Melanoma highly expressed competing endogenous lncRNA for miR-425 and miR489	0.0373	2.4
ARL14	ADP ribosylation factor like GTPase 14	0.0211	2.4
PIK3IP1	Phosphoinositide-3-kinase interacting protein 1	0.0063	2.4
LINC01431	Long intergenic non-protein coding RNA 1431	0.0484	2.3
LINC02482	Long intergenic non-protein coding RNA 2482	0.0027	2.3
C12orf76	Chromosome 12 open reading frame 76	0.0302	2.3
KLHL24	Kelch like family member 24	0.0091	2.3
RND1	Rho family GTPase 1	0.0282	2.2
TCP11L2	T-complex 11 like 2	0.0372	2.2
PNRC1	Proline rich nuclear receptor coactivator 1	0.0395	2.1
PRKAR2A-AS1	Protein kinase cAMP-dependent type II regulatory subunit alpha antisense RNA 1	0.0101	2.1
CDKN1C	Cyclin dependent kinase inhibitor 1C	0.0288	2.0
RNF39	Ring finger protein 39	0.0149	2.0
FHOD3	Formin homology 2 domain containing 3	0.0349	2.0
ZEB1-AS1	Zinc finger E-box binding homeobox 1 antisense RNA 1	0.0122	2.0
DBP	D-box binding PAR bZIP transcription factor	0.0052	2.0
LOC440934	uncharacterized ncRNA	0.0230	2.0
LENG8-AS1	Leukocyte receptor cluster, member 8 antisense RNA 1	0.0325	2.0
MST1	Macrophage stimulating 1	0.0073	2.0
LCMT2	Leucine carboxyl methyltransferase 2	0.0025	-2.0
SHOX2	Short stature homeobox 2	0.0091	-2.0
TRIM25	Tripartite motif containing 25	0.0236	-2.0
IBA57	IBA57 homolog, iron-sulfur cluster assembly	0.0043	-2.0
URB2	URB2 ribosome biogenesis homolog	0.0177	-2.0
ZNF778	Zinc finger protein 778	0.0263	-2.0
RGMB	Repulsive guidance molecular family member b	0.0153	-2.0
CLN8	Transmembrane endoplasmic reticulum (ER) and ER-Golgi intermediate Compartment protein	0.0137	-2.1
CD3EAP	CD3e molecule associated protein	0.0122	-2.1
NBPF12	Neuroblastoma breakpoint family member 12	0.0084	-2.1
SLC46A1	Solute carrier family 46 member 1	0.0019	-2.1
CYB561D1	Cytochrome b561 family member D1	0.0469	-2.1
EN2	Engrailed homeobox 2	0.0278	-2.1
CEBPA	CCAAT enhancer binding protein alpha	0.0105	-2.1
DHRS9	Dehydrogenase reductase 9	0.0379	-2.2
CHAC2	ChaC cation transport regulator homolog 2	0.0084	-2.2
FBXO9	F-box protein 9	0.0280	-2.2
ADAM1A	ADAM metallopeptidase domain 1A	0.0321	-2.3
ZNF283	Zinc finger protein 283	0.0147	-2.3
MIR22HG	lncRNA MIR22 host gene	0.0424	-2.4
LRRC26	Leucine rich repeat containing 26	0.0158	-2.4
POC1B-GALNT4	POC1 centriolar protein B - Polypeptide N-acetylgalactosaminyltransferase 4 readthrough	0.0159	-2.5
EIF5	Eukaryotic translation initiation factor 4E	0.0293	-2.6
DUSP2	Dual specificity phosphatase 2	0.0146	-2.6
CDK5R1	Cyclin dependent kinase 5 regulatory subunit 1	0.0145	-2.8
FGF18	Fibroblast growth factor 18	0.0347	-2.8
KBTBD8	Kelch repeat and BTB domain containing 8	0.0338	-3.1
SNAR-G1	Small ILF3/NF90-associated RNA G1	0.0196	-5.7
SNORA64	Small nucleolar RNA, H/ACA box 64	0.0056	-7.8
MIR3648-1	microRNA 3648-1	0.0088	-8.0
MIR3648-2	microRNA 3648-2	0.0088	-8.0

For the *in vitro S. suis* ST2 infected PCPEC samples, a total of 430 genes were identified as significantly differentially regulated with an uncorrected *p*-value ≤ 0.05. However, only a total of 50 genes displayed a significant differential regulation, of which 46 genes exhibited an up-regulation of at least 2-fold, and 4 genes exhibited a down-regulation of at least 2-fold.

Table 14 summarizes the significant DEGs for *S. suis* ST2 infected versus uninfected primary PCPEC, which showed a fold change of at least 2 (up- and down-regulated).

Interestingly, the *in vitro* infected primary PCPEC displayed a very strong cellular response during the infection with *S. suis* ST2, with a maximum of 134-fold up-regulation for IL1β. A total of 21 genes exhibited an up-regulation of at least 3-fold, with the majority of these genes known to being involved in the inflammatory response and regulation. The differential gene fold change observed in *S. suis* ST2 infected PCPEC shows a much stronger response of the porcine epithelial cells in comparison to the human epithelial cells.

In contrast, a total of only four genes encoding for VSIG4, DLGAP5, KNL1, and STRC were significantly differentially down-regulated during *S. suis* ST2 infection. The gene encoding for STRC was the highest significantly down-regulated gene, which exhibited a maximum down-regulation of 3-fold change.

When evaluating the DEG list of genes with a corrected *p*-value, only one gene encoding for ACOD1 remained significant ($p = 0.025$; data not shown).

Table 14. A total of 50 genes were significantly differentially expressed in *S. suis* ST2 infected versus uninfected PCPEC. The significance and gene fold change were determined with the PartekGS software implementing the one-way ANOVA test. Significant DEGs with a ±2 fold change and an uncorrected *p*-value ≤ 0.05 are presented.

Gene Symbol	Gene Name	*p*-value	Fold Change
IL1β	interleukin 1 beta	0.041	134.0
TNF	tumor necrosis factor	0.006	70.7
ACOD1	aconitate decarboxylase 1	0.000	52.2
ENSSSCG00000032343	uncharacterized	0.001	39.3
IL1α	interleukin 1 alpha	0.002	29.3
CCL3L1	chemokine (C-C motif) ligand 3-like 1	0.006	27.9
CXCL8	C-X-C motif chemokine ligand 8 (aka IL8)	0.006	22.6
AMCF-II	alveolar macrophage-derived chemotactic factor II (aka CXCL6)	0.009	15.1
CXCL2	chemokine (C-X-C motif) ligand 2	0.017	13.8
CCL2	chemokine (C-C motif) ligand 2	0.026	12.1
SLAMF7	SLAM family member 7	0.025	11.4
RND1	Rho family GTPase 1	0.023	10.9
ENSSSCG00000008954	uncharacterized	0.006	10.4
CCL11	chemokine (C-C motif) ligand 11	0.008	9.1
VCAM1	vascular cell adhesion molecule 1	0.019	8.0
PLEK	pleckstrin	0.003	5.1
DEPP1	DEPP1 autophagy regulator	0.009	5.0
RELB	avian reticuloendotheliosis viral (v-rel) oncogene related B	0.005	4.6
NFKBIZ	nuclear factor of kappa light polypeptide gene enhancer in B cells inhibitor, zeta	0.041	4.5
NFKBIA	nuclear factor of kappa light polypeptide gene enhancer in B cells inhibitor, alpha	0.016	3.9
CEBPD	CCAAT/enhancer binding protein (C/EBP), delta	0.027	3.2
GDF15	growth differentiation factor 15	0.001	2.8
IRF1	interferon regulatory factor 1	0.017	2.7
MAFF	v-maf musculoaponeurotic fibrosarcoma oncogene family, protein F (avian)	0.001	2.7
TCIM	Transcriptional and immune response regulator	0.001	2.7
SIK1	salt inducible kinase 1	0.000	2.6
CABP1	calcium binding protein 1	0.007	2.4
CCL5	chemokine (C-C motif) ligand 5	0.031	2.4
ICAM1	intercellular adhesion molecule 1	0.005	2.4
JUNB	jun B proto-oncogene	0.004	2.4
MAP3K8	mitogen-activated protein kinase kinase kinase 8	0.015	2.4
RSAD2	radical S-adenosyl methionine domain containing 2	0.034	2.3
STC2	stanniocalcin 2	0.036	2.3
PLAU	plasminogen activator, urokinase	0.020	2.3
PLEKHS1	pleckstrin homology domain containing, family S member 1	0.006	2.3
NEURL3	neuralized E3 ubiquitin protein ligase 3	0.015	2.3
SLCO1B3	solute carrier organic anion transporter family member 1B3	0.012	2.2
PDE4B	phosphodiesterase 4B, cAMP specific	0.001	2.2
IL6	interleukin 6	0.026	2.2
ELF3	E74-like factor 3	0.036	2.2
PFKFB3	6-phosphofructo-2-kinase/fructose-2,6-biphosphatase 3	0.003	2.1
SRGN	serglycin	0.050	2.1
ZC3H12A	zinc finger CCCH type containing 12A	0.004	2.1
FAM83D	family with sequence similarity 83, member D	0.005	2.0
TIFA	TRAF-interacting protein with forkhead-associated domain	0.023	2.0
KCNK3	potassium channel, subfamily K, member 3	0.020	2.0
VSIG4	V-set and immunoglobulin domain containing 4	0.017	-2.1
DLGAP5	DLG associated protein 5	0.046	-2.6
KNL1	kinetochore scaffold 1	0.029	-2.7
STRC	stereocilin	0.037	-3.0

Finally, a total of 3355 DEGs with an uncorrected *p*-value of ≤ 0.05 were identified in the CP of pigs suffering from *S. suis* ST2 – induced meningitis in relation to meningitis-free pigs. The DEG list of significant genes with an uncorrected *p*-value ≤ 0.05 presented 479 genes, which were at least ± 2-fold regulated, of which 171 genes were up-regulated and 308 genes were down-regulated (data not shown). Due to this large size, the significant DEGs with corrected *p*-values are presented in Table 15.

In total, 30 genes which were significantly differentially regulated exhibited a fold change of at least ± 2 with a corrected *p*-value of ≤ 0.05. 12 of the 30 genes displayed an up-regulation and 18 genes displayed a down-regulation. Table 15 summarizes the significant DEGs found in the CP, from animals suffering from meningitis versus meningitis-free piglets which showed a fold change of at least 2 (up- and down-regulated) and a corrected *p*-value of ≤ 0.05.

The strongest up-regulation was 11.3-fold for the gene encoding INSM1, whereas the strongest down-regulation was 6.3-fold for the gene encoding for TIMD4. Furthermore, of the 30 genes identified in Table 15, 13 genes exhibited a fold change ± 3.

Table 15. A total of 30 genes were found to be significant Differentially Expressed Genes in the choroid plexus of pigs suffering from *S. suis* ST2 – induced meningitis versus meningitis-free pigs. The significance and gene fold change were determined with the PartekGS software implementing the one-way ANOVA test. Significant DEGs with a ±2 fold change and a corrected *p*-value ≤ 0.05 are presented.

Gene Symbol	Gene Name	*p*-value	Fold Change
INSM1	insulinoma-associated 1	0.0002	11.3
GABRB1	gamma-aminobutyric acid A receptor, subunit beta 1	0.0002	5.0
INHBB	inhibin beta-B	0.0003	5.0
ENSSSCG00000000659	uncharacterized	0.0001	4.9
PVR	poliovirus receptor	0.0003	3.8
CUBN	cubilin	0.0001	2.9
EMP2	epithelial membrane protein 2	0.0003	2.7
CRNN	cornulin	0.0002	2.7
DERL3	Der1-like domain family, member 3	0.0002	2.7
HSP90B1	heat shock protein 90 kDa beta member 1	0.0000	2.2
GPR3	G-protein coupled receptor 3	0.0004	2.2
GPR146	G-protein coupled receptor 146	0.0004	2.0
ALDH3B1	aldehyde dehydrogenase 3 family member B1	0.0002	-2.0
DNAAF1	dynein, axonemal assembly factor 1	0.0002	-2.2
ENSSSCG00000036652	uncharacterized	0.0003	-2.3
HYKK	hydroxylysine kinase 1	0.0001	-2.3
MTMR8	myotubularin related protein 8	0.0003	-2.3
EIF2D	eukaryotic translation initiation factor 2D	0.0002	-2.4
SYTL1	synaptotagmin-like 1	0.0000	-2.5
POLE	polymerase (DNA directed), epsilon	0.0004	-2.5
ENSSSCG00000013144	uncharacterized	0.0000	-2.9
SORD	sorbitol dehydrogenase	0.0003	-2.9
VWA5A	von Willebrand factor A domain containing 5A	0.0002	-3.1
PRDM16	PR domain containing 16	0.0002	-3.3
RBM3	RNA binding motif protein 3	0.0002	-3.9
FLRT1	fibronectin leucine rich transmembrane protein 1	0.0004	-4.8
ACEA_U3		0.0001	-5.5
U3		0.0001	-5.5
TYMS	thymidylate synthase	0.0002	-6.1
TIMD4	T cell immunoglobulin and mucin domain containing 4	0.0002	-6.3

When comparing the PartekGS-generated significant DEG lists with an uncorrected p-value, the CP isolated following the *in vivo* infection experiments with *S. suis* ST2 resulted in the highest number of significantly DEGs, with a total of 479 genes which exhibited a fold change of at least 2 or below -2. In contrast, the infected HIBCPP cells and PCPEC displayed 63 and 50, respectively, significantly DEGs with a fold change above 2 or below -2. Furthermore, the highest observed fold change for infected HIBCPP cells was 8, whereas for the infected PCPEC the highest observed fold change was 134. For the data resulting from the *in vivo* samples, a significant fold change 3 or above was observed for 5 genes, with the highest being 11.3. Only two overlapping significant DEGs were identified in the infected CP epithelial cells, HIBCPP cells and PCPEC, and included transcriptional and immune response regulator (TCIM) and Rho family GTPase 1 (RND1).

The DEG lists give a first indication of individual significantly differentially regulated genes during the state of a *S. suis* ST2 infection in epithelial cells or at the CP during acute meningitis in comparison to uninfected cells or the CP of meningitis-free animals. In order to gain further insight and understand the biological processes, a GSEA was performed.

4.5.2. GSEA

In addition to identifying the significance of differential expression of individual genes, we also performed a GSEA in order to evaluate the data in terms of biologically relevant functions. The GSEA was originally developed by Mootha and colleagues, and first described by Subramanian and colleagues, in order to give a biological interpretation of data generated during high-throughput analysis (Mootha et al., 2003; Subramanian et al., 2005). The GSEA makes use of the MSigDB, which contains annotated Gene Sets (GSs) that are divided into eight large categories, composed of genes sharing or being involved in a biological function (Liberzon et al., 2011; Subramanian et al., 2005). Through an algorithm applied by the GSEA software, individual genes, which are assigned to GSs based on *a priori* knowledge, are ranked and assigned an enrichment score based on how strong they distinguish between, for e.g., the state of infection compared to an uninfected state, but also how often the gene is encountered (Subramanian et al., 2005).

However, the enrichment score reflects gene enrichment within a single GS. Since different GS are composed of a varying amount of genes, the GS size needs to be taken into consideration in order to draw comparisons of the enrichment between different GSs, thereby resulting in a normalized enrichment score (NES). In this study, a positive NES represents GSs, which are positively enriched in infected epithelial cells or the CP of pigs suffering from meningitis, whereas a negative NES

represents enriched GSs in either uninfected host cells or the CP of meningitis-free pigs. GSs which exhibited a NES of ± 2 were further taken into considered during the evaluation of the data.

Furthermore, when evaluating an enriched GS, the most important aspect to take into consideration is the probability of the results presenting a true or false positive, which is identified through the FDR. A FDR value of below or equal to 0.25 is considered significant in the GSEA, which is indicative of the result being statistically a true-positive in 75 % of the cases (Subramanian et al., 2005).

In addition to attributing enriched genes to pre-defined GSs, GSEA also evaluated the individual genes for their enrichment and how well their expression differentiates in the two phenotypes. Figure 15 depicts the heat-map generated in the GSEA analysis of the top 50 genes, which were found to be most distinguishing between *S. suis* ST2 infected epithelial cells or animals suffering from meningitis and uninfected epithelial cells or meningitis-free animals. The dark red is indicative of genes, which show the strongest differentiation in a positive direction in the infected/meningitis phenotype, whereas dark blue represent a strong differential expression towards a negative direction in the uninfected/meningitis-free phenotype.

The strongest coherent differential expression between the biological triplicates for each phenotype can be observed for the samples, which originated from the porcine *in vivo* experiments. However, strong coherence was observed for the majority of the biological HIBCPP cells and PCPEC replicates.

Furthermore, the majority of the GSEA enriched genes was also identified with the PartekGS software, and which can be found in the presented DEG lists in section 4.5.1.

Overall, the majority of the top 50 enriched genes displayed coherent differentiation in all biological replicates for the investigated phenotype. Interestingly, the top enriched genes determined by the GSEA software were also identified through the DEG analysis performed with the PartekGS software.

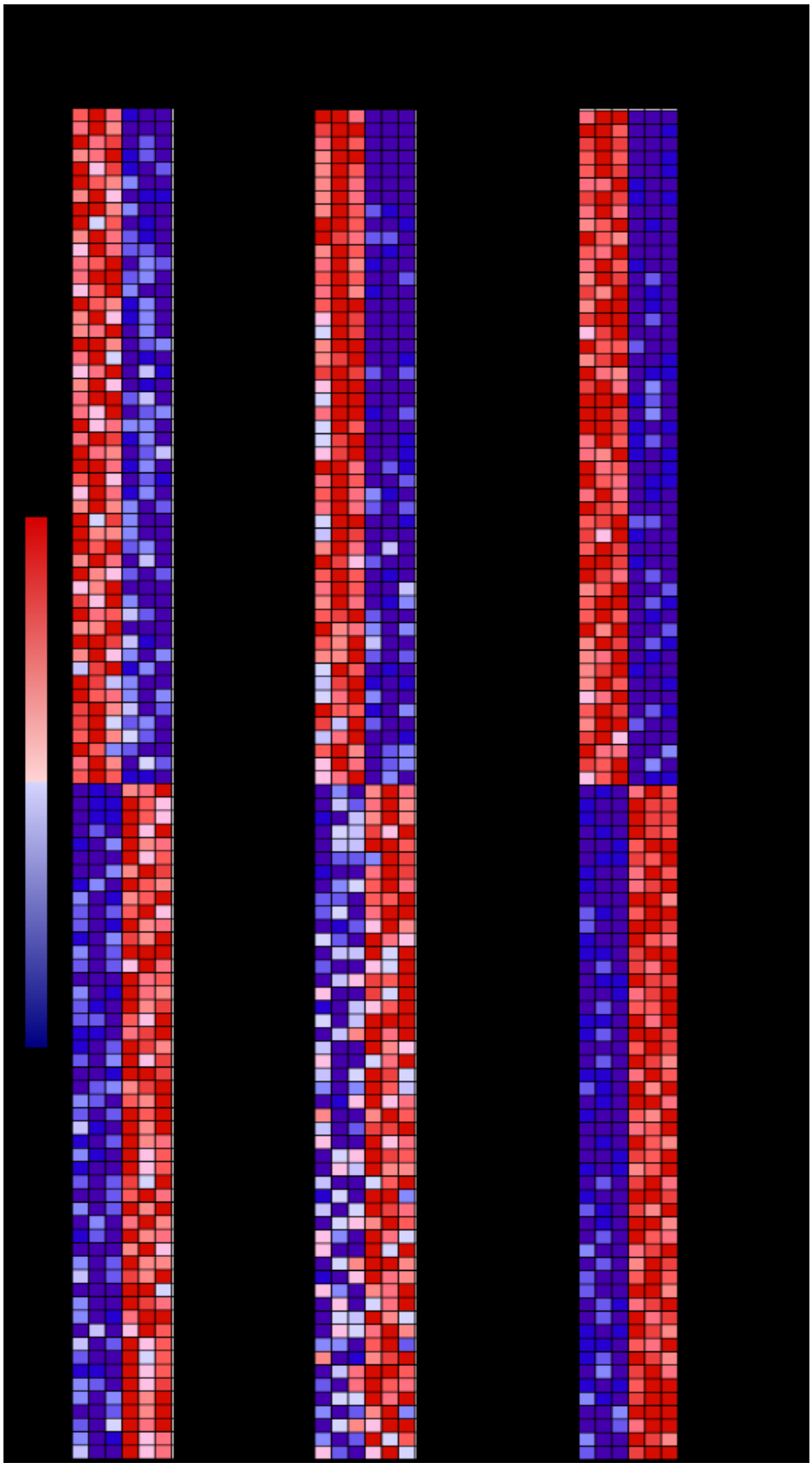

Figure 15. The GSEA generated heat-map depicts a coherent expression of the biological triplicates for all sample sets of the top 50 ranked genes. Dark red reflects gene enrichment of infected cells or animals suffering from meningitis. Dark blue reflects gene enrichment in uninfected cells or meningitis-free pigs.

4.5.2.1. The enrichment of hallmark GSs in infected human and porcine CP cells, and the in vivo CP response

The hallmark GS was first described by Liberzon and colleagues, and consists of 50 GSs, which represent well-defined and coherent biological states (Liberzon et al., 2015). They were generated from GSs published in the seven major categories, and were created in order to reduce redundancy. Furthermore, these 50 GSs are divided into eight major biological categories of: cellular components, development, immune reaction, cellular metabolism, pathways, cellular proliferation, signaling, and DNA damage (Liberzon et al., 2015). The hallmark GS collection is usually the first step in the data assessment to gain an overview of significant biological functions of the sample set in order to explore new targets and develop new hypotheses.

The GSEA of analyzed HIBCPP cell samples revealed that a total of 18 GSs out of the 50 hallmark GS collection were found to be significantly enriched in 6 h *S. suis* ST2 infected cells. Table 16 presents the significantly enriched hallmark GSs, which exhibited a FDR *q*-value of less than or equal to 0.25. The majority of the significantly enriched GSs can be categorized into cell signaling, and include TNFα signaling via NFκB, IL2-STAT5, GSs with up- and down-regulated genes by KRAS activation, and transforming growth factor beta (TGFβ) signaling. Additionally, five GSs belonging to the immune cellular processes were significantly enriched and include inflammatory response, interferon γ response, IL6-JAK/STAT3 signaling, allograft rejection, and complement system. Furthermore, the most significantly enriched GS was hypoxia (NES 3.24, *q*-value 0.000), and is categorized into the cellular pathways, along with apoptosis (NES 1.53, *q*-value 0.032). The GS epithelial-mesenchymal transition (EMT) was the third significantly enriched GS (NES 1.98, *q*-value 0.001) and belongs to the category of cellular development along with myogenesis (NES 1.54, *q*-value 0.030). Lastly, the apical surface GS belonging to the category of cellular component, and the P53 pathway belonging to cellular proliferation were also found to be significantly enriched. A summary of the significantly enriched GSs designated to the respective cellular processes, as well as the percentage of the designated enriched GSs of the total number of significant GSs, are depicted in Figure 16.

Table 16. GSEA of 18 hallmark GSs, which are significantly enriched in *S. suis* ST2 infected HIBCPP cells. The normalized enrichment score (NES) represents the extent of GS enrichment, taking the number of genes ("size"), which compose the GS, into account. The false discovery rate (FDR) is considered significant if *q* is ≤ 0.25.

Hallmark Gene Set Name	Size	NES	FDR *q*-value
Hypoxia	158	3.24	0.000
TNFα Signaling via NFκB	168	2.87	0.000
Epithelial-Mesenchymal transition	112	1.98	0.001
Apical surface	29	1.85	0.002
Glycolysis	171	1.78	0.012
Cholesterol homeostasis	68	1.73	0.012
Inflammatory Response	111	1.69	0.014
IL2-STAT5 Signaling	146	1.60	0.022
Myogenesis	107	1.54	0.030
Apoptosis	126	1.53	0.032
P53 Pathway	177	1.48	0.045
KRAS Signaling_up	124	1.45	0.057
Interferon γ response	159	1.44	0.056
KRAS Signaling_down	70	1.35	0.089
IL6-JAK/STAT3 Signaling	55	1.34	0.090
Allograft rejection	105	1.20	0.210
TGFβ Signaling	48	1.19	0.210
Complement	132	1.19	0.208

Table 17 summarizes the enriched GSs of the response of the infected PCPEC. A total of 28 GSs were found to be significantly enriched and displayed a FDR of $q \leq 0.25$. The majority of enriched GSs are categorized into the cellular signaling and include the GSs TNFα signaling via NFκB, IL2-STAT5, Wnt/β-catenin, early estrogen response, up- and down-regulated genes by KRAS activation, NOTCH, TGFβ, androgen response, and mTORC1 signaling. The category with the second most enriched GSs were found to belong to the immune response and include interferon α, γ, and inflammatory response, allograft rejection, IL6-JAK/STAT3 signaling, complement system, and coagulation. Interestingly, the top five enriched GSs display involvement of the immune response. The category containing the third most enriched GSs for the infected or meningitis phenotype was the cellular pathway and included hypoxia, apoptosis, unfolded protein response, and reactive oxygen species pathway. Furthermore, GSs categorized into cellular metabolism were also found to be enriched and included xenobiotic metabolism, glycolysis, and cholesterol homeostasis. The GSs angiogenesis and EMT, which are categorized into cellular development, were found to be enriched. Lastly, the GSs containing genes up-regulated in response to UV-radiation, categorized into cellular DNA damage response, and the P53 pathway belonging to the category of cellular proliferation, were enriched. A summary of the significantly enriched GSs designated to the respective cellular processes, as well as the percentage of the designated enriched GSs of the total number of significant GSs, are depicted in Figure 16.

Table 17. GSEA of 28 hallmark GSs, which are significantly enriched in infected primary PCPEC. The normalized enrichment score (NES) represents the extent of GS enrichment, taking the number of genes ("size"), which compose the GS, into account. The false discovery rate (FDR) is considered significant if *q* is ≤ 0.25.

Hallmark Gene Set Name	Size	NES	FDR *q*-value
TNFα signaling via NFκB	151	3.12	0.000
Interferon γ response	135	2.49	0.000
Inflammatory response	105	2.48	0.000
Allograft Rejection	108	2.20	0.000
IL6-JAK/STAT3 Signaling	48	2.19	0.000
Hypoxia	146	2.12	0.000
IL2-STAT5 Signaling	129	1.99	0.000
Interferon α response	73	1.90	0.001
Complement	136	1.88	0.001
UV response_up	115	1.87	0.001
Apoptosis	123	1.85	0.002
P53 Pathway	154	1.64	0.016
Coagulation	78	1.54	0.034
Unfolded protein response	93	1.51	0.044
Wnt/β-catenin	31	1.49	0.047
Reactive oxigen species pathway	40	1.47	0.051
Estrogen response_early	136	1.41	0.083
KRAS Signaling_up	127	1.39	0.090
Angiogenesis	23	1.37	0.101
NOTCH Signaling	25	1.36	0.102
KRAS Signaling_down	78	1.28	0.178
TGFβ Signaling	47	1.27	0.177
Xenobiotic Metabolism	129	1.24	0.200
Epithelial-Mesenchymal transition	153	1.24	0.192
Glycolysis	145	1.23	0.195
Cholesterol homeostasis	63	1.23	0.187
Androgen response	86	1.23	0.187
MTORC1 Signaling	162	1.20	0.210

Table 18 summarizes the enriched GSs of the response of the CP in animals, which suffered from meningitis. In total, 21 GSs were significantly (FDR $q \leq 0.25$) enriched.

The majority of the GSs belong in the category of cellular signaling, with these GSs being TNFα signaling via NFκB, IL2-STAT5, TGFβ, and Wnt/β-catenin signaling, early and late estrogen response, as well as androgen response, and the GS containing up-regulated genes following KRAS signaling. The categories for immune system, cellular development, and pathways all displayed an equal amount of enriched GSs. The inflammatory response, IL6-JAK/STAT3 signaling, and coagulation are categorized as immune response. The GSs angiogenesis, myogenesis, and EMT can be categorized under development, and hypoxia, unfolded protein response, and reactive oxygen species pathway are categorized under cellular pathways. Cholesterol homeostasis is categorized into cellular

metabolism, Myc targets fall under the category of proliferation, and the enriched GSs of genes up- or down-regulated in response to UV radiation belong to the cellular DNA damage response. A summary of the significantly enriched GSs designated to the respective cellular processes, as well as the percentage of the designated enriched GSs of the total number of significant GSs, are depicted in Figure 16.

Table 18. GSEA of the 21 hallmark GSs, which are significantly enriched in animals suffering from meningitis. The normalized enrichment score (NES) represents the extent of GS enrichment, taking the number of genes ("size"), which compose the GS, into account. The false discovery rate (FDR) is considered significant if *q* is ≤ 0.25.

Hallmark Gene Set Name	Size	NES	FDR *q*-value
TNFα signaling via NFκB	181	2.77	0.000
Inflammatory response	168	1.98	0.001
IL6-JAK/STAT3 Signaling	69	1.82	0.006
IL2-STAT5 Signaling	174	1.79	0.006
TGFβ Signaling	49	1.73	0.008
Hypoxia	167	1.70	0.008
Estrogen response_early	168	1.58	0.020
Androgen response	89	1.52	0.029
Wnt/β-catenin	36	1.52	0.026
UV response_up	133	1.47	0.036
Myc targets	49	1.40	0.059
Angiogenesis	30	1.36	0.074
Cholesterol homeostasis	66	1.35	0.073
UV response_down	129	1.33	0.078
Coagulation	106	1.33	0.074
Estrogen response_late	167	1.33	0.071
Unfolded protein response	94	1.29	0.089
KRAS Signaling_up	174	1.25	0.118
Reactive oxigen species pathway	40	1.24	0.115
Myogenesis	165	1.19	0.172
Epithelial-Mesenchymal transition	178	1.17	0.186

GSs which are enriched in uninfected cells or meningitis-free animals in comparison to the infected or diseased state were also evaluated and are summarized in Table 19. These GSs display a negative NES score and a FDR $q \leq 0.25$.

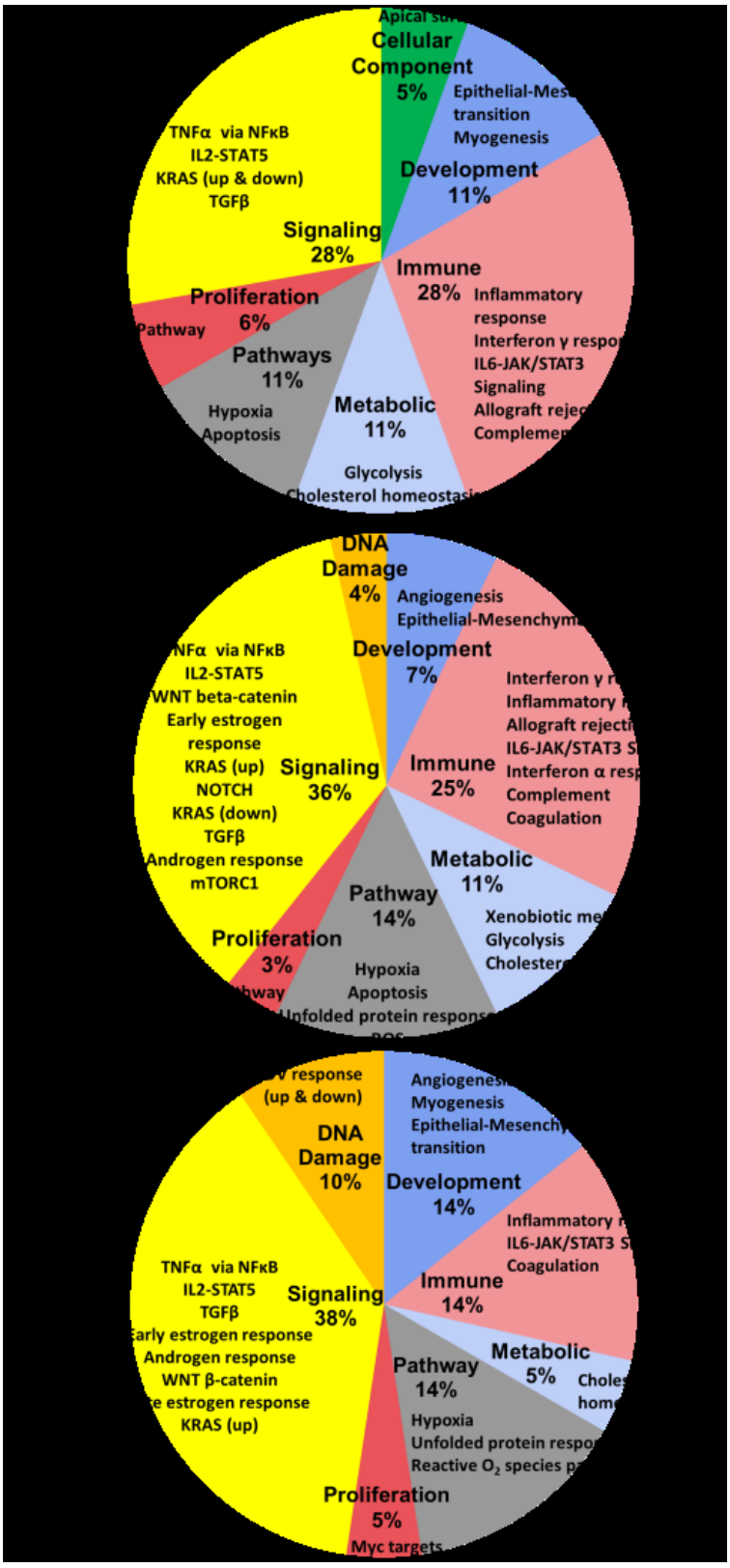

Figure 16. Summary of the enriched GSs of the hallmark GSEA for *S. suis* ST2 infected HIBCPP cells, PCPEC, and pigs. These pie-charts summarize the enriched GSs from Table 16 - Table 18. The percentage, which is listed under the bold labels indicating the cellular process category, is based on the total number of significantly (FDR $q \leq 0.025$) enriched GSs for the sample. The outer labels of the pie chart represent the significantly enriched GS for each sample which falls under the respective cellular process category.

In uninfected HIBCPP cells, the majority of enriched GSs were found to belong to the category of cellular proliferation and include the enrichment of the GSs, version 1 and 2, of genes regulated by Myc family members, genes regulated by the E2F transcription factors, and genes involved in the G2/M checkpoint of the cell division cycle. Furthermore, an enrichment of the GSs of unfolded proteins response, DNA repair, and spermatogenesis belonging to the cellular categories of pathways, DNA damage, and development, was observed.

The uninfected PCPEC displayed the least amount of significant enriched GSs. The GS containing genes regulated by the E2F transcription factors, belonging to the cellular proliferation category displayed a significant enrichment. Furthermore, the GS containing genes up-regulated in pancreatic beta cells displayed enrichment. However, due to the small GS size and a relative high FDR, this enrichment may indicate a false-positive.

The majority of enriched GSs in uninfected cells or meningitis-free pigs are involved in the immune response and cellular metabolism. The interferon α and γ response, as well as the allograft rejection GSs are categorized under immune response, whereas the metabolic processes include oxidative phosphorylation, as well as fatty acid and bile acid metabolism.

Table 19. The hallmark GSs, which are enriched in uninfected cells or meningitis-free animals. The normalized enrichment score (NES) represents the extent of GS enrichment, taking the number of genes ("size"), which compose the GS, into account. The false discovery rate (FDR) is considered significant if *q* is ≤ 0.25.

Hallmark Gene Set Name	Size	NES	FDR q-val
uninfected HIBCPP cells			
MYC targets V2	58	-2.29	0.000
MYC targets V1	197	-1.90	0.000
E2F targets	197	-1.86	0.000
Unfolded protein response	109	-1.57	0.020
G2M Checkpoint	195	-1.56	0.016
DNA repair	138	-1.50	0.035
Spermatogenesis	64	-1.42	0.075
uninfected PCPEC			
E2F Targets	150	-1.54	0.128
Pancreas Beta Cells	18	-1.37	0.245
meningitis-free pigs			
Interferon α response	81	-2.57	0.000
Interferon γ response	163	-1.99	0.000
Oxidative phosphorylation	152	-1.72	0.003
E2F Targets	166	-1.62	0.010
DNA Repair	119	-1.40	0.122
Fatty Acid Metabolism	130	-1.38	0.122
Allograft Rejection	173	-1.32	0.186
Bile acid metabolism	97	-1.30	0.202

When comparing the 18, 28, and 21 significantly enriched GSs from *S. suis* ST2 infected HIBCPP cells, PCPEC, and animals suffering from meningitis, respectively, a total of eight GSs were found to overlap. These eight GSs were TNFα signaling via NFκB, inflammatory response, hypoxia, IL2-STAT5 signaling, IL6-JAK/STAT3 signaling, TGFβ signaling, EMT, and KRAS signaling. In contrast to the infected cell samples, samples that were either uninfected or animals that were meningitis-free had one GS in common, which was significantly enriched in this phenotype. This enriched GS contains gene targets which are involved in the cell cycle and are regulated by the E2F transcription factors.

4.6. Selected genes could be validated utilizing qPCR

Following the sequencing analysis, the generated data was validated. The most common practice, as was also done for this study, is the validation with the relative quantification method via qPCR for selected genes, to determine the gene fold change of the gene of interest in relation to an internal control, such as a house-keeping gene.

The DEG lists presented in section 4.5.1 were used in order to select candidate genes for the validation of the sequencing data. All fold changes were calculated via the $2^{-\Delta\Delta CT}$ method, and the house-keeping gene encoding for glyceraldehyde 3-phosphate dehydrogenase (GAPDH) was used as an internal control in order to calculate the relative fold change of the gene of interest.

Table 20 summarizes the fold change and the corresponding significance (uncorrected *p*-value of a one-way ANOVA test) of differentially regulated genes during the RNA-seq analysis, as determined by the PartekGS software. Additionally, Table 20 also summarizes the relative FC ($2^{-\Delta\Delta CT}$) between infected versus uninfected samples, along with the S.D., of the qPCR results. These genes were selected for subsequent qPCR validation, and the data from Table 20 will be discussed in relation to the data presented in Figure 17 - Figure 19.

Table 20. Summary of the fold changes (FCs) and uncorrected *p*-values of selected genes from the RNA-seq data and the FC of infected samples in relation to uninfected samples. The FC and *p*-values of the RNA-seq data were determined by the software PartekGS. The FC for the qPCR data was calculated via the $2^{-\Delta\Delta CT}$ method using GAPDH as an internal control, and the relative FC was determine between infected versus uninfected samples with the S.D. Genes are considered significantly differentially regulated if the *p*-value ≤ 0.05. These listed genes were selected for subsequent qPCR validation.

	HIBCPP cells				PCPEC				*in vivo*			
	RNA-seq		qPCR		RNA-seq		qPCR		RNA-seq		qPCR	
	FC	*p*-value	relative $2^{-\Delta\Delta Ct}$	S.D.	FC	*p*-value	relative $2^{-\Delta\Delta Ct}$	S.D.	FC	*p*-value	relative $2^{-\Delta\Delta Ct}$	S.D.
IL1β	-1.1	0.925	2.0	3.4	134.0	0.041	136.4	83.0	2.8	0.127	4.6	15.3
IL8	3.8	0.386	3.8	7.3	22.6	0.006	20.5	12.8	22.0	0.014	7.6	17.7
CXCL2	4.9	0.258	4.7	5.3	13.8	0.017	19.4	5.5	9.9	0.005	13.0	25.1
TNFα	12.1	0.256	12.0	17.1	70.7	0.006	19.8	2.6	1.1	0.909	1.2	0.3
NFκBIA	4.2	0.266	2.6	3.5	3.9	0.016	3.5	1.2	1.3	0.173	1.7	0.4
ZC3H12A	3.3	0.220	3.1	2.4	2.1	0.004	2.0	1.2	2.9	0.107	1.4	0.6
TCIM	3.1	0.025	2.6	4.6	2.7	0.001	2.7	0.4	2.2	0.114	3.1	1.9
HIF1α	1.1	0.732	0.8	0.3	-1.6	0.306	1.0	0.2	-1.3	0.008	1.0	0.1
VEGFA	2.0	0.075	1.6	0.5	1.6	0.006	1.4	0.3	1.4	0.003	1.4	0.2
MXI1	2.5	0.043	2.8	12.1	1.2	0.008	1.0	0.03	1.1	0.416	1.1	0.1
DUSP2	-2.6	0.015	-4.2	2.2	5.2	0.016	1.3	1.5	8.1	0.004	9.7	1.9

FC, fold change; S.D., standard deviation

First, genes, which are implicated during inflammation, were selected for the verification. For this, genes, which were significantly upregulated on the DEG list of the infected PCPEC (Table 14), were selected and are summarized in Table 20. The relative fold change of the genes encoding for the cytokines and chemokines IL1β, IL8, C-X-C ligand 2 chemokine (CXCL2), and TNFα in all sample sets are summarized in Figure 17.

The average fold change of infected cells or animals with meningitis in relation to uninfected cells or meningitis-free animals (± the standard deviation) for IL1β was 2.0 (± 3.4), 136.4 (± 83.0; $p = 0.047$), and 4.6 (± 15.3), for infected HIBCPP cells, PCPEC, and the CP from *in vivo* infection experiments, respectively. This is comparable to the data generated following the RNA-seq, which also displayed significance in PCPEC ($p = 0.041$; Table 20).

The average fold change of infected cells or animals with meningitis in relation to uninfected cells or meningitis-free animals (± the standard deviation) for IL8 was 3.8 (± 7.3), 20.5 (± 12.8; $p = 0.009$), and 7.6 (± 17.7), for infected HIBCPP cells, PCPEC, and the CP from *in vivo* infection experiments, respectively. The fold changes and significance were in accordance with the RNA-seq data, with the exception of the *in vivo* – generated samples (Table 20). The RNA-seq data of pigs suffering from meningitis revealed a 22-fold change of IL8 with a significance of $p = 0.014$ (Table 20).

The average fold change of infected cells or animals with meningitis in relation to uninfected cells or meningitis-free animals (± the standard deviation) for CXCL2 was 4.7 (± 5.3), 19.4 (± 5.5; $p = 0.011$), and 13.0 (± 25.1), for infected HIBCPP cells, PCPEC, and the CP from *in vivo* infection experiments,

respectively. These results were comparable to the results obtained with the PartekGS software following RNA-seq, with the exception that the *in vivo* data displayed a significance (p = 0.005) of the fold change in meningitis versus meningitis-free animals, which was not achieved by the qPCR validation (Table 20).

The average fold change of infected cells or animals with meningitis in relation to uninfected cells or meningitis-free animals (± the standard deviation) for TNFα was 12.0 (± 17.1), 19.8 (± 2.6; p = 0.0002), and 1.2 (± 0.3), for infected HIBCPP cells, PCPEC, and the CP from *in vivo* infection experiments, respectively. With the exception of the PCPEC samples, which displayed a fold change of approximately 70 in the RNA-seq analysis, the qPCR data corresponded to the RNA-seq determined data (Table 20).

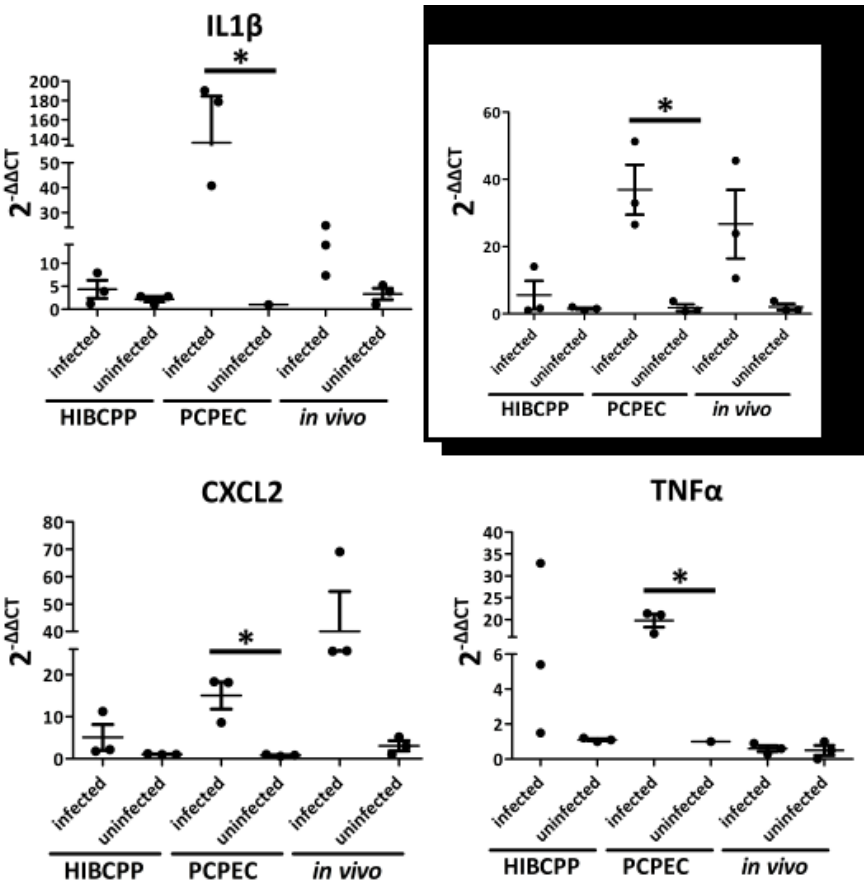

Figure 17. Quantitative PCR validation for the RNA-seq data of genes expressing for cytokines and chemokines. The relative fold change of each gene was calculated by using the $2^{-\Delta\Delta CT}$ method using the gene encoding for GAPDH as an internal control. Each biological replicate is represented in the graphs, along with the mean and standard deviation. A significance of $p \leq 0.05$ between the infected state versus uninfected state is indicated by an asterisk (*).

In addition to the genes encoding for the cytokines and chemokines, genes, which are implicated in regulating the inflammatory response, were evaluated. At least one of the selected genes was found to be significantly differentially regulated in infected HIBCPP cells and PCPEC (Table 13 and Table 14),

as summarized in Table 20. The relative fold change of the genes encoding for NFκB inhibitor alpha (NFκBIA), zinc finger CCCH-type containing 12A (ZC3H12A; also known as Regnase), and TCIM in all sample sets are summarized in Figure 18.

The average fold change of infected cells or animals with meningitis in relation to uninfected cells or meningitis-free animals (± the standard deviation) for NFκBIA was 2.6 (± 3.5), 3.5 (± 1.2; p = 0.016), and 1.7 (± 0.4; p = 0.023), for infected HIBCPP cells, PCPEC, and the CP from *in vivo* infection experiments, respectively. These results were congruent with the results obtained from the RNA-seq analysis (Table 20).

The average fold change of infected cells or animals with meningitis in relation to uninfected cells or meningitis-free animals (± the standard deviation) for ZC3H12A was 3.1 (± 2.4), 2.0 (± 1.2), and 1.4 (± 0.6), for infected HIBCPP cells, PCPEC, and the CP from *in vivo* infection experiments, respectively). These results matched the observations from the RNA-seq results, with the exception that the fold change observed in the PCPEC samples was significant (p = 0.004; Table 20) in comparison to the qPCR results, which detected no significance.

The average fold change of infected cells or animals with meningitis in relation to uninfected cells or meningitis-free animals (± the standard deviation) for TCIM was 2.6 (± 4.6), 2.7 (± 0.4; p = 0.005), and 3.1 (± 1.9), for infected HIBCPP cells, PCPEC, and the CP from *in vivo* infection experiments, respectively. These qPCR results are comparable to the RNA-seq results, with the exception that expression-fold change yielded significance (p = 0.025) in the HIBCPP cell sample set (Table 20).

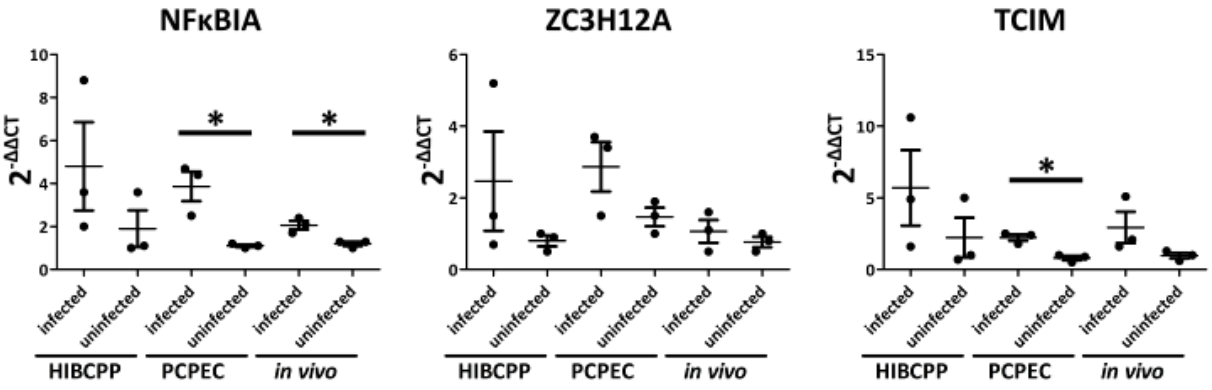

Figure 18. Quantitative PCR validation for the RNA-seq data of genes expressing immune response regulators. The relative fold change of each gene was calculated by using the $2^{-\Delta\Delta CT}$ method using the gene encoding for GAPDH as an internal control. Each biological replicate is represented in the graphs, along with the mean and standard deviation. A significance of $p \leq 0.05$ between the infected state versus uninfected state is indicated by an asterisk (*).

Furthermore, based on the results generated by the GSEA (section 4.5.2), genes known to play a key role during hypoxia, or are known to have their expression influenced in a hypoxic environment, were chosen for validation. The relative fold change of the genes encoding for hypoxia-inducible factor 1 alpha (HIF1α), vascular endothelial growth factor a (VEGFA), MAX interactor 1 (MXI1), and dual specificity phosphatase 2 (DUSP2) in all sample sets are summarized in Figure 19, and the data generated during the RNA-seq analysis are summarized in Table 20. Additionally, MXI1 and DUSP2 were found to be significantly differentially expressed in *S. suis* ST2 infected HIBCPP cells (Table 13).

The average fold change of infected cells or animals with meningitis in relation to uninfected cells or meningitis-free animals (± standard deviation) observed for HIF1α was 0.8 (± 0.3), 1.0 (± 0.2), and 1.0 (± 0.1), for infected HIBCPP cells, PCPEC, and the CP from *in vivo* infection experiments, respectively. These observations corresponded to the RNA-seq DEG data, with the exception of the *in vivo* samples, which displayed a significant differential expression (p = 0.008; Table 20).

The average fold change of infected cells or animals with meningitis in relation to uninfected cells or meningitis-free animals (± standard deviation) observed for VEGFA was 1.6 (± 0.5), 1.4 (± 0.3), and 1.4 (± 0.2; *p* = 0.048), for infected HIBCPP cells, PCPEC, and the CP from *in vivo* infection experiments, respectively. Again, these values were in line with the data obtained from RNA-seq, with the exception that the PCPEC sample set displayed significant differential fold change (0.006; Table 20).

The average fold change of infected cells or animals with meningitis in relation to uninfected cells or meningitis-free animals (± standard deviation) observed for MXI1 was 2.8 (± 12.1), 1.0 (± 0.03), and 1.1 (± 0.1), for infected HIBCPP cells, PCPEC, and the CP from *in vivo* infection experiments, respectively. With the exception of the PCPEC samples set, which displayed a significant differential expression (p = 0.008; Table 20) following the RNA-seq data analysis, the qPCR matched the RNA-seq data.

The average fold change of infected cells or animals with meningitis in relation to uninfected cells or meningitis-free animals (± standard deviation) observed for DUSP2 was - 4.2 (± 2.2), 1.3 (± 1.5), and 9.7 (± 1.9; *p* = 0.005), for infected HIBCPP cells, PCPEC, and the CP from *in vivo* infection experiments, respectively. From the RNA-seq data analysis, the gene encoding DUSP2 displayed a significant (*p* = 0.015) 2.6 down-regulation in the infected HIBCPP cell sample set (Table 20), which corresponded approximately to the data generated via qPCR, where an approximate 4-fold down-regulation was observed, although this was not significant in infected cells in comparison to uninfected HIBCPP cells. Furthermore, RNA-seq revealed a significant (*p* = 0.016) 5.2-fold up-regulation in *S. suis* ST2 infected PCPEC (Table 20), which yielded no significance in the qPCR validation. Congruence was observed for the sample set obtained from the *in vivo* experiments.

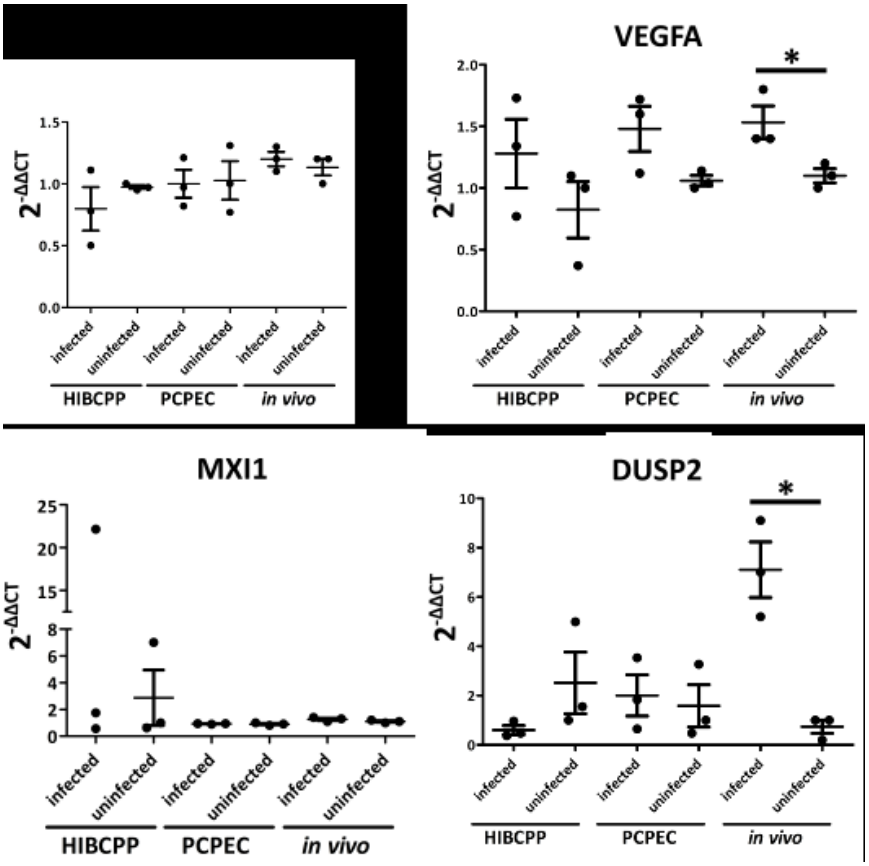

Figure 19. Quantitative PCR validation for the RNA-seq data of genes regulated during a hypoxic physiological state correlate to the RNA-seq data. The relative fold change of each gene was calculated by using the $2^{-\Delta\Delta CT}$ method using the gene encoding for GAPDH as an internal control. Each biological replicate is represented in the graphs, along with the mean and standard deviation. A significance of $p \leq 0.05$ between the infected state versus uninfected state is indicated by an asterisk (*).

Overall, the gene fold change determined following the RNA-seq data analysis could be validated with the qPCR method, and the significances determined following the qPCR analysis largely corresponded to the significant fold change determined with the PartekGS software. Genes encoding for the cytokines and chemokines displayed a higher fold change in the PCPEC and in samples from the porcine *in vivo* infection experiments, an observation also made from the DEG lists (section 4.5.1).

4.7. Comparing two sequencing methods: conventional RNA-seq versus MACE

In addition to the conventional Illumina's RNA-seq technology, many different sequencing methods exist, since each method has its own strengths and weaknesses. An alternative and relative new method was developed by GenXPro and is called MACE (Rotter et al., 2017). This sequencing method, which sequences only the 3` end of the transcript, brings advantages with it, in comparison to the conventional RNA-seq method. For example, with MACE it is possible to sequence the sample at a deeper level since each read is representative of one transcript in the sample, whereas conventional RNA-seq could have multiple reads from the same transcript, since sequencing is performed on the entirety of randomly fragmented transcripts (Rotter et al., 2017).

In this study, a comparative analysis of samples sequenced via the conventional and the MACE sequencing methods was performed. The samples utilized for this evaluation were obtained from the porcine *in vivo S. suis* infection experiments (section 3.3.2).

4.7.1. A high concordance of significantly DEGs was observed when comparing conventional RNA-seq and MACE data

The first step in the data analysis post-sequencing was to generate and evaluate a list of significant DEGs. Following the DEG analysis, 2,263 and 1,919 DEGs with an uncorrected $p \leq 0.05$, and which showed at least 10 raw reads in one class for all biological replicates for the conventional RNA-seq and MACE, respectively, were identified. Of these significant DEGs, 1,102 concordant genes were identified following both sequencing methods.

Figure 20 depicts a positive correlation of concordant DEGs identified in pigs suffering from meningitis versus meningitis-free pigs following the conventional RNA-seq analysis (x-axis) and MACE analysis (y-axis).

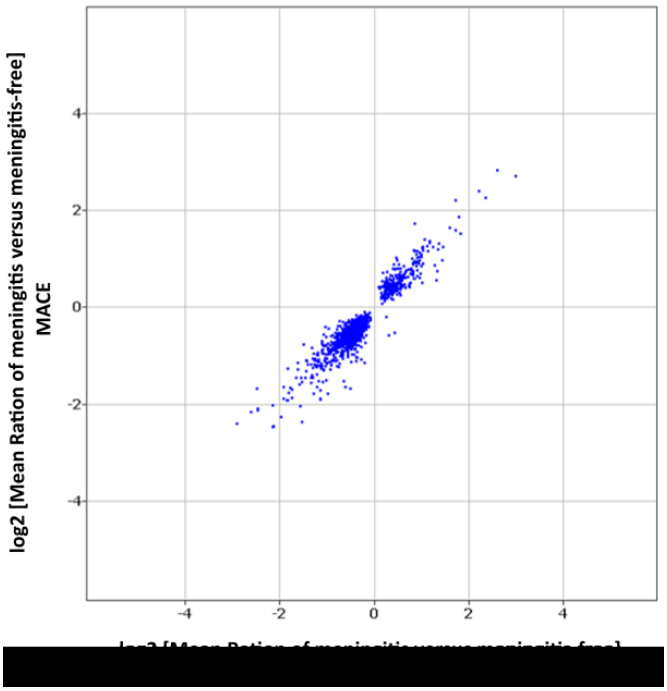

Figure 20. 1,102 concordant DEGs from the conventional RNA-sequencing and MACE generated data. Genes with an uncorrected *p*-value of below or equal to 0.05 and at least 10 raw reads in all biological replicates of one class (meningitis versus meningitis-free) are presented.

In addition to comparing the differential gene expression of individual genes, a GSEA was carried out in order to evaluate the enrichment of hallmark GSs following the MACE sequencing method.

4.7.2. GSEA analysis yielded similar hallmark GS enrichment

A GSEA, as described in section 4.5.2, was carried out with the data generated from the MACE sequencing. In total, 21 significant GSs were identified (Table 21), which is the same quantity identified following the conventional RNA-seq (Table 18).

The majority of the GSs belong in the category of cellular signaling, with these GSs being TNFα signaling via NFκB, IL2-STAT5, TGFβ, Wnt/β-catenin, and MTORC1 signaling, early estrogen response, as well as the GS containing up-regulated genes following KRAS signaling. The category containing the second most enriched GS was for the immune system and included inflammatory response, IL6-JAK/STAT3 signaling, allograft rejection, coagulation, and complement. The category with the third most enriched GSs included reactive oxygen species pathway, hypoxia, unfolded protein response, and apoptosis, which are categorized under cellular pathways. The GSs myogenesis, angiogenesis, and EMT can be categorized under development, and the enriched GSs of genes up- or down-regulated in response to UV radiation belong to the cellular DNA damage response.

The GSEA of the MACE data revealed four different enriched GSs (apoptosis, allograft rejection, MTORC1 signaling, and complement) in comparison to the samples sequenced via the conventional sequencing method, which displayed enrichment for androgen response, Myc targets, cholesterol homeostasis, and late estrogen response.

Table 21. GSEA of the MACE sequenced samples reveals 21 hallmark GSs, which are significantly enriched in animals suffering from meningitis. The normalized enrichment score (NES) represents the extent of GS enrichment, taking the number of genes ("size") into account. The false discovery rate (FDR) is considered significant if *q* is ≤ 0.25.

Hallmark Gene Set Name	Size	NES	FDR q-value
TNFα signaling via NFκB	109	3.01	0.000
Inflammatory response	79	2.29	0.000
IL6-JAK/STAT3 Signaling	44	2.24	0.000
Myogenesis	90	1.95	0.003
Angiogenesis	20	1.91	0.003
Reactive oxygen species pathway	36	1.84	0.004
Hypoxia	112	1.75	0.007
IL2-STAT5 Signaling	88	1.70	0.012
Unfolded protein response	84	1.63	0.019
Apoptosis	110	1.58	0.023
Early estrogen response	99	1.58	0.021
Epithelial-Mesenchymal transition	112	1.52	0.029
TGFβ Signaling	38	1.50	0.032
KRAS Signaling	92	1.48	0.034
Wnt/β-catenin	23	1.47	0.036
UV response_up	100	1.44	0.043
UV response_down	95	1.39	0.063
Allograft rejection	88	1.33	0.084
MTORC1 Signaling	141	1.20	0.210
Coagulation	60	1.17	0.238
Complement	109	1.17	0.230

Only four GSs were identified as being significantly enriched at the CP of meningitis-free pigs following the MACE analysis. These included interferon α (NES -2.25, *q* = 0.000) and γ (NES -1.71, *q* = 0.006) response, belonging to the category of immune response. Additionally, the metabolism categorized GSs, oxidative phosphorylation (NES -1.89, *q* = 0.000) and bile acid metabolism (NES -1.40, *q* = 0.183), were also found to be significantly enriched. These four GSs were also identified as being significantly enriched in the same samples which underwent conventional RNA-seq.

5. Discussion

S. suis, as a zoonotic opportunistic pathogen, is capable of causing disease in its natural host, the pig, as well as in humans by predominantly presenting itself clinically as meningitis (Dutkiewicz et al., 2017). *In vivo* and *in vitro* evidence exists, which demonstrate and implicate the CP at the BCSFB, in acting as an entry gate for this pathogen into the CNS (Schwerk et al., 2012; Tenenbaum et al., 2009; Williams and Blakemore, 1990). In this study, the global transcriptome response of *in vitro S. suis* infected human papilloma (HIBCPP) and primary porcine CP epithelial cells (PCPEC), as well as the CP tissue of *in vivo* infected piglets, which developed *S. suis*-induced meningitis, was evaluated via RNA-seq. Subsequent to sequencing, the generated data was evaluated on the differential expression of individual genes and was also biologically interpreted by evaluating the enrichment of GSs via the GSEA between the infected versus uninfected phenotypes. The data produced by the RNA-seq method via the Illumina sequencing technology was then validated with the qPCR method. For this, genes were selected based on the generated DEG list and on key genes playing a role in significantly enriched GSs (e.g. hypoxia). The gene fold change determined via qPCR analysis revealed a high congruence with the fold change calculated by the RNA-seq data analysis software.

5.1. The DEG analysis of *S. suis* ST2 infected CP cells of pigs and humans

5.1.1. The implications of individual differentially regulated genes at the CP involved in inflammation and hypoxia

5.1.1.1. Primary PCPEC

A previous transcriptome investigation, utilizing microarray technology, of apically *S. suis* ST2 infected PCPEC, which *in vivo* would reflect the state of infection following bacterial translocation into the CNS, revealed that the CP epithelial cells contributed to the inflammatory response *in vitro* (Schwerk et al., 2011). For the 6 h basolateral infected PCPEC in this current study, which *in vivo* would reflect the state before bacteria enter the CNS, it was observed that infection with *S. suis* ST2 induced a strong response in the primary porcine cells, with the majority of the identified significant DEGs being involved in inflammation as well. Part of the inflammatory response is the upregulation of cytokines and chemokines, which in this present study included IL1β, TNF, IL1α, CCL3L1, CXCL8, AMCF-II, CXCL2, CCL2, CCL11, CCL5, and IL6, many of which were also identified in the study by Schwerk and colleagues of apically infected PCPEC (Schwerk et al., 2011). IL1β was found to be the strongest up-regulated gene, with a 134-fold change 6 h post-infection, and is known to be involved in many physiological functions, among others, being a potent inducer of inflammatory signaling

expressed by many different cell types, including the CNS (Hewett et al., 2012). In previous studies evaluating the *S. suis*-dependent cytokine production, IL1β, along with other key inflammatory cytokines, such as IL6 and IL8, was found to be produced by porcine monocytes and polymorphonuclear lymphocytes in a whole-blood system in response to infection, as well as in human THP-1 monocytes (Segura et al., 2002; Segura et al., 2006). Furthermore, utilizing a murine *in vivo S. suis* infection model, the transcription of IL1β, TNF, and CCL2 in the brain during cerebral inflammation was demonstrated via *in situ* hybridization (Dominguez-Punaro et al., 2007). In addition to the cytokine and chemokine upregulation observed in this present work, the inflammatory response regulators SLAMF7, RELB, NFKBIZ, NFKBIA, and ZC3H12A were identified, further underlining the strong inflammatory response elicited by PCPEC during to infection.

5.1.1.2. HIBCPP cells

The transcriptome of HIBCPP cells was previously investigated following the *in vitro* infection with *N. meningitidis* from the basolateral cell side (Borkowski et al., 2014). In the experimental set-up from Borkowski and colleagues, the HIBCPP cells demonstrated a strong inflammatory response, which included the production of cytokines and chemokines. Previous studies involving infection of other human cells with *S. suis*, such as a human brain endothelial cell line (HBMEC) or human immune cells (e.g. THP-1 monocytes and dendritic cells), mainly focused their research on the inflammatory response of host cells, too, or on bacterial survival and interaction with host cells (Charland et al., 2000; Liu et al., 2011b; Meijerink et al., 2012; Segura et al., 2002). Interestingly, in this present study, whereas PCPEC displayed a strong inflammatory response to infection, genes attributed to hypoxia were found to play a more important role during infection in HIBCPP cells. The significant DEGs identified in basolaterally infected HIBCPP cells involved in hypoxia included ZFP36L1, MXI1, KLHL24, PNRC1, CDKN1C, and DUSP2.

In addition to the hypoxic response, it was also interesting to observe the significant differential regulation of various RNA types, which are known to have a regulatory function and are non-protein coding. These regulatory RNAs included the anti-sense (AS) RNAs HLA-F, LIFR, PRKAR2A, ZEB1, and long intergenic non-coding RNAs (LINC) 887, 1431, 2482, as well as microRNAs (MIRs) 22HG and 3648, which are associated with viral inflammation and cancer and cellular proliferation, respectively (Rashid et al., 2017; Razooky et al., 2017; Zhang et al., 2018). This suggests that non-coding RNAs play a role in human CP epithelial cells during infection.

5.1.1.3. CP of in vivo infected pigs

Finally, for the first time the transcriptome of cells found at the CP of pigs was investigated. For this sample set, it is important to take into consideration that the CP tissue obtained from the *in vivo* infected pigs consists of a heterogeneous cell population, such as CP epithelial, endothelial cells, and immune cells located at or recruited to the BCSFB (Strazielle and Ghersi-Egea, 2000). Therefore, due to the tissue heterogeneity, the results of the CP tissues samples cannot directly be compared to that of the *in vitro* infection experiments with homogenous epithelial cell populations, such as the PCPEC and HIBCPP cells. However, this data is rich in information, which helps to understand the CP tissue-specific response during *S. suis* infection. Previous studies carried out utilizing *in vivo* porcine *S. suis* infection models investigated the transcriptome of different organs (brain, lung, monocytes, spleen), but not specifically the CP (Li et al., 2010; Liu et al., 2011a). These studies evaluated the transcriptome at pre-defined time points (24 hours and 3 days post-infection) of 4 to 5-week old piglets, as compared to this present study, where the response of 8-week old pigs was analyzed which developed acute meningitis, finding differentially regulated genes to be predominantly associated with the host's inflammatory response.

Although gene transcription and regulation is of high interest, genes have to be translated to biologically active proteins in order to perform their functions in the cell. Liu and colleagues were the first to investigate the protein profile of the CSF in piglets suffering from meningoencephalitis. They found enriched up-regulated proteins were extracellular, participated in protein metabolism, and displayed cysteine-type peptidase activity. Down-regulated proteins were also identified as belonging to exosomes of cellular components, energy pathways in biological processes, and proteins possessing catalytic activity (Liu et al., 2018). Proteomic investigation has also been performed of *S. suis in vivo* in its natural host during disease, giving insight into virulence contribution. However, dual RNA-seq methods exist, which can evaluate the host and pathogen's transcriptional response simultaneously and should therefore be taken into consideration in the future when investigating specific niches (Saliba et al., 2017; Yu et al., 2018).

Interestingly, the final *in vivo* DEG list obtained in this present study contained many more gene targets than the lists generated following the analysis for the HIBCPP cell and PCPEC samples, likely due to the cell heterogeneity found *in vivo*. For example, from the generated DEG list generated post-sequencing of the CP tissue it can be deduced, based on the DEG lists generated from the homogenous epithelial cell culture, which genes are found not expressed by the human CP (CRNN and FLRT1), or likely do not originate from CP epithelial cells (TIMD4). For the future, one could investigate individual cells or single cell types out of the *in vivo* environment by making use of advanced techniques, such as laser-capture microdissection in combination with single-cell RNA-seq

(Kukurba and Montgomery, 2015). An *in situ* hybridization method could also be applied in order to evaluate the transcript origin in the heterogeneous tissue.

Additionally, the samples obtained from the *in vivo* infection experiments were subject to an alternative sequencing method called MACE, which performs deep-sequencing by sequencing only the 3'-end of a transcript (Rotter et al., 2017). For the approximately 2,000 significantly ($p \leq 0.05$) DEGs identified in both the conventional RNA-seq method and the MACE sequencing method, an overlap of approximately 50 % was observed. It should be considered, that the varying degree of the library preparation and a difference in the sequencing depth (only the 3'-transcript end versus random fragments of a transcript) of the MACE and conventional RNA-seq approaches could potentially introduce sequencing biases, which account for a variation in the quantification, and thereby affect the evaluation of differential expression (Alberti et al., 2014; Fang and Cui, 2011). Only a few comparative RNA-seq methods have previously been performed and found a higher concordance (80-99 %) of genes identified between the different sequencing methods (Harris et al., 2010; Tian et al., 2010). However, in these studies, RNA profiles from a specific RNA population (micro RNA) from non-pathological tissue or homogenous cell population were investigated, whereas in this present work, the global transcriptome profile of a heterogeneous cell population in a pathological state was investigated, which is known to affect the estimations of transcript abundances (Kukurba and Montgomery, 2015). Cell homogeneity was previously discussed to result in more accurate quantification (Kukurba and Montgomery, 2015). Taking these details into consideration, 50 % gene concordance between the two different sequencing methods employed in this thesis could be viewed as a promising result, and MACE could be applied to future studies with homogenous cell populations as cheaper sequencing alternative.

5.1.2. The DEG comparison between *S. suis* ST2 infected CP cells displayed limited gene overlap

Despite *S. suis* most commonly presenting itself clinically the same way in both the natural host and humans, a differing transcriptional response was identified between the three samples in terms of gene fold change intensity and the biological functions attributed to the genes. When evaluating and comparing the PartekGS-generated DEGs between the analyzed sample sets, the upregulation of only two genes was found to overlap in the human and porcine *in vitro* infected epithelial samples during infection. These two genes were identified as TCIM and RND1. TCIM, which is also well known under the aliases TC1 and C8orf4, is a gene regulator often found in association with poor survival outcome during cancer, due to its involvement in regulating the Wnt/β-catenin pathway (Kim et al., 2009). Furthermore, TCIM was found to be upregulated by the pro-inflammatory cytokines TNFα and IL1β

(Kim et al., 2006), but in return also influences the up-regulation of inflammatory cytokines and the adhesion molecules ICAM1 and VCAM1 (Kim et al., 2009). The latter is known to be expressed by CP epithelial cells and has been implicated in being manipulated by bacterial pathogens in order to aid in invasion of the CNS (Al-Obaidi and Desa, 2018; Steffen et al., 1996). In a study performed by Kim and colleagues, TCIM was described as a novel inflammatory regulator in endothelial cells, since it was found to be regulated by, and conversely also regulating, and thereby enhancing, the transcription factor NFκB (Kim et al., 2009). To date, there has been no clear implication of TCIM during infection of the CNS. However, its upregulation has been observed for malignant cancers in the CNS (Wang et al., 2017). RND1 functions in the actin cytoskeletal arrangement and cellular adhesion, and has been implicated in viral infections, e.g. Nipah virus, which is known to affect the CNS (Glennon et al., 2015; Nobes et al., 1998). Interestingly, both TCIM and RND1 were previously found to be up-regulated during an *in vitro N. meningitidis* infection experimental set-up with HIBCPP cells (Borkowski et al., 2014).

The lack of genes overlapping in the identified DEGs may be due to various reasons. It could be speculated that the cell line background, i.e. whether the cells originated from papilloma cells or are primary cells cultivated *ex vivo*, plays a role since immortalization may have an impact on how a cell responds to a defined stressor. Furthermore, due to the swine being the natural host organism of *S. suis*, another theory could be that porcine cells may be more evolutionary attuned to responding to this pathogen than human cells. Along these lines, this may explain why *N. meningitidis*, which is known for its host specificity towards humans, elicited a strong inflammatory response in the HIBCPP cells *in vitro* (Borkowski et al., 2014; Hill et al., 2010). With the advancement of transcriptome studies being able to perform sequencing of RNA with low integrity, the CP of patients, whom succumbed to *S. suis*-induced meningitis, could potentially be evaluated post-mortem in future studies. Furthermore, the utilization of 3D cell culture models, such as brain organoids, which are currently used to study infection with Zika virus, could be optimized, since these have been shown to develop a CP-like structure (Renner et al., 2017).

5.2. The GSEA of *S. suis* ST2 infected CP cells of pigs and humans

Although the DEG analysis was able to determine individual genes regulated during infection with *S. suis*, the identification of biological pathways, in which multiple differentially expressed genes are connected to a common or networked performance, is of high interest in understanding cellular processes. One such tool, which allows the identification of enrichment of genes sharing a common biological function, is the GSEA.

5.2.1. The enrichment of GSs in the individual human and porcine CP

5.2.1.1. GS enrichment in infected primary PCPEC

In the GSEA, a total of 28 GSs was identified to be significantly enriched in *S. suis*-infected PCPEC. The top enriched GSs are implicated in the immune response, which corresponded and complemented the data obtained in the DEG analysis. In a previous transcriptome study analyzing apically *S. suis*-infected PCPEC cells, Gene Ontology (GO) analysis, which evaluates high through-put data, based on biological processes, molecular functions, and cellular components, also identified many enriched cellular processes to be involved in inflammation (Ashburner et al., 2000; Schwerk et al., 2011). This is revealed by the over-represented GO terms for cytokine activity, inflammatory response, defense response, and IκB kinase/NFκB cascade, as well as programmed cell death, which can be induced as a consequence of inflammation (Schwerk et al., 2011).

5.2.1.2. GS enrichment of infected HIBCPP cells

For the HIBCPP cell samples set, 18 GSs were found to be significantly enriched, with the most significant enrichment being for the GS containing genes in the hypoxia cellular stress response. As observed with the PCPEC, the GSEA for the HIBCPP cell samples confirmed its corresponding DEG analysis as well, since this also identified hypoxia related genes. In addition to the gene enrichment in hypoxia, the GSEA revealed an enrichment of GSs participating in inflammation. A previous GSEA and a GO analysis of *N. meningitides*-infected HIBCPP cells revealed a predominant inflammatory response, with cytokine and chemokine activity playing a significant role (Borkowski et al., 2014). Additionally, a GS involved in wound healing was identified (Borkowski et al., 2014), which is often associated with EMT. The EMT GS was identified in the present study to be the third most enriched GS in infected HIBCPP cells. In a different study investigating the transcriptome of a human monocyte cell line (THP-1 cells) exposed to *S. suis*, GO analysis revealed a cellular response including the participation of intracellular signaling pathways involved in inflammation, such as apoptosis and host defense and immunity, as well as other cellular processes involving cellular metabolism, gene transcription, and gene translation (Liu et al., 2011b).

5.2.1.3. GS enrichment of the CP from in vivo infected piglets with meningitis

The GSEA of the CP isolated from *in vivo*-infected piglets identified 21 significantly enriched GSs. The majority of the GSs displayed involvement in the inflammatory host response, as was also observed with the PCPEC samples. A previous porcine *in vivo* investigation revealed that the brains of *S. suis*-infected piglets displayed gene enrichment also involved in inflammation, and could be categorized

into the GO terms of biological processes responding to a stimulus via signal transducer activity, cytokine activity and binding, defense response, inflammatory response, immune response, and innate immune response (Liu et al., 2011a). However, it was noted that many GO categories overlapped, due to the same genes being involved in multiple biological processes (Liu et al., 2011a). A further transcriptome study utilizing a zebrafish *S. suis*-infection model, underscored the role of inflammation and host defense during infection, and highlighting the zebrafish as a suitable model to study *S. suis* infection (Wu et al., 2010).

When comparing the overlapping GSs of the CP samples from the porcine *in vivo* studies subject of conventional RNA-seq and MACE sequencing, the GSEA revealed a high overlap in the detected enriched biological functions during infection. This further underlines the MACE sequencing method as a suitable alternative. For both sequencing methods, a total of 21 significantly enriched GSs were identified. 17 GSEA GSs were found to overlap between both analyzed sequencing methods, with non-overlapping GSs being enriched in the androgen response, Myc gene targets, cholesterol homeostasis, and late estrogen response for the conventional sequenced samples, and apoptosis, allograft rejection, mTORC1 signaling, and complement GSs for the MACE analysis.

5.2.1.4. Down-regulated GSs at the CP during S. suis infection

Not only were enriched GSs evaluated in infected or meningitis samples, but GSs, which were enriched in uninfected samples in comparison to infected samples, were also evaluated. The number of significantly enriched GSs was observed to be overall fewer in uninfected or meningitis-free samples than in the infected or meningitis samples. The majority of the significantly enriched GS identified in the uninfected samples can be categorized into cellular metabolism or cellular proliferation. One enriched GS, which contains genes regulated by family members of E2F transcription factors, was found to overlap between all of the samples. The E2F transcription factors are important for the regulation of genes involved in DNA replication and the cell division cycle, and in the context of infection, they were investigated during viral infections, such as human immunodeficiency virus and adenovirus (Bracken et al., 2004; Kundu et al., 1997; Zheng et al., 2016). It is noteworthy, that the enrichment of the GS containing E2F targets corresponds to the GS containing genes involved in the G2/M checkpoint of the cell division cycle.

Furthermore, the enrichment of the GS constituted by gene targets of the Myc transcription factor was observed in the HIBCPP cell samples. Myc is often involved in the development in cancer, due to the role it plays in cellular growth, but in the context of infection Myc was shown to be manipulated during infection with the intracellular parasite *Toxoplasma gondii,* which is known to implicate the CP

during infection of the CNS (Dang, 2012; Falangola and Petito, 1993; Franco et al., 2014). The enrichment of these GSs, especially in the HIBCPP cell samples, is indicative that cellular proliferation is altered or stopped during *S. suis* ST2 infection.

Additionally, the enrichment of GSs involved in cellular metabolism was observed for the *in vivo* analyzed CP samples of meningitis-free pigs. These GSs include genes involved in oxidative phosphorylation, as well as the metabolism of fatty acids and bile acids and salts. Oxidative phosphorylation plays an important role in aerobic ATP synthesis, and its down-regulation is found in association with a hypoxic environment (Fuhrmann and Brune, 2017). In an *in vivo* zebrafish infection model for *S. suis*, a down-regulation of metabolic pathways was also observed following infection (Wu et al., 2010). However, the identified genes were involved in glycolysis, and the metabolism of amino acids and carbohydrates (Wu et al., 2010). The enrichment of these GSs gives insight into metabolic alterations which occurred *in vivo* at the CP during *S. suis* infection.

5.2.2. The overlap of enriched GSs found in all infected CP models

Through the GSEA analysis, 18, 28, and 21 hallmark GSs were identified to be significantly enriched in infected HIBCPP cells, PCPEC, and the CP of pigs suffering from meningitis, respectively (Figure 21 A). Of these GSs, eight GSs were found to be significantly enriched in all three samples sets and are summarized in Figure 21 B. These included the five GSs TNFα signaling via NFκB, inflammatory response, IL2-STAT5 signaling, IL6-JAK/STAT3 signaling, TGFβ signaling, which were previously implicated during *S. suis*-infection, whereas the three GSs for hypoxia, EMT, and a set of genes up-regulated by KRAS signaling, were not. Furthermore, the previously *S. suis*-implicated GSs identified in this study, had also been demonstrated to be involved in the brains of *in vivo S. suis*-infected pigs (Liu et al., 2011a).

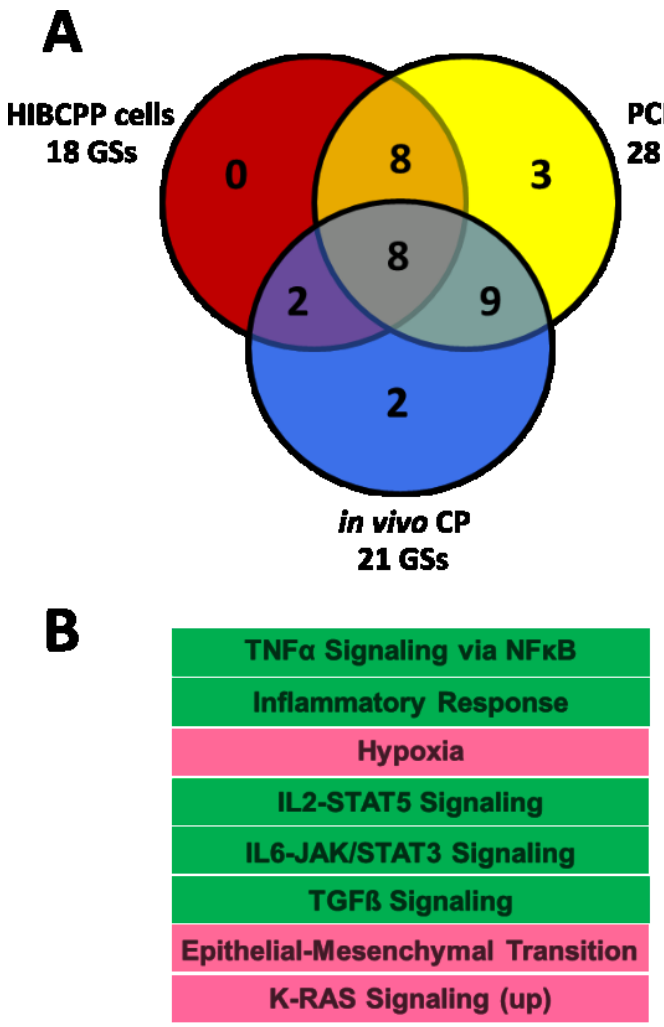

Figure 21. Overlap of the GSEA identified GSs for *S. suis* ST2 infected HIBCPP cells, PCPEC, and the CP of pigs suffering from *S. suis*-induced meningitis. The Venn diagram depicts the number of significantly enriched GSs attributed to each sample set with the number of GSs which were found to overlap between the infected epithelial cells (HIBCPP cells and PCPEC) and the epithelial cells with the *in vivo* CP tissue from meningitis cases, as well as the number of GSs overlapping between all three samples sets analyzed (A). Eight GSs were found to overlap in the three analyzed samples sets, and the name of the enriched GS is listed in (B), where the green boxes are indicative of cellular process previously implicated with *S. suis* ST2 infection, whereas the cellular processes in the red boxes have not been previously associated with the infection of *S. suis*.

It is well described that the activation of the transcription factor NFκB regulates the expression of genes involved in the inflammatory response, including the expression of cytokines and chemokines, such as TNFα (Liu et al., 2017). An increase of TNFα, along with other pro-inflammatory cytokines, was detected in the brain, blood, and kidney of *S. suis* infected mice, as well as in a porcine *in vivo* infection model, which investigated the brain, mononuclear cells, and lung (Liu et al., 2011a; Nakayama et al., 2011). Furthermore, the virulence associated factor, SLY, of *S. suis* was shown to induce the release of TNFα in human monocytes (Lun et al., 2003). However, not just experiments

performed *in vivo* or using whole-blood cells demonstrated the TNFα response, but by utilizing PCPEC, microarray analysis following *S. suis* infection from the apical cell side, also elicited a strong induction of TNFα and other inflammatory cytokines, thereby implying the contribution of the CP epithelial cells in the immune response at the BCSFB (Schwerk et al., 2011). Interestingly, the release of TNFα was found to promote the permeability in a human BCSFB *in vitro* model, by inducing cell death (Schwerk et al., 2010). The release of cytokines is known to elicit a down-stream cellular signaling cascade. One such signaling cascade is the IL6 induction of JAK/STAT3 signaling, which has been described to influence cell growth and differentiation, and is therefore often implicated in cancer when dysregulated (Huynh et al., 2017). Furthermore, as with IL6, IL2 has been described to stimulate the STAT5 signaling cascade, which is known to mainly regulate cellular proliferation and modulate the immune response of T cells (Lin and Leonard, 2000). In the context of *S. suis* infection, STAT3 and STAT5 were found up-regulated in the porcine brain *in vivo* (Liu et al., 2011a). However, the role of these signaling cascades during *S. suis* infection have not been further investigated.

Another well described signaling cascade can be induced by the cytokine TGFβ, which was previously found to be upregulated in the porcine spleen and brain of *S. suis in vivo* infected piglets (Li et al., 2010; Liu et al., 2011a). The induction of TGFβ signaling was previously implicated during the colonization of *S. pneumoniae* and *H. influenzae*, which are other common bacterial meningitis-causative agents, in lung epithelial cells and was accompanied by an inflammatory response (Beisswenger et al., 2009). However, this signaling cascade can impact distinct cell types in different ways depending on the context, and it was described to regulate cellular proliferation and differentiation, as well as other functions that include cell adhesion, migration, survival, as well as tissue homeostasis (Massague, 2012).

To date, hypoxia, EMT, and genes regulated by KRAS signaling have not been directly linked to *S. suis* infection. KRAS signaling is important in the regulation of cellular proliferation and a mutation of the KRAS gene is often implicated in cancer development (Downward, 2003). Its role during infection is not clear, however, in one study it was observed that gastric cancer patients infected with the carcinogenic bacterium, *Helicobacter pylori*, were significantly more likely to exhibit a mutation of KRAS (Jabini et al., 2019). It should be considered that an enrichment of the KRAS GS in this present study was observed due to overlapping genes found with the GS EMT, since genes participating in the cellular EMT program can depend on, among other signaling cascades, the RAS signaling cascade. For example, KRAS was previously shown to regulate EMT in a colon cancer cell line (Kalluri and Weinberg, 2009; Shao et al., 2014). EMT is a cellular program which reverts epithelial cells to mesenchymal cells, and is often implicated in cancer, since it promotes metastasis and invasion, which is easier for mesenchymal cells than epithelial cells to perform (Kalluri and Weinberg, 2009).

EMT is also often involved in wound healing and tissue regeneration, which occurs following a physical trauma or injury caused by inflammation as a result of, e.g., an infection (Hofman and Vouret-Craviari, 2012; Kalluri and Weinberg, 2009). Furthermore, previous studies, especially in cancer research, have demonstrated that a hypoxic environment is a prerequisite in order for EMT to occur (Cannito et al., 2008).

5.3. A new avenue of *S. suis*-induced meningitis: *S. suis* ST2 infected CP epithelial cells exhibit a stress response to the hypoxic environment

A hypoxic microenvironment is often associated in infected tissues or with tumors, and is known to elicit a stress response due to oxygen being a necessity in order for animal cells to carry out their normal physiological functions (Taylor and Colgan, 2017). Furthermore, hypoxia has been implicated during injury to the CNS, which includes stroke or infection (Mukandala et al., 2016; van der Flier et al., 2003). Once a low-oxygen environment occurs, the induction of the hypoxia transcription factors is initiated in order to regulate specific genes, with the main goal of sustaining cell survival by reprograming cellular metabolism (anaerobic glycolysis), increase red blood cell production (erythropoiesis), or promote new blood vessel formation (angiogenesis) (Chen and Sang, 2016). Another interesting aspect of hypoxia is that it is known to affect the global transcription and translation of mRNA molecules by reducing both of these molecular processes, which allows for energy conservation during cellular stress (Koritzinsky and Wouters, 2007). Since the hypoxia GS was the top significantly enriched GS in the infected HIBCPP samples, it could be speculated as a reason for why the HIBCPP cells did not exhibit a strong fold change in the DEG analysis, with a maximal up-regulation of 3.6-fold for ZFP36L1 and the strong down-regulation of 8-fold for MIR3648 was observed, as compared to the PCPEC 6 h post-infection.

Hypoxia stress response can be induced either in a HIF-dependent or HIF-independent manner, most notably via the NFκB transcription factor, with complex overlaps and cross-talks described between these two pathways (Rius et al., 2008; Schaffer and Taylor, 2015). Furthermore, cytokine release, most notable being IL1β and TNFα, is known to be associated in the acute phase of hypoxia, as well as NFκB activation (Mukandala et al., 2016). Additionally, IL1β and TNFα have been shown to activate the HIF transcription factor in an oxygen-independent and NFκB-dependent pathway during inflammation (Lin and Simon, 2016). Interestingly, the inflammatory cytokine IL1β was observed to affect BBB permeability by influencing blood vessel plasticity via HIF regulation in the angiogenesis program in multiple sclerosis patients (Argaw et al., 2006). A further study investigating the cytokine presence in the CSF of infants who suffered a perinatal hypoxia event, found that infants who

displayed an elevated amount of TNFα and IL6 in the CSF, were significantly more likely to suffer from severe neurological abnormalities 12 months post-partum; a phenomenon, which was also observed in survivors of bacterial meningitis and cerebral malaria (John et al., 2008; Perdomo-Celis et al., 2015; Sumanovic-Glamuzina et al., 2017).

Hypoxia does not only induce a cellular stress response, but is also described to modulate cell functions. For example, in an *in vitro* hypoxic environment, changes of the immune response in extracellular trap formation, which is a cellular process that releases the intracellular content known to contain antimicrobial properties, and phagocytosis were observed. This included a decrease of NET formation by neutrophil immune cells and an increase of extracellular traps stemming from mast cells, along with a reduced phagocytic activity (Branitzki-Heinemann et al., 2016; Mollerherm et al., 2017). However, in a limited number of studies, hypoxia was also described to modulate and affect other cell types, such as epithelial cells during infection (Schaffer and Taylor, 2015; Taylor and Colgan, 2017). In two previous studies, it was demonstrated that a hypoxic environment during the infection with *Pseudomonas aeruginosa* of lung epithelial cells reduced the host's cellular uptake of the pathogen, thereby diminishing host cell death, as well as causing a decline in the invasion of *Yersinia enterocolitica* into intestinal epithelial cells *in vitro* (Schaible et al., 2013; Zeitouni et al., 2016). Furthermore, hypoxia also negatively affected the virulence factor expression (Schaible et al., 2017). These studies demonstrate that a hypoxic environment was able to aid in containing the infection.

In this present study, it was observed for the first time to our knowledge, that hypoxia-related cellular processes were significantly increased in relation to *S. suis* ST2 infection *in vitro* with human CP epithelial cells and PCPEC, as well as in the *in vivo* infected porcine CP samples. Since the HIF1α subunit of the heterodimeric HIF transcription factor is known to have a very short half-life of approximately 5 minutes, future studies could examine the impact of hypoxia over a time course caused by *S. suis* infection on its host cells at the BCSFB in the context of acute and chronic hypoxia (Chatard et al., 2017; Mukandala et al., 2016). *In vitro* models of the BBB are in place to study hypoxic effects on the BBB cells and the barrier, and this application should be applied to BCSFB *in vitro* models with human and porcine cells (Chatard et al., 2017). Additionally, a previously established monitoring system is in place for investigating mammalian cell culture pH and oxygen presence (Naciri et al., 2008). Noteworthy, one gene in particular stood out in the enriched hypoxia GS in all three analyzed samples sets. VEGF was found to be one of the top enriched genes in the hypoxia GS of all analyzed samples (data not shown), which is indicative of angiogenesis, and in turn has been implicated in chronic hypoxia response (Mukandala et al., 2016).

Lastly, the hypoxia transcription factor HIF has be discussed as a potential target for adjunctive therapy options, with already successful candidates against methicillin-sensitive and -resistant *Staphylococcus aureus* strains, in order to improve outcome or potentially replace antimicrobial therapeutics due to a rise in microbial resistance (Okumura et al., 2012; Santos and Andrade, 2017; Zinkernagel et al., 2008). Importantly, HIF therapy would not be solely limited to infections, but could also be applied in the setting of cancer treatment or chronic inflammatory disorders (Santos and Andrade, 2017).

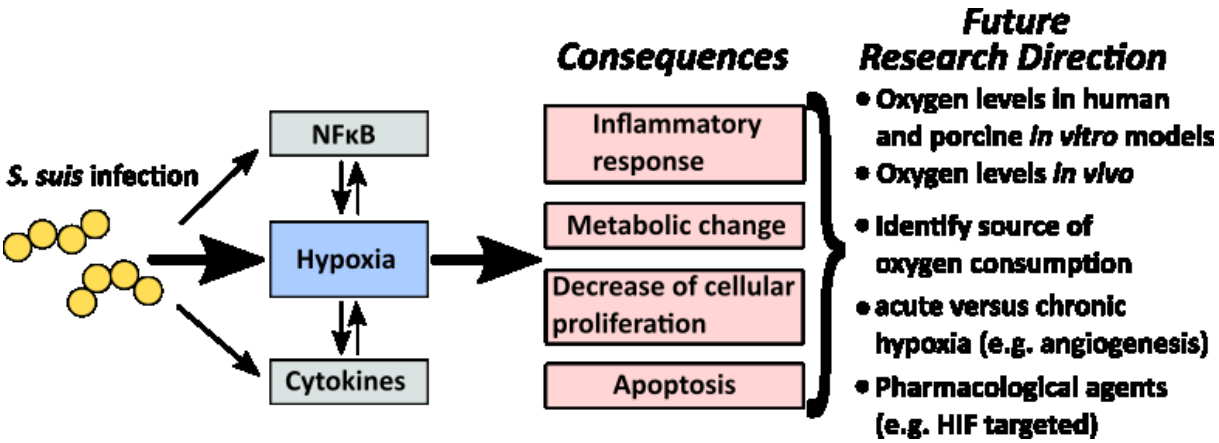

Figure 22. Hypoxia, its role during *S. suis* ST2 infection, and future avenues of research. *S. suis* infection was shown to induce genes involved during a hypoxic state, along with cytokines and NFκB known to also play a role during hypoxia, leading to multiple consequences of the cell response. In order to gain a deeper understanding of hypoxia during *S. suis* infection, multiple avenues relevant to hypoxia are suggested.

The future avenues involving the investigation of hypoxia during *S. suis* infection are summarized in Figure 22. By investigating the role of hypoxia in the context of *S. suis* infection, with a focus on the significance of the BCSFB, a long-term aim could be explored of alternative therapy options. Those alternative therapy options could potentially limit infection severity, which is often found corresponding to long-term sequelae of survivors, such as full or partial auditory loss frequently associated with *S. suis* infection in humans, or death.

6. Conclusion and Future Perspectives

Despite the availability of vaccines and antibiotic therapeutic agents, bacterial meningitis remains a leading cause of morbidity worldwide, frequently resulting in long-term neurological impairments or death. The zoonotic pathogenic agent *S. suis* is a leading cause for adult bacterial meningitis in south-east Asia, and occurrences in other large pig-husbandry nations, but is also responsible for major economic losses worldwide due to post-weaned piglets being at a particularly high risk for disease development.

From this study, the vital role the CP plays during infection was further elucidated. With a state-of-the-art bioinformatic approach, which evaluated the global transcriptome response via RNA-seq, new insights were gained on how different host cells respond to *S. suis in vitro* and *in vivo*. Not only was the contribution by the CP to the immune response observed, but new cellular processes occurring at the transcriptome level were identified, such as hypoxia. Therefore, these novel insights lay a new foundation for future perspective studies in order to aid in further elucidating cellular mechanisms playing an essential role during an infection with *S. suis*.

However, one main limiting factor of this study was that a transcriptome snapshot was obtained following a 6 hour infection time point. Therefore, it would be of interest to evaluate the transcriptional changes occurring over time *in vitro*, as well as at different stages *in vivo*, in order to further clarify how the inflammatory response is initiated and progresses. This is important, since an exasperated immune response and infection progression is linked to a bleak outcome, early intervention could result in the most ideal outcome and counteract debilitating sequelae.

Furthermore, the development of improved treatment options should be established. Although the use of antibiotics, and in some cases the use of dexamethasone as adjunctive therapy to reduce inflammation, is currently in place, the rise of antibiotic resistance remains a global threat. One alternative therapy option was presented by Shen and colleagues, who suggested the use of a natural compound found to limit virulence and inflammation specifically during *S. suis in vitro* and *in vivo* infections, and with the use of this compound simultaneously decreased the selection pressure towards antibiotic resistant genes (Shen et al., 2018). However, since hypoxia was observed in the present thesis to play a significant role during infection with *S. suis*, especially in the human *in vitro* BCSFB, further investigations to fully elucidate this role need to be performed to understand the impact during infection and consequences for the host. This would be especially relevant since studies investigating the effective pharmaceutical targeting of the hypoxia pathway have been described.

Understanding the cellular processes occurring at the BCSFB is one of the first steps for development of effective therapeutics. The CP is not only pivotal in producing the CSF of the CNS, but evidence exists which implicates the CP beyond infections, in debilitating diseases, such as multiple sclerosis and cancer metastasis. Therefore, for the future, more research needs to be dedicated to this small tissue structure, which plays a vital role in maintaining a healthy CNS.

I. Reference List

Abbott, N.J., Patabendige, A.A., Dolman, D.E., Yusof, S.R., and Begley, D.J. (2010). Structure and function of the blood-brain barrier. Neurobiol Dis *37*, 13-25.

Abbott, N.J., Ronnback, L., and Hansson, E. (2006). Astrocyte-endothelial interactions at the blood-brain barrier. Nat Rev Neurosci *7*, 41-53.

Agier, L., Martiny, N., Thiongane, O., Mueller, J.E., Paireau, J., Watkins, E.R., Irving, T.J., Koutangni, T., and Broutin, H. (2017). Towards understanding the epidemiology of *Neisseria meningitidis* in the African meningitis belt: a multi-disciplinary overview. Int J Infect Dis *54*, 103-112.

Al-Obaidi, M.M.J., and Desa, M.N.M. (2018). Mechanisms of blood brain barrier disruption by different types of bacteria, and bacterial-host interactions facilitate the bacterial pathogen invading the brain. Cell Mol Neurobiol *38*, 1349-1368.

Al Ahmad, A., Gassmann, M., and Ogunshola, O.O. (2012). Involvement of oxidative stress in hypoxia-induced blood-brain barrier breakdown. Microvasc Res *84*, 222-225.

Alberti, A., Belser, C., Engelen, S., Bertrand, L., Orvain, C., Brinas, L., Cruaud, C., Giraut, L., Da Silva, C., Firmo, C.*, et al.* (2014). Comparison of library preparation methods reveals their impact on interpretation of metatranscriptomic data. BMC Genomics *15*, 912.

Argaw, A.T., Zhang, Y., Snyder, B.J., Zhao, M.L., Kopp, N., Lee, S.C., Raine, C.S., Brosnan, C.F., and John, G.R. (2006). IL-1beta regulates blood-brain barrier permeability via reactivation of the hypoxia-angiogenesis program. J Immunol *177*, 5574-5584.

Ashburner, M., Ball, C.A., Blake, J.A., Botstein, D., Butler, H., Cherry, J.M., Davis, A.P., Dolinski, K., Dwight, S.S., Eppig, J.T.*, et al.* (2000). Gene ontology: tool for the unification of biology. The Gene Ontology Consortium. Nat Genet *25*, 25-29.

Baums, C.G., Kaim, U., Fulde, M., Ramachandran, G., Goethe, R., and Valentin-Weigand, P. (2006). Identification of a novel virulence determinant with serum opacification activity in *Streptococcus suis*. Infect Immun *74*, 6154-6162.

Baums, C.G., Kock, C., Beineke, A., Bennecke, K., Goethe, R., Schroder, C., Waldmann, K.H., and Valentin-Weigand, P. (2009). *Streptococcus suis* bacterin and subunit vaccine immunogenicities and protective efficacies against serotypes 2 and 9. Clin Vaccine Immunol *16*, 200-208.

Beisswenger, C., Lysenko, E.S., and Weiser, J.N. (2009). Early bacterial colonization induces toll-like receptor-dependent transforming growth factor beta signaling in the epithelium. Infect Immun *77*, 2212-2220.

Bernd, A., Ott, M., Ishikawa, H., Schroten, H., Schwerk, C., and Fricker, G. (2015). Characterization of efflux transport proteins of the human choroid plexus papilloma cell line HIBCPP, a functional *in vitro* model of the blood-cerebrospinal fluid barrier. Pharm Res *32*, 2973-2982.

Berthelot-Herault, F., Gottschalk, M., Labbe, A., Cariolet, R., and Kobisch, M. (2001). Experimental airborne transmission of *Streptococcus suis* capsular type 2 in pigs. Vet Microbiol *82*, 69-80.

Bolger, A.M., Lohse, M., and Usadel, B. (2014). Trimmomatic: a flexible trimmer for Illumina sequence data. Bioinformatics *30*, 2114-2120.

Borkowski, J., Li, L., Steinmann, U., Quednau, N., Stump-Guthier, C., Weiss, C., Findeisen, P., Gretz, N., Ishikawa, H., Tenenbaum, T*., et al.* (2014). *Neisseria meningitidis* elicits a pro-inflammatory response involving IkappaBzeta in a human blood-cerebrospinal fluid barrier model. J Neuroinflammation *11*, 163.

Bracken, A.P., Ciro, M., Cocito, A., and Helin, K. (2004). E2F target genes: unraveling the biology. Trends Biochem Sci *29*, 409-417.

Branitzki-Heinemann, K., Mollerherm, H., Vollger, L., Husein, D.M., de Buhr, N., Blodkamp, S., Reuner, F., Brogden, G., Naim, H.Y., and von Kockritz-Blickwede, M. (2016). Formation of neutrophil extracellular traps under low oxygen level. Front Immunol *7*, 518.

Cannito, S., Novo, E., Compagnone, A., Valfre di Bonzo, L., Busletta, C., Zamara, E., Paternostro, C., Povero, D., Bandino, A., Bozzo, F*., et al.* (2008). Redox mechanisms switch on hypoxia-dependent epithelial-mesenchymal transition in cancer cells. Carcinogenesis *29*, 2267-2278.

Chandran, A., Herbert, H., Misurski, D., and Santosham, M. (2011). Long-term sequelae of childhood bacterial meningitis: an underappreciated problem. Pediatr Infect Dis J *30*, 3-6.

Chang, C.W., Ye, L., Defoe, D.M., and Caldwell, R.B. (1997). Serum inhibits tight junction formation in cultured pigment epithelial cells. Invest Ophthalmol Vis Sci *38*, 1082-1093.

Charland, N., Nizet, V., Rubens, C.E., Kim, K.S., Lacouture, S., and Gottschalk, M. (2000). *Streptococcus suis* serotype 2 interactions with human brain microvascular endothelial cells. Infect Immun *68*, 637-643.

Chatard, M., Puech, C., Perek, N., and Roche, F. (2017). Hydralazine is a suitable mimetic agent of hypoxia to study the impact of hypoxic stress on *in vitro* blood-brain barrier model. Cell Physiol Biochem *42*, 1592-1602.

Chen, S., and Sang, N. (2016). Hypoxia-inducible factor-1: A critical player in the survival strategy of stressed cells. J Cell Biochem *117*, 267-278.

Cloutier, G., D'Allaire, S., Martinez, G., Surprenant, C., Lacouture, S., and Gottschalk, M. (2003). Epidemiology of *Streptococcus suis* serotype 5 infection in a pig herd with and without clinical disease. Vet Microbiol *97*, 135-151.

Conesa, A., Madrigal, P., Tarazona, S., Gomez-Cabrero, D., Cervera, A., McPherson, A., Szczesniak, M.W., Gaffney, D.J., Elo, L.L., Zhang, X*., et al.* (2016). A survey of best practices for RNA-seq data analysis. Genome Biol *17*, 13.

Dando, S.J., Mackay-Sim, A., Norton, R., Currie, B.J., St John, J.A., Ekberg, J.A., Batzloff, M., Ulett, G.C., and Beacham, I.R. (2014). Pathogens penetrating the central nervous system: infection pathways and the cellular and molecular mechanisms of invasion. Clin Microbiol Rev *27*, 691-726.

Dang, C.V. (2012). MYC on the path to cancer. Cell *149*, 22-35.

de Buhr, N., Reuner, F., Neumann, A., Stump-Guthier, C., Tenenbaum, T., Schroten, H., Ishikawa, H., Muller, K., Beineke, A., Hennig-Pauka, I*., et al.* (2017). Neutrophil extracellular trap formation in the *Streptococcus suis*-infected cerebrospinal fluid compartment. Cell Microbiol *19*.

De, S.K., and Baron, M. (2012). Step-up and step-down methods for testing multiple hypotheses in sequential experiments. J Stat Plan Inference *142*, 2059-2070.

Del Maestro, R.F. (1998). Leonardo da Vinci: the search for the soul. J Neurosurg *89*, 874-887.

Dinner, S., Borkowski, J., Stump-Guthier, C., Ishikawa, H., Tenenbaum, T., Schroten, H., and Schwerk, C. (2016). A choroid plexus epithelial cell-based model of the human blood-cerebrospinal fluid barrier to study bacterial infection from the basolateral side. J Vis Exp *111*, 54061.

Dobin, A., Davis, C.A., Schlesinger, F., Drenkow, J., Zaleski, C., Jha, S., Batut, P., Chaisson, M., and Gingeras, T.R. (2013). STAR: ultrafast universal RNA-seq aligner. Bioinformatics *29*, 15-21.

Dominguez-Punaro, M.C., Segura, M., Plante, M.M., Lacouture, S., Rivest, S., and Gottschalk, M. (2007). *Streptococcus suis* serotype 2, an important swine and human pathogen, induces strong systemic and cerebral inflammatory responses in a mouse model of infection. J Immunol *179*, 1842-1854.

Doran, K.S., Fulde, M., Gratz, N., Kim, B.J., Nau, R., Prasadarao, N., Schubert-Unkmeir, A., Tuomanen, E.I., and Valentin-Weigand, P. (2016). Host-pathogen interactions in bacterial meningitis. Acta Neuropathol *131*, 185-209.

Downward, J. (2003). Targeting RAS signalling pathways in cancer therapy. Nat Rev Cancer *3*, 11-22.

Du, P., Zheng, H., Zhou, J., Lan, R., Ye, C., Jing, H., Jin, D., Cui, Z., Bai, X., Liang, J*., et al.* (2017). Detection of multiple parallel transmission outbreak of *Streptococcus suis* human infection by use of genome epidemiology, China, 2005. Emerg Infect Dis *23*, 204-211.

Dutkiewicz, J., Sroka, J., Zajac, V., Wasinski, B., Cisak, E., Sawczyn, A., Kloc, A., and Wojcik-Fatla, A. (2017). *Streptococcus suis*: a re-emerging pathogen associated with occupational exposure to pigs or pork products. Part I - Epidemiology. Ann Agric Environ Med *24*, 683-695.

Dutkiewicz, J., Zajac, V., Sroka, J., Wasinski, B., Cisak, E., Sawczyn, A., Kloc, A., and Wojcik-Fatla, A. (2018). *Streptococcus suis*: a re-emerging pathogen associated with occupational exposure to pigs or pork products. Part II - Pathogenesis. Ann Agric Environ Med *25*, 186-203.

Egelund, G.B., Ertner, G., Kristensen, K.L., Jensen, A.V., Benfield, T.L., and Brandt, C.T. (2017). Cerebrospinal fluid pleocytosis in infectious and noninfectious central nervous system disease: A retrospective cohort study. Medicine *96*, e6686.

Ehrlich, P. (1885). Das Sauerstoff-Bedürfnis des Organismus. Eine farbenanalytische Studie. Herschwald, Berlin, 69-72.

Engelhardt, B., Vajkoczy, P., and Weller, R.O. (2017). The movers and shapers in immune privilege of the CNS. Nat Immunol *18*, 123-131.

Falangola, M.F., and Petito, C.K. (1993). Choroid plexus infection in cerebral toxoplasmosis in AIDS patients. Neurology *43*, 2035-2040.

Fang, Z., and Cui, X. (2011). Design and validation issues in RNA-seq experiments. Brief Bioinform *12*, 280-287.

Fittipaldi, N., Segura, M., Grenier, D., and Gottschalk, M. (2012). Virulence factors involved in the pathogenesis of the infection caused by the swine pathogen and zoonotic agent *Streptococcus suis*. Future Microbiol *7*, 259-279.

Franco, M., Shastri, A.J., and Boothroyd, J.C. (2014). Infection by *Toxoplasma gondii* specifically induces host c-Myc and the genes this pivotal transcription factor regulates. Eukaryot Cell *13*, 483-493.

Fuhrmann, D.C., and Brune, B. (2017). Mitochondrial composition and function under the control of hypoxia. Redox Biol *12*, 208-215.

Gallego Romero, I., Pai, A.A., Tung, J., and Gilad, Y. (2014). RNA-seq: impact of RNA degradation on transcript quantification. BMC Biol *12*, 42.

Gath, U., Hakvoort, A., Wegener, J., Decker, S., and Galla, H.J. (1997). Porcine choroid plexus cells in culture: expression of polarized phenotype, maintenance of barrier properties and apical secretion of CSF-components. Eur J Cell Biol *74*, 68-78.

Ghersi-Egea, J.F., Strazielle, N., Catala, M., Silva-Vargas, V., Doetsch, F., and Engelhardt, B. (2018). Molecular anatomy and functions of the choroidal blood-cerebrospinal fluid barrier in health and disease. Acta Neuropathol *135*, 337-361.

Glaser, C.A., Honarmand, S., Anderson, L.J., Schnurr, D.P., Forghani, B., Cossen, C.K., Schuster, F.L., Christie, L.J., and Tureen, J.H. (2006). Beyond viruses: clinical profiles and etiologies associated with encephalitis. Clin Infect Dis *43*, 1565-1577.

Glennon, N.B., Jabado, O., Lo, M.K., and Shaw, M.L. (2015). Transcriptome profiling of the virus-induced innate immune response in *Pteropus vampyrus* and its attenuation by Nipah virus interferon antagonist functions. J Virol *89*, 7550-7566.

Goldmann, E. (1913). Vitalfärbung am Zentralnervensystem. Abh Preuss Wissensch Phys Math *1*, 1-60.

Goralska, K., Blaszkowska, J., and Dzikowiec, M. (2018). Neuroinfections caused by fungi. Infection *46*, 443-459.

Gottschalk, M.G., Lacouture, S., and Dubreuil, J.D. (1995). Characterization of *Streptococcus suis* capsular type 2 haemolysin. Microbiology *141 (Pt 1)*, 189-195.

Goyette-Desjardins, G., Auger, J.P., Xu, J., Segura, M., and Gottschalk, M. (2014). *Streptococcus suis*, an important pig pathogen and emerging zoonotic agent-an update on the worldwide distribution based on serotyping and sequence typing. Emerg Microbes Infect *3*, e45.

Graeff-Teixeira, C., da Silva, A.C., and Yoshimura, K. (2009). Update on eosinophilic meningoencephalitis and its clinical relevance. Clin Microbiol Rev *22*, 322-348.

Grandgirard, D., Gaumann, R., Coulibaly, B., Dangy, J.P., Sie, A., Junghanss, T., Schudel, H., Pluschke, G., and Leib, S.L. (2013). The causative pathogen determines the inflammatory profile in cerebrospinal fluid and outcome in patients with bacterial meningitis. Mediators Inflamm *2013*, 312476.

Grimwood, K., Anderson, V.A., Bond, L., Catroppa, C., Hore, R.L., Keir, E.H., Nolan, T., and Roberton, D.M. (1995). Adverse outcomes of bacterial meningitis in school-age survivors. Pediatrics *95*, 646-656.

Haas, B., and Grenier, D. (2018). Understanding the virulence of *Streptococcus suis*: A veterinary, medical, and economic challenge. Med Mal Infect *48*, 159-166.

Hakvoort, A., Haselbach, M., Wegener, J., Hoheisel, D., and Galla, H.J. (1998). The polarity of choroid plexus epithelial cells *in vitro* is improved in serum-free medium. J Neurochem *71*, 1141-1150.

Harris, R.A., Wang, T., Coarfa, C., Nagarajan, R.P., Hong, C., Downey, S.L., Johnson, B.E., Fouse, S.D., Delaney, A., Zhao, Y*., et al.* (2010). Comparison of sequencing-based methods to profile DNA methylation and identification of monoallelic epigenetic modifications. Nat Biotechnol *28*, 1097-1105.

Haselbach, M., Wegener, J., Decker, S., Engelbertz, C., and Galla, H.J. (2001). Porcine choroid plexus epithelial cells in culture: regulation of barrier properties and transport processes. Microsc Res Tech *52*, 137-152.

Head, S.R., Komori, H.K., LaMere, S.A., Whisenant, T., Van Nieuwerburgh, F., Salomon, D.R., and Ordoukhanian, P. (2014). Library construction for next-generation sequencing: overviews and challenges. Biotechniques *56*, 61-64, 66, 68, passim.

Hewett, S.J., Jackman, N.A., and Claycomb, R.J. (2012). Interleukin-1beta in central nervous system injury and repair. Eur J Neurodegener Dis *1*, 195-211.

Hill, D.J., Griffiths, N.J., Borodina, E., and Virji, M. (2010). Cellular and molecular biology of *Neisseria meningitidis* colonization and invasive disease. Clin Sci (Lond) *118*, 547-564.

Ho Dang Trung, N., Le Thi Phuong, T., Wolbers, M., Nguyen Van Minh, H., Nguyen Thanh, V., Van, M.P., Thieu, N.T., Van, T.L., Song, D.T., Thi, P.L*., et al.* (2012). Aetiologies of central nervous system infection in Viet Nam: a prospective provincial hospital-based descriptive surveillance study. PLoS One *7*, e37825.

Hofman, P., and Vouret-Craviari, V. (2012). Microbes-induced EMT at the crossroad of inflammation and cancer. Gut Microbes *3*, 176-185.

Hrdlickova, R., Toloue, M., and Tian, B. (2017). RNA-Seq methods for transcriptome analysis. Wiley Interdiscip Rev RNA *8*, 1-17.

Hu, X., Zhu, F., Wang, H., Chen, S., Wang, G., Sun, J., Hua, C., and Yang, H. (2000). [Studies on human streptococcal infectious syndrome caused by infected pigs]. Zhonghua Yu Fang Yi Xue Za Zhi *34*, 150-152.

Huong, V.T., Ha, N., Huy, N.T., Horby, P., Nghia, H.D., Thiem, V.D., Zhu, X., Hoa, N.T., Hien, T.T., Zamora, J*., et al.* (2014). Epidemiology, clinical manifestations, and outcomes of *Streptococcus suis* infection in humans. Emerg Infect Dis *20*, 1105-1114.

Huong, V.T.L., Turner, H.C., Kinh, N.V., Thai, P.Q., Hoa, N.T., Horby, P., van Doorn, H.R., and Wertheim, H.F.L. (2019). Burden of disease and economic impact of human *Streptococcus suis* infection in Viet Nam. Trans R Soc Trop Med Hyg.

Huynh, J., Etemadi, N., Hollande, F., Ernst, M., and Buchert, M. (2017). The JAK/STAT3 axis: A comprehensive drug target for solid malignancies. Semin Cancer Biol *45*, 13-22.

International Human Genome Sequencing, C. (2004). Finishing the euchromatic sequence of the human genome. Nature *431*, 931-945.

Ishiwata, I., Ishiwata, C., Ishiwata, E., Sato, Y., Kiguchi, K., Tachibana, T., Hashimoto, H., and Ishikawa, H. (2005). Establishment and characterization of a human malignant choroids plexus papilloma cell line (HIBCPP). Hum Cell *18*, 67-72.

Jabini, R., Eghbali, S.A., Ayatollahi, H., Sheikhi, M., and Farzanehfar, M. (2019). Analysis of KRAS gene mutation associated with *Helicobacter pylori* infection in patients with gastric cancer. Iran J Basic Med Sci *22*, 529-533.

John, C.C., Panoskaltsis-Mortari, A., Opoka, R.O., Park, G.S., Orchard, P.J., Jurek, A.M., Idro, R., Byarugaba, J., and Boivin, M.J. (2008). Cerebrospinal fluid cytokine levels and cognitive impairment in cerebral malaria. Am J Trop Med Hyg *78*, 198-205.

Kalluri, R., and Weinberg, R.A. (2009). The basics of epithelial-mesenchymal transition. J Clin Invest *119*, 1420-1428.

Kim, J., Kim, Y., Kim, H.T., Kim, D.W., Ha, Y., Kim, J., Kim, C.H., Lee, I., and Song, K. (2009). TC1(C8orf4) is a novel endothelial inflammatory regulator enhancing NF-kappaB activity. J Immunol *183*, 3996-4002.

Kim, K.S. (2008). Mechanisms of microbial traversal of the blood-brain barrier. Nat Rev Microbiol *6*, 625-634.

Kim, K.S. (2010). Acute bacterial meningitis in infants and children. Lancet Infect Dis *10*, 32-42.

Kim, S., Hwang, Y., Lee, D., and Webster, M.J. (2016). Transcriptome sequencing of the choroid plexus in schizophrenia. Transl Psychiatry *6*, e964.

Kim, Y., Kim, J., Park, J., Bang, S., Jung, Y., Choe, J., Song, K., and Lee, I. (2006). TC1(C8orf4) is upregulated by IL-1beta/TNF-alpha and enhances proliferation of human follicular dendritic cells. FEBS Lett *580*, 3519-3524.

King, S.J., Leigh, J.A., Heath, P.J., Luque, I., Tarradas, C., Dowson, C.G., and Whatmore, A.M. (2002). Development of a multilocus sequence typing scheme for the pig pathogen *Streptococcus suis*: identification of virulent clones and potential capsular serotype exchange. J Clin Microbiol *40*, 3671-3680.

Koritzinsky, M., and Wouters, B.G. (2007). Hypoxia and regulation of messenger RNA translation. Methods Enzymol *435*, 247-273.

Kukurba, K.R., and Montgomery, S.B. (2015). RNA sequencing and analysis. Cold Spring Harb Protoc *2015*, 951-969.

Kundu, M., Guermah, M., Roeder, R.G., Amini, S., and Khalili, K. (1997). Interaction between cell cycle regulator, E2F-1, and NF-kappa B mediates repression of HIV-1 gene transcription. J Biol Chem *272*, 29468-29474.

Lakkitjaroen, N., Takamatsu, D., Okura, M., Sato, M., Osaki, M., and Sekizaki, T. (2011). Loss of capsule among *Streptococcus suis* isolates from porcine endocarditis and its biological significance. J Med Microbiol *60*, 1669-1676.

Lauer, A.N., Tenenbaum, T., Schroten, H., and Schwerk, C. (2018). The diverse cellular responses of the choroid plexus during infection of the central nervous system. Am J Physiol Cell Physiol *314*, C152-C165.

Li, R., Zhang, A., Chen, B., Teng, L., Wang, Y., Chen, H., and Jin, M. (2010). Response of swine spleen to *Streptococcus suis* infection revealed by transcription analysis. BMC Genomics *11*, 556.

Liberzon, A., Birger, C., Thorvaldsdottir, H., Ghandi, M., Mesirov, J.P., and Tamayo, P. (2015). The Molecular Signatures Database (MSigDB) hallmark gene set collection. Cell Syst *1*, 417-425.

Liberzon, A., Subramanian, A., Pinchback, R., Thorvaldsdottir, H., Tamayo, P., and Mesirov, J.P. (2011). Molecular signatures database (MSigDB) 3.0. Bioinformatics *27*, 1739-1740.

Liddelow, S.A. (2015). Development of the choroid plexus and blood-CSF barrier. Front Neurosci *9*, 32.

Lin, J.X., and Leonard, W.J. (2000). The role of Stat5a and Stat5b in signaling by IL-2 family cytokines. Oncogene *19*, 2566-2576.

Lin, N., and Simon, M.C. (2016). Hypoxia-inducible factors: key regulators of myeloid cells during inflammation. J Clin Invest *126*, 3661-3671.

Liu, H., Jia, L., Guo, W., Sun, Y., Zhu, R., Li, S., Qu, G., Jiang, H., Wang, J., Gu, J*., et al.* (2018). Differential protein profiling of cerebrospinal fluid in piglets with severe meningoencephalitis caused by *Streptococcus suis* type 2 compared to controls. Front Cell Infect Microbiol *8*, 35.

Liu, M., Fang, L., Tan, C., Long, T., Chen, H., and Xiao, S. (2011a). Understanding *Streptococcus suis* serotype 2 infection in pigs through a transcriptional approach. BMC Genomics *12*, 253.

Liu, M., Tan, C., Fang, L., Xiao, S., and Chen, H. (2011b). Microarray analyses of THP-1 cells infected with *Streptococcus suis* serotype 2. Vet Microbiol *150*, 126-131.

Liu, T., Zhang, L., Joo, D., and Sun, S.C. (2017). NF-kappaB signaling in inflammation. Signal Transduct Target Ther *2*.

Livak, K.J., and Schmittgen, T.D. (2001). Analysis of relative gene expression data using real-time quantitative PCR and the 2(-Delta Delta C(T)) Method. Methods *25*, 402-408.

Lun, S., Perez-Casal, J., Connor, W., and Willson, P.J. (2003). Role of suilysin in pathogenesis of *Streptococcus suis* capsular serotype 2. Microb Pathog *34*, 27-37.

Martin, J.A., and Wang, Z. (2011). Next-generation transcriptome assembly. Nat Rev Genet *12*, 671-682.

Massague, J. (2012). TGFbeta signalling in context. Nat Rev Mol Cell Biol *13*, 616-630.

Meeker, R.B., Williams, K., Killebrew, D.A., and Hudson, L.C. (2012). Cell trafficking through the choroid plexus. Cell Adh Migr *6*, 390-396.

Meijerink, M., Ferrando, M.L., Lammers, G., Taverne, N., Smith, H.E., and Wells, J.M. (2012). Immunomodulatory effects of *Streptococcus suis* capsule type on human dendritic cell responses, phagocytosis and intracellular survival. PLoS One *7*, e35849.

Metzker, M.L. (2005). Emerging technologies in DNA sequencing. Genome Res *15*, 1767-1776.

Metzker, M.L. (2010). Sequencing technologies - the next generation. Nat Rev Genet *11*, 31-46.

Mollerherm, H., Branitzki-Heinemann, K., Brogden, G., Elamin, A.A., Oehlmann, W., Fuhrmann, H., Singh, M., Naim, H.Y., and von Kockritz-Blickwede, M. (2017). Hypoxia modulates the response of mast cells to *Staphylococcus aureus* infection. Front Immunol *8*, 541.

Mootha, V.K., Lindgren, C.M., Eriksson, K.F., Subramanian, A., Sihag, S., Lehar, J., Puigserver, P., Carlsson, E., Ridderstrale, M., Laurila, E.*, et al.* (2003). PGC-1alpha-responsive genes involved in oxidative phosphorylation are coordinately downregulated in human diabetes. Nat Genet *34*, 267-273.

Mortazavi, A., Williams, B.A., McCue, K., Schaeffer, L., and Wold, B. (2008). Mapping and quantifying mammalian transcriptomes by RNA-Seq. Nat Methods *5*, 621-628.

Mukandala, G., Tynan, R., Lanigan, S., and O'Connor, J.J. (2016). The effects of hypoxia and inflammation on synaptic signaling in the CNS. Brain Sci *6*.

Naciri, M., Kuystermans, D., and Al-Rubeai, M. (2008). Monitoring pH and dissolved oxygen in mammalian cell culture using optical sensors. Cytotechnology *57*, 245-250.

Nakayama, T., Takeuchi, D., Akeda, Y., and Oishi, K. (2011). *Streptococcus suis* infection induces [corrected] bacterial accumulation in the kidney. Microb Pathog *50*, 87-93.

Nobes, C.D., Lauritzen, I., Mattei, M.G., Paris, S., Hall, A., and Chardin, P. (1998). A new member of the Rho family, Rnd1, promotes disassembly of actin filament structures and loss of cell adhesion. J Cell Biol *141*, 187-197.

O'Neil, D., Glowatz, H., and Schlumpberger, M. (2013). Ribosomal RNA depletion for efficient use of RNA-seq capacity. Curr Protoc Mol Biol *Chapter 4*, Unit 4 19.

Okumura, C.Y., Hollands, A., Tran, D.N., Olson, J., Dahesh, S., von Kockritz-Blickwede, M., Thienphrapa, W., Corle, C., Jeung, S.N., Kotsakis, A.*, et al.* (2012). A new pharmacological agent (AKB-4924) stabilizes hypoxia inducible factor-1 (HIF-1) and increases skin innate defenses against bacterial infection. J Mol Med (Berl) *90*, 1079-1089.

Pallares, F.J., Halbur, P.G., Schmitt, C.S., Roth, J.A., Opriessnig, T., Thomas, P.J., Kinyon, J.M., Murphy, D., Frank, D.E., and Hoffman, L.J. (2003). Comparison of experimental models for *Streptococcus suis* infection of conventional pigs. Can J Vet Res *67*, 225-228.

Pappas, G. (2013). Socio-economic, industrial and cultural parameters of pig-borne infections. Clin Microbiol Infect *19*, 605-610.

Perch, B., Kristjansen, P., and Skadhauge, K. (1968). Group R streptococci pathogenic for man. Two cases of meningitis and one fatal case of sepsis. Acta Pathol Microbiol Scand *74*, 69-76.

Perdomo-Celis, F., Torres, M.A., Ostos, H., Gutierrez-Achury, J., Molano, V., Duran, L.F., Gonzalez, G., and Narvaez, C.F. (2015). Patterns of local and systemic cytokines in bacterial meningitis and its relation with severity and long-term sequelae. Biomark Insights *10*, 125-131.

Ransohoff, R.M., and Engelhardt, B. (2012). The anatomical and cellular basis of immune surveillance in the central nervous system. Nat Rev Immunol *12*, 623-635.

Rashid, F., Awan, H.M., Shah, A., Chen, L., and Shan, G. (2017). Induction of miR-3648 upon ER stress and its regulatory role in cell proliferation. Int J Mol Sci *18*.

Rayanakorn, A., Goh, B.H., Lee, L.H., Khan, T.M., and Saokaew, S. (2018). Risk factors for *Streptococcus suis* infection: A systematic review and meta-analysis. Sci Rep *8*, 13358.

Razooky, B.S., Obermayer, B., O'May, J.B., and Tarakhovsky, A. (2017). Viral infection identifies micropeptides differentially regulated in smORF-containing lncRNAs. Genes (Basel) *8*.

Renner, M., Lancaster, M.A., Bian, S., Choi, H., Ku, T., Peer, A., Chung, K., and Knoblich, J.A. (2017). Self-organized developmental patterning and differentiation in cerebral organoids. EMBO J *36*, 1316-1329.

Rieckmann, K., Seydel, A., Szewczyk, K., Klimke, K., Rungelrath, V., and Baums, C.G. (2018). *Streptococcus suis* cps7: an emerging virulent sequence type (ST29) shows a distinct, IgM-determined pattern of bacterial survival in blood of piglets during the early adaptive immune response after weaning. Vet Res *49*, 48.

Rius, J., Guma, M., Schachtrup, C., Akassoglou, K., Zinkernagel, A.S., Nizet, V., Johnson, R.S., Haddad, G.G., and Karin, M. (2008). NF-kappaB links innate immunity to the hypoxic response through transcriptional regulation of HIF-1alpha. Nature *453*, 807-811.

Robinson, J.T., Thorvaldsdottir, H., Winckler, W., Guttman, M., Lander, E.S., Getz, G., and Mesirov, J.P. (2011). Integrative genomics viewer. Nat Biotechnol *29*, 24-26.

Rotter, B., Rodriguez, A., Krezdorn, N., Jost, L., and Winter, P. (2017). Massive Analysis of cDNA Ends (MACE): eine effektive RNA-Seq-Variante. BIOspektrum Springer *23*, 58-60.

Rozen, S., and Skaletsky, H. (2000). Primer3 on the WWW for general users and for biologist programmers. Methods Mol Biol *132*, 365-386.

Rungelrath, V., Weisse, C., Schutze, N., Muller, U., Meurer, M., Rohde, M., Seele, J., Weigand, P.V., Kirschfink, M., Beineke, A*., et al.* (2018). IgM cleavage by *Streptococcus suis* reduces IgM bound to the bacterial surface and is a novel complement evasion mechanism. Virulence *9*, 1314-1337.

Saliba, A.E., S, C.S., and Vogel, J. (2017). New RNA-seq approaches for the study of bacterial pathogens. Curr Opin Microbiol *35*, 78-87.

Sanford, S.E. (1987). Gross and histopathological findings in unusual lesions caused by *Streptococcus suis* in pigs. II. Central nervous system lesions. Can J Vet Res *51*, 486-489.

Sanger, F., Nicklen, S., and Coulson, A.R. (1977). DNA sequencing with chain-terminating inhibitors. Proc Natl Acad Sci U S A *74*, 5463-5467.

Santos, S.A.D., and Andrade, D.R.J. (2017). HIF-1alpha and infectious diseases: a new frontier for the development of new therapies. Rev Inst Med Trop Sao Paulo *59*, e92.

Schaffer, K., and Taylor, C.T. (2015). The impact of hypoxia on bacterial infection. FEBS J *282*, 2260-2266.

Schaible, B., McClean, S., Selfridge, A., Broquet, A., Asehnoune, K., Taylor, C.T., and Schaffer, K. (2013). Hypoxia modulates infection of epithelial cells by *Pseudomonas aeruginosa*. PLoS One *8*, e56491.

Schaible, B., Rodriguez, J., Garcia, A., von Kriegsheim, A., McClean, S., Hickey, C., Keogh, C.E., Brown, E., Schaffer, K., Broquet, A.*, et al.* (2017). Hypoxia reduces the pathogenicity of *Pseudomonas aeruginosa* by decreasing the expression of multiple virulence factors. J Infect Dis *215*, 1459-1467.

Schmittgen, T.D., and Livak, K.J. (2008). Analyzing real-time PCR data by the comparative C(T) method. Nat Protoc *3*, 1101-1108.

Schroeder, A., Mueller, O., Stocker, S., Salowsky, R., Leiber, M., Gassmann, M., Lightfoot, S., Menzel, W., Granzow, M., and Ragg, T. (2006). The RIN: an RNA integrity number for assigning integrity values to RNA measurements. BMC Molecular Biology *7*.

Schroten, M., Hanisch, F.G., Quednau, N., Stump, C., Riebe, R., Lenk, M., Wolburg, H., Tenenbaum, T., and Schwerk, C. (2012). A novel porcine *in vitro* model of the blood-cerebrospinal fluid barrier with strong barrier function. PLoS One *7*, e39835.

Schwerk, C., Adam, R., Borkowski, J., Schneider, H., Klenk, M., Zink, S., Quednau, N., Schmidt, N., Stump, C., Sagar, A.*, et al.* (2011). *In vitro* transcriptome analysis of porcine choroid plexus epithelial cells in response to *Streptococcus suis*: release of pro-inflammatory cytokines and chemokines. Microbes Infect *13*, 953-962.

Schwerk, C., Papandreou, T., Schuhmann, D., Nickol, L., Borkowski, J., Steinmann, U., Quednau, N., Stump, C., Weiss, C., Berger, J.*, et al.* (2012). Polar invasion and translocation of *Neisseria meningitidis* and *Streptococcus suis* in a novel human model of the blood-cerebrospinal fluid barrier. PLoS One *7*, e30069.

Schwerk, C., Rybarczyk, K., Essmann, F., Seibt, A., Molleken, M.L., Zeni, P., Schroten, H., and Tenenbaum, T. (2010). TNFalpha induces choroid plexus epithelial cell barrier alterations by apoptotic and nonapoptotic mechanisms. J Biomed Biotechnol *2010*, 307231.

Schwerk, C., Tenenbaum, T., Kim, K.S., and Schroten, H. (2015). The choroid plexus-a multi-role player during infectious diseases of the CNS. Front Cell Neurosci *9*, 80.

Seele, J., Tauber, S.C., Bunkowski, S., Baums, C.G., Valentin-Weigand, P., de Buhr, N., Beineke, A., Iliev, A.I., Bruck, W., and Nau, R. (2018). The inflammatory response and neuronal injury in *Streptococcus suis* meningitis. BMC Infect Dis *18*, 297.

Segura, M. (2015). *Streptococcus suis* vaccines: candidate antigens and progress. Expert Rev Vaccines *14*, 1587-1608.

Segura, M., Fittipaldi, N., Calzas, C., and Gottschalk, M. (2017). Critical *Streptococcus suis* virulence factors: Are they all really critical? Trends Microbiol *25*, 585-599.

Segura, M., Vadeboncoeur, N., and Gottschalk, M. (2002). CD14-dependent and -independent cytokine and chemokine production by human THP-1 monocytes stimulated by *Streptococcus suis* capsular type 2. Clin Exp Immunol *127*, 243-254.

Segura, M., Vanier, G., Al-Numani, D., Lacouture, S., Olivier, M., and Gottschalk, M. (2006). Proinflammatory cytokine and chemokine modulation by *Streptococcus suis* in a whole-blood culture system. FEMS Immunol Med Microbiol *47*, 92-106.

Shao, D.D., Xue, W., Krall, E.B., Bhutkar, A., Piccioni, F., Wang, X., Schinzel, A.C., Sood, S., Rosenbluh, J., Kim, J.W.*, et al.* (2014). KRAS and YAP1 converge to regulate EMT and tumor survival. Cell *158*, 171-184.

Shen, X., Niu, X., Li, G., Deng, X., and Wang, J. (2018). Amentoflavone ameliorates *Streptococcus suis*-induced infection *in vitro* and *in vivo*. Appl Environ Microbiol *84*.

Smith, H.E., Damman, M., van der Velde, J., Wagenaar, F., Wisselink, H.J., Stockhofe-Zurwieden, N., and Smits, M.A. (1999). Identification and characterization of the cps locus of *Streptococcus suis* serotype 2: the capsule protects against phagocytosis and is an important virulence factor. Infect Immun *67*, 1750-1756.

Soneson, C., and Delorenzi, M. (2013). A comparison of methods for differential expression analysis of RNA-seq data. BMC Bioinformatics *14*, 91.

Staats, J.J., Feder, I., Okwumabua, O., and Chengappa, M.M. (1997). *Streptococcus suis*: past and present. Vet Res Commun *21*, 381-407.

Steffen, B.J., Breier, G., Butcher, E.C., Schulz, M., and Engelhardt, B. (1996). ICAM-1, VCAM-1, and MAdCAM-1 are expressed on choroid plexus epithelium but not endothelium and mediate binding of lymphocytes *in vitro*. Am J Pathol *148*, 1819-1838.

Strazielle, N., and Ghersi-Egea, J.F. (2000). Choroid plexus in the central nervous system: biology and physiopathology. J Neuropathol Exp Neurol *59*, 561-574.

Strazielle, N., and Ghersi-Egea, J.F. (2016). Potential pathways for CNS drug delivery across the blood-cerebrospinal fluid barrier. Curr Pharm Des *22*, 5463-5476.

Subramanian, A., Tamayo, P., Mootha, V.K., Mukherjee, S., Ebert, B.L., Gillette, M.A., Paulovich, A., Pomeroy, S.L., Golub, T.R., Lander, E.S.*, et al.* (2005). Gene set enrichment analysis: a knowledge-based approach for interpreting genome-wide expression profiles. Proc Natl Acad Sci U S A *102*, 15545-15550.

Sumanovic-Glamuzina, D., Culo, F., Culo, M.I., Konjevoda, P., and Jerkovic-Raguz, M. (2017). A comparison of blood and cerebrospinal fluid cytokines (IL-1beta, IL-6, IL-18, TNF-alpha) in neonates with perinatal hypoxia. Bosn J Basic Med Sci *17*, 203-210.

Tang, J., Wang, C., Feng, Y., Yang, W., Song, H., Chen, Z., Yu, H., Pan, X., Zhou, X., Wang, H.*, et al.* (2006). Streptococcal toxic shock syndrome caused by *Streptococcus suis* serotype 2. PLoS Med *3*, e151.

Tarazona, S., Garcia-Alcalde, F., Dopazo, J., Ferrer, A., and Conesa, A. (2011). Differential expression in RNA-seq: a matter of depth. Genome Res *21*, 2213-2223.

Taylor, C.T., and Colgan, S.P. (2017). Regulation of immunity and inflammation by hypoxia in immunological niches. Nat Rev Immunol *17*, 774-785.

Tenenbaum, T., Adam, R., Eggelnpohler, I., Matalon, D., Seibt, A., GE, K.N., Galla, H.J., and Schroten, H. (2005). Strain-dependent disruption of blood-cerebrospinal fluid barrier by *Streptoccocus suis in vitro*. FEMS Immunol Med Microbiol *44*, 25-34.

Tenenbaum, T., Essmann, F., Adam, R., Seibt, A., Janicke, R.U., Novotny, G.E., Galla, H.J., and Schroten, H. (2006). Cell death, caspase activation, and HMGB1 release of porcine choroid plexus epithelial cells during *Streptococcus suis infection in vitro*. Brain Res *1100*, 1-12.

Tenenbaum, T., Matalon, D., Adam, R., Seibt, A., Wewer, C., Schwerk, C., Galla, H.J., and Schroten, H. (2008). Dexamethasone prevents alteration of tight junction-associated proteins and barrier function in porcine choroid plexus epithelial cells after infection with *Streptococcus suis in vitro*. Brain Res *1229*, 1-17.

Tenenbaum, T., Papandreou, T., Gellrich, D., Friedrichs, U., Seibt, A., Adam, R., Wewer, C., Galla, H.J., Schwerk, C., and Schroten, H. (2009). Polar bacterial invasion and translocation of *Streptococcus suis* across the blood-cerebrospinal fluid barrier *in vitro*. Cell Microbiol *11*, 323-336.

Tian, G., Yin, X., Luo, H., Xu, X., Bolund, L., Zhang, X., Gan, S.Q., and Li, N. (2010). Sequencing bias: comparison of different protocols of microRNA library construction. BMC Biotechnol *10*, 64.

Tsutsumi, M., Skinner, M.K., and Sanders-Bush, E. (1989). Transferrin gene expression and synthesis by cultured choroid plexus epithelial cells. Regulation by serotonin and cyclic adenosine 3',5'-monophosphate. J Biol Chem *264*, 9626-9631.

van der Flier, M., Geelen, S.P., Kimpen, J.L., Hoepelman, I.M., and Tuomanen, E.I. (2003). Reprogramming the host response in bacterial meningitis: how best to improve outcome? Clin Microbiol Rev *16*, 415-429.

van Ettekoven, C.N., van de Beek, D., and Brouwer, M.C. (2017). Update on community-acquired bacterial meningitis: guidance and challenges. Clin Microbiol Infect *23*, 601-606.

van Samkar, A., Brouwer, M.C., Schultsz, C., van der Ende, A., and van de Beek, D. (2015). *Streptococcus suis* meningitis: A systematic review and meta-analysis. PLoS Negl Trop Dis *9*, e0004191.

van Sorge, N.M., Ebrahimi, C.M., McGillivray, S.M., Quach, D., Sabet, M., Guiney, D.G., and Doran, K.S. (2008). Anthrax toxins inhibit neutrophil signaling pathways in brain endothelium and contribute to the pathogenesis of meningitis. PLoS One *3*, e2964.

Vandenhaute, E., Stump-Guthier, C., Lasierra Losada, M., Tenenbaum, T., Rudolph, H., Ishikawa, H., Schwerk, C., Schroten, H., Durken, M., Marz, M., *et al.* (2015). The choroid plexus may be an underestimated site of tumor invasion to the brain: an *in vitro* study using neuroblastoma cell lines. Cancer Cell Int *15*, 102.

Vecht, U., Wisselink, H.J., Jellema, M.L., and Smith, H.E. (1991). Identification of two proteins associated with virulence of *Streptococcus suis* type 2. Infect Immun *59*, 3156-3162.

Vercellino, M., Votta, B., Condello, C., Piacentino, C., Romagnolo, A., Merola, A., Capello, E., Mancardi, G.L., Mutani, R., Giordana, M.T.*, et al.* (2008). Involvement of the choroid plexus in multiple sclerosis autoimmune inflammation: a neuropathological study. J Neuroimmunol *199*, 133-141.

Wang, M.-H., Jiang, G.-Y., Zhang, X.-P., Yang, L.-H., Xu, H.-T., Li, Q.-C., and Wang, E.-H. (2017). The expression of TC1 (C8orf4) and beta-catenin were correlated with the malignant phenotype of gliomas and meningiomas. Int J Clin Exp Pathol *10*, 625-631.

Wang, Z., Gerstein, M., and Snyder, M. (2009). RNA-Seq: a revolutionary tool for transcriptomics. Nat Rev Genet *10*, 57-63.

Weller, R.O., Sharp, M.M., Christodoulides, M., Carare, R.O., and Mollgard, K. (2018). The meninges as barriers and facilitators for the movement of fluid, cells and pathogens related to the rodent and human CNS. Acta Neuropathol *135*, 363-385.

Wertheim, H.F., Nghia, H.D., Taylor, W., and Schultsz, C. (2009). *Streptococcus suis*: an emerging human pathogen. Clin Infect Dis *48*, 617-625.

Wewer, C., Seibt, A., Wolburg, H., Greune, L., Schmidt, M.A., Berger, J., Galla, H.J., Quitsch, U., Schwerk, C., Schroten, H.*, et al.* (2011). Transcellular migration of neutrophil granulocytes through the blood-cerebrospinal fluid barrier after infection with *Streptococcus suis*. J Neuroinflammation *8*, 51.

Whiteford, N., Skelly, T., Curtis, C., Ritchie, M.E., Lohr, A., Zaranek, A.W., Abnizova, I., and Brown, C. (2009). Swift: primary data analysis for the Illumina Solexa sequencing platform. Bioinformatics *25*, 2194-2199.

Wilhelm, B.T., and Landry, J.R. (2009). RNA-Seq-quantitative measurement of expression through massively parallel RNA-sequencing. Methods *48*, 249-257.

Williams, A.E., and Blakemore, W.F. (1990). Pathogenesis of meningitis caused by *Streptococcus suis* type 2. J Infect Dis *162*, 474-481.

Wolburg, H., and Lippoldt, A. (2002). Tight junctions of the blood-brain barrier: development, composition and regulation. Vascul Pharmacol *38*, 323-337.

Wolburg, H., and Paulus, W. (2010). Choroid plexus: biology and pathology. Acta Neuropathol *119*, 75-88.

Wolburg, H., Wolburg-Buchholz, K., Liebner, S., and Engelhardt, B. (2001). Claudin-1, claudin-2 and claudin-11 are present in tight junctions of choroid plexus epithelium of the mouse. Neurosci Lett *307*, 77-80.

Wright, W.F., Pinto, C.N., Palisoc, K., and Baghli, S. (2019). Viral (aseptic) meningitis: A review. J Neurol Sci *398*, 176-183.

Wu, Z., Zhang, W., Lu, Y., and Lu, C. (2010). Transcriptome profiling of zebrafish infected with *Streptococcus suis*. Microb Pathog *48*, 178-187.

Yu, H., Jing, H., Chen, Z., Zheng, H., Zhu, X., Wang, H., Wang, S., Liu, L., Zu, R., Luo, L.*, et al.* (2006). Human *Streptococcus suis* outbreak, Sichuan, China. Emerg Infect Dis *12*, 914-920.

Yu, Y.F., Qian, Y.Y., Du, D.C., Li, Q., Xu, C.Y., Liu, H.Z., Chen, M.M., Yao, H.C., Lu, C.P., and Zhang, W. (2018). Infection and adaption-based proteomic changes of *Streptococcus suis* serotype 2 in a pig model. J Proteomics *180*, 41-52.

Zeitouni, N.E., Dersch, P., Naim, H.Y., and von Kockritz-Blickwede, M. (2016). Hypoxia decreases invasin-mediated *Yersinia enterocolitica* internalization into Caco-2 cells. PLoS One *11*, e0146103.

Zhang, D.Y., Zou, X.J., Cao, C.H., Zhang, T., Lei, L., Qi, X.L., Liu, L., and Wu, D.H. (2018). Identification and functional characterization of long non-coding RNA MIR22HG as a tumor suppressor for hepatocellular carcinoma. Theranostics *8*, 3751-3765.

Zheng, W., and Zhao, Q. (2002). Establishment and characterization of an immortalized Z310 choroidal epithelial cell line from murine choroid plexus. Brain Res *958*, 371-380.

Zheng, Y., Stamminger, T., and Hearing, P. (2016). E2F/Rb family proteins mediate interferon induced repression of adenovirus immediate early transcription to promote persistent viral infection. PLoS Pathog *12*, e1005415.

Zinkernagel, A.S., Peyssonnaux, C., Johnson, R.S., and Nizet, V. (2008). Pharmacologic augmentation of hypoxia-inducible factor-1alpha with mimosine boosts the bactericidal capacity of phagocytes. J Infect Dis *197*, 214-217.

II. List of Figures

III. List of Tables

Acknowledgements

First and foremost I want to thank Prof. Horst Schroten for his support throughout the project and for allowing me to carry out this project in his lab, as well as supporting my travelling to be involved in the external collaborations throughout Germany and presenting this research during numerous international conferences.

I want to thank Prof. Michael Lanzer for taking on the responsibility of first referee for this thesis.

I want to thank Prof. Christian Schwerk for the scientific supervision, support and encouragement, countless times of meticulous proof reading, as well as always being open for discussion.

I want to thank you to my fellow PhD students: Steffi, Tobias, Marie, Franjo, Rosanna, and Lea for scientific exchange and fun conversations.

I want to thank Svenja, Ummaya, Carolin, Julia B., and Ulrike for their technical support, theoretical expertise and scientific discussions, as well as fellow lab members over the past few years for making work a fun and pleasant place to be.

I want to thank the following collaboration partners …

… Dr. Ludger Klein-Hitpass and his group, as well as Dr. Rene Scholtysik, at the Institute for Cell Biology, University Hospital Essen in Essen, Germany, for their support with acquiring all the bioinformatic data, answering any related questions, welcoming me to participate in their laboratory, and giving me further insight into their area of expertise.

… Prof. Christoph Georg Baums and the members of his institute, at the Institute for Bacteriology and Mycology, Center for Infectious Diseases, at the Faculty of Veterinary Medicine, University of Leipzig in Leipzig, Germany, for allowing me to gain insight and participate in the animals experiments, and ensuring the collection of the CP tissue samples.

… Prof. Andreas Beineke at the Institute for Pathology, University of Veterinary Medicine in Hannover, Germany, for performing the veterinary pathology of the *in vivo* infected piglets.

I want to thank the Grimminger-Stiftung für Zoonosenforschung (Grimminger Foundation for Zoonotic Research) for awarding a grant which financially supported part of this project.

Most importantly I want thank my family: my parents, Elizabeth & Hank and Nico & Dine, my siblings, Ari, Finn, and Malin, as well as Katja and Rainer for their unconditional love and support.

I want to thank my friends, especially Becca, Cihan, Alina, Chris, and Sven for their support in many aspects and motivating me throughout the past few years. And last, but not least, thank you to the most loving and loyal companion, Georgie.